

Bulgarian Geophysical Journal

2019, Vol. 42

Contents

<i>R. Bojilova</i> – Influence of geomagnetic activity on the ionosphere critical frequencies.	3
<i>E. Oynakov, I. Aleksandrova, D. Solakov</i> – Variations of the parameters of background seismic noise in the stage of preparation of strong earthquakes in the Vrancea region storms.	10
<i>N. Dimitrov, P. Danchev, I. Georgiev</i> – Investigation of the impact of atmospheric refraction on precision leveling measurements.	28
<i>N. Miloshev, P. Trifonova</i> – What the National Geo information Center is going to change?.	37
<i>P. Trifonova, M. Metodiev, I. Buchvarov</i> – Digital data records in PAG Geomagnetic Observatory available for a 60 years period.	46
<i>M. Metodiev, P. Trifonova</i> – Annual report of the observed geomagnetic activity in Panagyurishte Observatory for 2014.	62
<i>A. Ivanov, I. Georgiev, N. Dimitrov</i> – Analysis of monthly sea level data from Varna tide gauge station.	77
<i>L. Christoskov, L. Dimitrova, D. Solakov, S. Simeonova</i> – Forty years National Operative Telemetric System for seismological information.	83
<i>V. Buchakchiev, E. Oynakov, D. Dragomirov, Y. Milkov</i> – Seismicity on the territory of Bulgaria and the adjacent lands recorded by NOTSSI in 2017. . .	94

D. Dragomirov, E. Oynakov, V. Buchakchiev, Y. Milkov – Seismicity on the territory of Bulgaria and the adjacent lands recorded by NOTSSI in 2018..... 105

INFLUENCE OF GEOMAGNETIC ACTIVITY ON THE IONOSPHERE CRITICAL FREQUENCIES

R. Bojilova

National Institute of Geophysics, Geodesy and Geography, Bulgarian Academy of Sciences, Acad.
G. Bonchev Str., bl. 3, Sofia 1113, Bulgaria, e-mail: rbojilova@geophys.bas.bg

DOI: 10.34975/bgj-2019.42.1

Abstract. The present work investigates the seasonal dependence of the geomagnetic activity influences on the diurnal variability of the maximum electron concentration of the ionosphere over Bulgaria. Data from the ionosonde station Sofia for the period of 1995-2014 are used. The geomagnetic activity is described by the planetary Kp-index. The ionospheric response to the geomagnetic storms is studied by considering the relative deviation of the diurnal variability from its median course for the two ionospheric characteristics foF2 (critical frequency of the ionospheric F-region) and MUF3000 (maximum usable frequency for a distance of 3000 km). It is found that the ionospheric reaction in summer is stronger than that in winter and the time delay of the ionospheric response in winter is longer than that in summer.

Key words: geomagnetic activity, critical frequency, ionospheric response.

Introduction

Ionospheric storm is a common term that describes the entirety of ionospheric variations induced by geomagnetic disturbances. The ionospheric storms primarily occur as a consequence of a sudden input of solar wind energy into the magnetosphere-ionosphere-thermosphere system (Astafyeva et al., 2015). The energy inputs during the geomagnetic disturbances lead to substantial effects in the upper atmosphere and the significant perturbation of the "quiet-time" ionosphere (Mukhtarov and Bojilova, 2017). Three main mechanisms of storm effects have been suggested to explain the positive and negative phases of ionospheric storms: (i) thermospheric composition changes, (ii) neutral wind perturbations, and (iii) the appearance of electric fields of magnetospheric origin. The negative phase of ionospheric storms is mainly due to the composition changes (Rishbeth, 1991), i.e. the thermosphere becomes rich-

er in molecular nitrogen (N_2) and oxygen (O_2) and poorer in atomic oxygen (O). The molecular species, however, determine the loss rate of ions hence their enhancement leads to an increase of the loss rate. The auroral heating can alter the mean global circulation of the thermosphere. Whereas for quiet conditions there is a general upwelling in the summer hemisphere flow toward the winter hemisphere at higher levels, and down-welling in the winter hemisphere, the storm-time heating adds a polar upwelling and equatorward flow in both hemispheres. The increased equatorward wind at middle latitudes tends to push the ionosphere higher up along magnetic field lines, where the loss rate is lower. The reasons of the positive ionospheric storms are the combined effects of disturbed thermospheric wind and electric fields (Balan et al., 2010 and Tanaka, 1979). Kelley et al. (2004) suggested that, in the presence of daytime ionization an eastward prompt penetration electric field (PPEF) can strengthen the equatorial plasma fountain to a super plasma fountain, which, in turn, can lead to positive ionospheric storms at sub-tropical and mid-latitudes. However, modelling studies later showed that an equatorward neutral wind is required also to produce positive ionospheric storms (Balan et al., 2010).

The present study investigates the seasonal dependence of the geomagnetic activity influences on the diurnal variability of the maximum electron concentration of the ionosphere over Bulgaria. The ionospheric response to the geomagnetic storms is studied by considering the deviation of the diurnal variability from its steady (median) course. It is found that the ionospheric reaction in summer is stronger than that in winter. Using the correlation analysis the seasonal dependence of the ionospheric response time delay for two ionospheric characteristics, foF2 and MUF3000, was determined. It is found that the time delay of the ionospheric response in winter is longer than that in summer.

Data

The geomagnetic activity is described by the planetary Kp-index and the values of the Kp-index are obtained from NOAA website: <https://www.ngdc.noaa.gov>. The data for foF2 and MUF3000 are taken from the ionosonde station Sofia- SQ143 (42.4°N, 23.2°E) at the NIGGG-BAS for the period of 1995-2014. This study is based on the representation suggested by (Muhtarov et al., 2002 and Mukhtarov et al., 2013) about the reaction of the relative deviation of ionospheric quantities to geomagnetic disturbances in an inertial model, described by a linear differential equation of first order with a given time constant. For this purpose, the Kp-index has been integrated with different time constants from 1 to 72 hours. For each time constant, the cross-correlation function between the integrated Kp-index and the relative deviation of foF2 and MUF3000 is calculated and the time constant with the highest correlation (positive or negative) is selected. It is assumed that this time constant characterizes the real inertness of the ionosphere. In order to get information about the seasonal differences, cross-correlation is calculated for each calendar month. The day and night-time conditions are considered separately.

Experimental results

The results of the cross-correlation analysis between the ionospheric characteristics foF2 and MUF3000 and geomagnetic activity will be illustrated and explained in detail by considering the presented below examples. The obtained results will be used to justify later the development of an empirical model for predicting the ionosphere state over Bulgaria.

Fig. 1 shows the seasonal courses of the negative correlations (left panel) and the optimal time constants (right panel) during daytime conditions for both parameters foF2 (full line) and MUF3000 (dash line). The left panel of Fig. 1 reveals that a significant negative correlation of 28-30% occurs in the summer and equinoctial months for both characteristics foF2 and MUF3000 oppositely to the winter months when the correlation is very small, only 3-8%. The right panel of Fig. 1 shows small time constants of the order of 2-15 hours for the months from February to September (we note that January and December are not shown because the response is always positive).

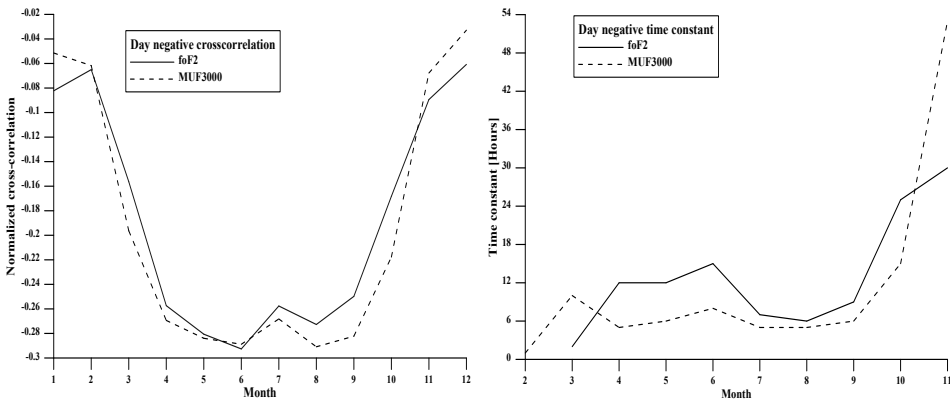


Fig. 1. Seasonal variability of the negative cross-correlation (left panel) and time constant (right panel) during daytime conditions.

Fig. 2 demonstrates the cross-correlation functions for two typical summer months, June and July, for the considered parameters foF2 (left panel) and MUF3000 (right panel) in daytime conditions. The figure shows a good negative cross-correlation during the months under consideration for both parameters, reaching in some cases 30%. The delay corresponding to the maximum negative cross-correlation for daytime conditions in the months June and July, presented in Fig. 2, is around 7 hours.

Fig. 3 is similar to Fig. 1 but for nighttime conditions. Again, we can see well-expressed negative cross-correlations valid for the two quantities foF2 and MUF3000 during the summer months, reaching about 30%. The winter months, shown in Fig. 3, are again characterized by a smaller negative cross-correlation (Fig. 3, left panel). The time constants, shown on the right panel of Fig. 3, demonstrate the smallest values (about 15

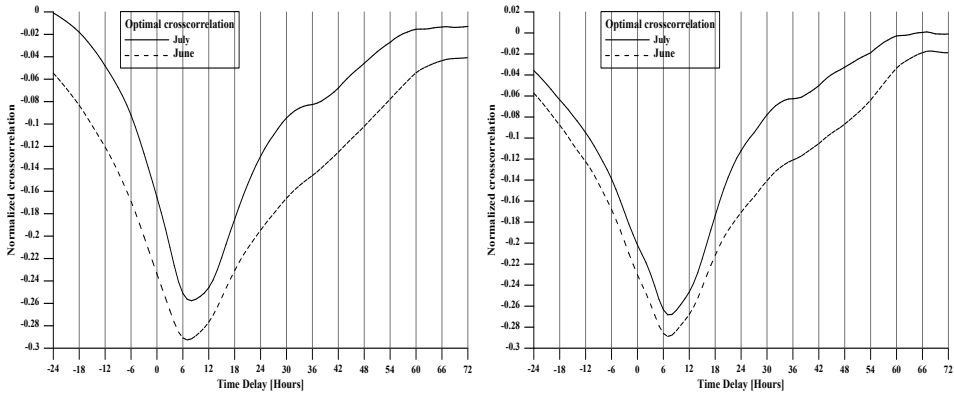


Fig. 2. Optimal negative cross-correlation functions for two months June and July for foF2 (left panel) and MUF3000 (right panel) during daytime conditions.

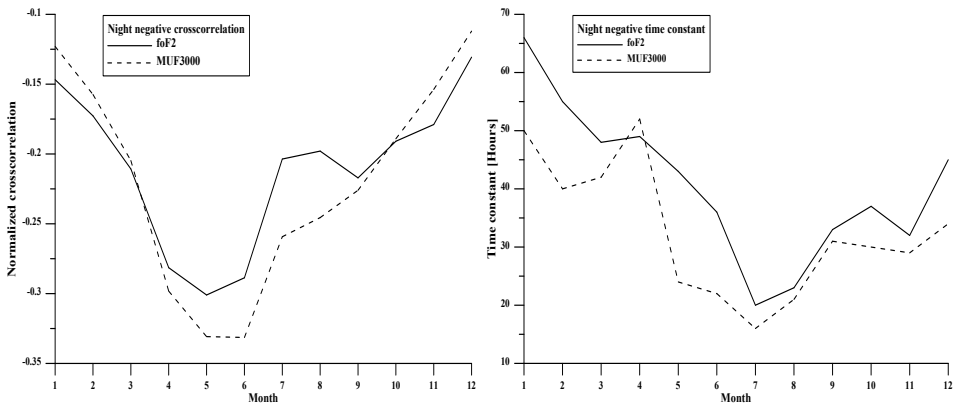


Fig. 3. Seasonal variability of the negative cross-correlation (left panel) and time constant (right panel) during nighttime conditions.

hours) in the summer months again while in the winter months the time constants begin to increase and reach about 66 hours.

Fig. 4 is analogous to Fig. 2 and presents the cross-correlation functions for two typical summer months, June and July, for the considered parameters foF2 (left panel) and MUF3000 (right panel), but this time for nighttime conditions. A good negative cross-correlation during the considered months for both quantities is observed; it reaches almost 30% for foF2 (left panel) and exceeds 32% for MUF3000 (right panel). The delay corresponding to the maximum negative cross-correlation for the nighttime conditions in June and July is presented in Fig. 4 (left and right panel), ranges from 6 to 11 hours.

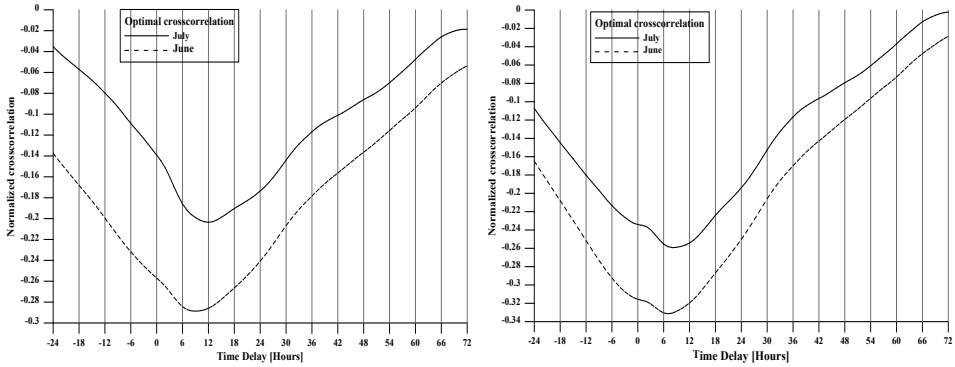


Fig. 4. Optimal negative cross-correlation functions for two months June and July for foF2 (left panel) and MUF3000 (right panel) during nighttime conditions.

Fig. 5 shows the cross-correlation functions in daytime conditions for two typical winter months December and January for the considered parameters foF2 (left panel) and MUF3000 (right panel). The presentation of these months in a separate figure was done because of the positive cross-correlation obtained at the practically zero value of the integrated time constant. The values of the time delay for both critical frequencies are around 2-9 hours for January and 6 and 11 hours for December. The maximum positive cross-correlation for foF2 (left panel) during these winter months is about 24%, whereas for MUF3000 it is approximately 15% (right panel). The delay corresponding to the maximum positive cross-correlation during the daytime conditions in December and January for foF2, presented in Fig. 5 (left panel), is between 3 and 9 hours. The same time delay corresponding to the maximum positive cross-correlation for MUF3000, shown in Fig. 5 (right panel), is about 10-11 hours, which is similar to the summer months presented in Fig. 4.

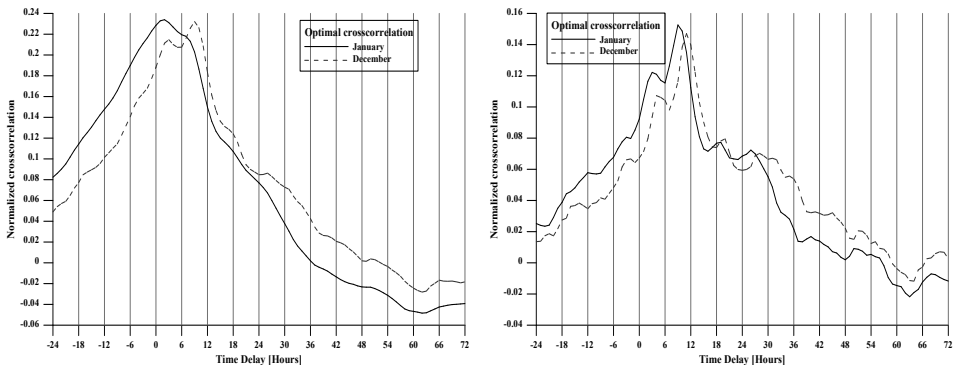


Fig. 5. Optimal positive cross-correlation functions for two winter months December and January for foF2 (left panel) and MUF3000 (right panel) during daytime conditions

Comments and conclusions

This study investigates the seasonal variability of the ionospheric response to geomagnetic activity over ionosonde station Sofia. For this purpose the cross-correlation analysis between the integrated Kp-index and the relative deviation of the parameters foF2 and MUF3000 is performed. It is well known that the values of the cross-correlation function, i.e. the cross-correlation coefficients, to a large extent determine the coefficients of linear regression between the studied quantities, as the negative/positive cross-correlation defines the inverse/direct relationship. The values themselves indicate the strength of the investigated relationship.

The analyses revealed that the negative reaction of the ionospheric parameters to the geomagnetic activity is stronger during summer and equinoctial months than that in winter. This is due to the thermospheric composition changes related to the Joule heating and particle precipitations during the geomagnetic storms which are moved to the middle latitude by the disturbed and 'quiet-time' seasonal circulations in summer. The increase in time constants, i.e. the delay of the negative reaction during the winter is caused by the need of extra time for strengthening of the disturbed circulation. Negative nighttime reaction turns out to be more significant than in daytime conditions. A positive reaction practically without delay is observed only in the winter months during daytime conditions.

The results obtained might prove useful in the development of an empirical model for predicting the ionosphere response to geomagnetic storms over Sofia.

Acknowledgments. This work was supported by the Bulgarian Ministry of Education and Science under the National Research Program "Young scientists and postdoctoral students" approved by DCM №577 / 17.08.2018 and by Contract No D01-161/28.08.2018 (Project "National Geoinformation Center (NGIC)" financed by the National Roadmap for Scientific Infrastructure 2017-2023.

References

- Astafyeva, E., Zakharenkova I. and Förster M., 2015. Ionospheric response to the 2015 St. Patrick's Day storm: A global multi-instrumental overview, *J. Geophys. Res. Space Physics*, **120**, 9023–9037, doi:10.1002/2015JA021629.
- Balan N., Shiokawa K., Otsuka Y., Kikuchi T., Vijaya Lekshmi D., Kawamura S., Yamamoto M., Bailey G. J., 2010. A physical mechanism of positive ionospheric storms at low latitudes and mid latitudes, *J. Geophys. Res.* **115**, A02304, doi:10.1029/2009JA014515.
- Blanc M., Richmond A. D., 1980. The ionospheric disturbance dynamo, *J. Geophys. Res.*, **85(A4)**, 1669–1699.
- Kelley M. C., Vlasov M. N., Foster J. C., Coster A. J., 2004. A quantitative explanation for the phenomenon known as storm enhanced density, *Geophys. Res. Lett.* **31**, L19809, doi:10.1029/2004GL020875.

- Muhtarov, P., Kutiev, I., & Cander, L., 2002. Geomagnetically correlated autoregression model for short-term prediction of ionospheric parameters. *Inverse Problems*, **18(1)**, 49.
- Mukhtarov, P., Andonov, B., & Pancheva, D., 2013. Global empirical model of TEC response to geomagnetic activity. *Journal of Geophysical Research: Space Physics*, **118(10)**, 6666-6685.
- Mukhtarov, P., and Bojilova, R., 2017. Influence of solar and geomagnetic activity on the ionosphere over Bulgaria. *Comptes Rendus de L'Academie Bulgare des Sciences*, **70(9)**, 1289-1296
- Rishbeth H., 1991. F-region storms and thermospheric dynamics, *J. Geomag. Geoelectr.*, **43 (suppl.)**, 513–524.
- Tanaka T., 1979. The worldwide distribution of positive ionospheric storms, *J. Atmos. Terr. Phys.*, **41**, 103–110.

Влияние на геомагнитната активност върху критичните честоти на йоносферата

Р. Божилова

Резюме: В настоящето изследване е представена сезонната зависимост на влиянието на геомагнитната активност върху отклонението от стационарния (среден) денонощен ход на максималната електронна концентрация на йоносферата за България. Използвани са данни от Йоносферна станция София за периода 1995–2014 г, както и индексът, характеризиращ геомагнитната активност K_p , за същия период време. Установява се, че получената реакция се увеличава през летния сезон в сравнение със зимния. Чрез използването на корелационен анализ е определен сезонният ход на времеконстантата на закъснение на реакцията на йоносферата за двете йоносферни характеристики – f_oF2 и $MUF3000$. Предложено е обяснение за получените резултати, които показват, че съответната времеконстанта е по-дълга през зимните месеци и ниска през лятото.

VARIATIONS OF THE PARAMETERS OF BACKGROUND SEISMIC NOISE IN THE STAGE OF PREPARATION OF STRONG EARTHQUAKES IN THE VRANCEA REGION

E. Oynakov, I. Aleksandrova, D. Solakov

National Institute of Geophysics, Geodesy and Geography, Bulgarian Academy of Sciences, Acad. G. Bonchev Str., bl.3, Sofia 1113, Bulgaria, e-mail: i.alex@abv.bg

DOI: 10.34975/bgj-2019.42.2

Abstract. The Balkans, including Bulgaria, is one of the most seismogenic zones in Europe. The relatively small depth of the hypocentres of earthquakes - up to 60-70 km, could greatly increase the effects on the ground surface. In conditions of relatively high population density and high urban constructions, even a moderate magnitude earthquake could lead to increased unfavourable consequences - destruction and human losses.

The global impacts of atmospheric and oceanic processes, tidal deformations of the earth's crust, as well as the less well-studied processes in the Earth's crust, are associated with accumulation and slow dissipation of tectonic energy in the lithosphere. These processes are the „participants“ in the formation of the random process, where the traditional apparatus of spectral analysis is less effective.

The usage of fractal analysis for decipher the structure of seismic noise is a good enough alternative. Since the early 1990s, the method is used in both: turbulence analysis and in financial and medical time series studies.

The development of new methods for earthquake forecasting based on data from geophysical and, in particular, seismic monitoring, is one of the priority goals of Earth science. Seismic records of twenty-three Balkan Peninsula stations were analyzed, at distances of 1 to 500 km far from the earthquake on 23.09.2016, 27.12.2016 and 28.10.2018 with magnitude more 5.5 in seismic zone Vrancea. For the analysis, the Lubusin method was used for fractal analysis of scalar time series.

A scientific goal is to detect common signals ignoring the „individual“ behavior of the elements of the monitoring systems.

Key words: earthquake indicators, seismic noise, fractal analysis of seismic noise

Introduction

Microseismic oscillations in a wide frequency range are one of the most widespread objects of geophysical studies. This is due to their accessibility, the presence of numerous regional and global seismic networks, and the well-developed practice of seismic observations. Even an approximate review of the literature, devoted to analysis of microseisms, apparently cannot be made.

This is particularly true for the analysis of high frequency (HF) microseisms (from 0.01 to 100 Hz and higher, up to seismoacoustic waves). The widespread occurrence of HF microseismic observations is due to the relative simplicity and mobility of instrumentation, free from rigid requirements on long-term stability of sensors that can by no means be neglected in problems of low frequency (LF) geophysical monitoring. McNamara and Buland [2004] presented results of detailed research into microseismic background of natural and industrial origin in the frequency band 0.01–16 Hz, including the construction of estimators for the temporal (diurnal and seasonal) and spatial distribution of power spectrum properties. With an increase in the period of microseismic background oscillations studied, the role of atmospheric and oceanic waves, as main sources of microseisms, becomes predominant. Berger et al. [2004] presented a review of the use of IRIS broadband seismic stations for the study of background microseisms. Microseismic oscillations in the period range 5–40 s were studied by Stehly et al. [2006], who established their oceanic origin. Continuously observed microseismic oscillations at periods of 100–500s were examined in Friedrich et al., [1998]. These oscillations are generated both by weak earthquakes and by processes in the atmosphere, although the atmospheric effects are predominant.

The effect of atmospheric processes (movement of cyclones) and oceanic waves, generated by them, as well as the impact of the waves on the shelf and coasts, contributes most to the energy of the LF microseismic background.

The origin of an LF seismic hum with a predominant period of 4 min was studied in Rhie and Romanowicz [2004, 2006]. A significant correlation was established between the intensity of these oscillations and the oceans wave height, caused by storms, and it was shown that the hum intensity is independent of the Earth's seismic activity: the authors presented an example of a seismically quiet time interval (January 31– February 3, 2000) characterized, however, by anomalously high amplitudes of microseismic background in the vicinity of the 4-min period. As a possible mechanism of excitation of such oscillations, they proposed the perturbation of the gravitational field by high waves, resulting in the excitation of LF seismic waves on the seafloor. The main regions of excitation of these oscillations are suggested to be the northern Pacific Ocean in winter and the southern Atlantic Ocean in summer.

Low frequency oscillations of microseismic background and the Earth's gravitational field with periods of a few tens to a few hundreds of minutes arising, due to the lithosphere–atmosphere coupling, were considered in Linkov, [1987]. It is important that the source of such oscillations is supposedly slow wavelike deformations of the lithosphere.

The present paper generalizes the experience, accumulated in studies of microseismic background in the (LF) range of periods from 1 to 300 min, observed in time inter-

vals, preceding a few strong earthquakes [Oynakov, Aleksandrova 2019; Oynakov E., et al. 2019].

This frequency range is the least studied and occupies an intermediate position between LF seismology and investigations of slow geophysical processes, such as gravity field variations, crustal strain and tilt variations, and so on. The range includes various modes of the Earth's free oscillations, excited by strong earthquakes; however, in the present paper, the main attention is given to the background behavior of microseisms. Note that this background contains continuous arrivals from near weak and far strong and moderate earthquakes.

In this paper, the main emphasis is placed on the study of synchronization effects, appearing in a joint multidimensional analysis of information from several stations. The synchronization effects of the microseismic background are also examined, as a means for detecting new precursors of strong earthquakes.

Method and Theory

Let F be some random fluctuations in the time interval $[t-\delta/2, t+\delta/2]$ (Figure 1) with duration δ and the reach of the random process for this interval - $\mu(t, \delta)$ (difference between the maximum and minimum amplitude values) and calculate the mean value of its power degree q : $M(\delta, q) = [(\mu_x(t, \delta))^q]$.

A random signal is scale-invariant [Taqqu, 1988] if $M(\delta, q) \sim \delta^{(q)}$ when $\delta \rightarrow 0$, that is, the following limit exists:

$$\rho(q) = \lim_{\delta \rightarrow 0} \left(\frac{\ln M(\delta, q)}{\ln(\delta)} \right). \quad (1)$$

If $\rho(q)$ is a linear function $\rho(q) = Hq$, where $H = const$, $0 < H < 1$, the process is called monofractal. In the case where $\rho(q)$ is a nonlinear concave function of q , the signal is called multifractal. To estimate the value of $\rho(q)$ using a finite sample $x(t)$, $t = 0, 1, \dots, N-1$ we used the method, which is based on the approach of detrended fluctuation analysis (DFA) [Kantelhardt et al., 2002]. Let us split the entire time series into non-overlapping intervals of length s :

$$\mathbf{I}_k^{(s)} = \left\{ t : 1 + (k-1)s \leq t \leq ks, k = 1, \dots, \left[\frac{N}{s} \right] \right\} \quad (2)$$

and let

$$\mathbf{y}_k^{(s)}(t) = \mathbf{x}((k-1)s + t), t = 1, \dots, s \quad (3)$$

be a part of the signal $x(t)$, corresponding to interval $\mathbf{I}_k^{(s)}$. Let $\mathbf{p}_k^{(s,m)}(t)$ be a polynomial of the order m , best fitted to the signal $\mathbf{y}_k^{(s)}(t)$. Let us consider the deflections from the local trend:

$$\Delta y_k^{(s,m)}(t) = y_k^{(s)}(t) - p_k^{(s,m)}(t), \quad t = 1, \dots, s \quad (4)$$

and calculate the values

$$Z^{(m)}(q, s) = \left(\frac{\left(\sum_{k=1}^{N/s} \left(\max_{1 \leq t \leq s} \Delta y_k^{(s,m)}(t) - \min_{1 \leq t \leq s} \Delta y_k^{(s,m)}(t) \right)^q \right)}{\frac{N}{s}} \right)^{\frac{1}{q}} \quad (5)$$

that can be regarded as the estimate of $(M(\delta_s, q))^{\frac{1}{q}}$. Let us define the function $h(q)$ as a coefficient of linear regression between $\ln(Z^{(m)}(q, s))$ and $\ln(s)$: $Z^{(m)}(q, s) \sim s^{h(q)}$ fitted for scales range $s_{min} \leq s \leq s_{max}$. It is evident that $(q) = qh(q)$ and, for a monofractal signal, $h(q) = H = const$. The multifractal singularity spectrum $F(\alpha)$ is equal to the fractal dimensionality of the set of time moments t for which the Hölder – Lipschitz exponent is equal to α i.e. for which $|x(t + \delta) - x(t)| \sim |\delta|^\alpha, \delta \rightarrow 0$ [Feder, 1988]. The singularity spectrum can be estimated using the standard multifractal formalism, which consists in calculating the Gibbs sum: multifractal formalism, which consists in calculating the Gibbs sum:

$$W(q, s) = \sum_{k=1}^{N/s} \left(\max_{1 \leq t \leq s} \Delta y_k^{(s,m)}(t) - \min_{1 \leq t \leq s} \Delta y_k^{(s,m)}(t) \right)^q \quad (6)$$

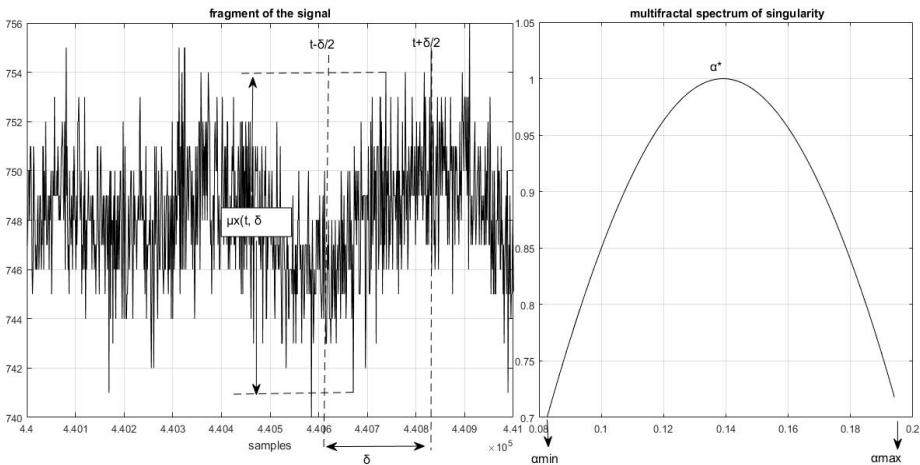


Fig. 1. Illustration of the multifractal spectrum of the singularity, where: $F(\alpha)$ – the multifractal spectrum of the singularity or fractal dimension of the set of times t ; $\Delta\alpha$ – width of the carrier of $F(\alpha)$; α^* – a general exponent Hurst

and in estimating the mass exponent $\tau(q)$ from the condition $W(q, s) \sim s^{\tau(q)}$. From (6) it follows that $\tau(q) = \rho(q) - 1 = qh(q) - 1$. In the next step, the spectrum $F(\alpha)$ is calculated with the Legendre transform:

$$F(\alpha) = \max_q \{ \min(\alpha q - \tau(q)), 0 \}. \quad (7)$$

If the singularity spectrum $F(\alpha)$ is estimated in a moving window, its evolution can give useful information on the variations in the structure of the “chaotic” pulsations of the series. In particular, the position and width of the support of the spectrum $F(\alpha)$, i.e., the values α_{\min} , α_{\max} , $\Delta\alpha = \alpha_{\max} - \alpha_{\min}$ and α^* , such that $F(\alpha^*) = \max_{\alpha} F(\alpha)$, are characteristics of the noisy signal. The value α^* can be called a generalized Hurst exponent and it gives the most typical value of Lipschitz-Holder exponent. Parameter $\Delta\alpha$, singularity spectrum support width, could be regarded as a measure of variety of stochastic behavior. In the case of a monofractal signal, the quantity $\Delta\alpha$ should vanish and $\alpha^* = H$. Usually $F(\alpha^*) = 1$, but there exist time windows for which $F(\alpha^*) < 1$. Estimates of minimum Hölder-Lipschitz exponent $\min \alpha$ are mainly positive. Nevertheless negative values of $\min \alpha$ are quite possible as well for time fragments which are characterized by high-amplitudes spikes and steps.

Used data

This article explores the time interval of 01.08.2016. - 30.12.2016, involving three seismic events with $M_w > 5.5$:

- the earthquake of 23.09.2016; $T_0=11:11:20$ GMT; with coordinates 45.71°N / 26.62°E; $M_w = 5.7$; $h = 92$ km;
- the Vrancea earthquake on 27.12.2016; $T_0=11:20:56.3$ GMT; with coordinates 45.72°N / 26.61°E; $M_w = 5.6$; $h = 91$ km;
- the Vrancea earthquake on 28.10.2018; $T_0= 00:38:15$ GMT; with coordinates 45.7°N / 26.4°E; $M_w=5.5$; $h = 150$ km.

For the study, vertical component records (Z) of 23 seismic stations (Table 1), with records of 100 reports per second (i.e., 8 640 000 reports for 24 hours) are used. In order to obtain 1/2-minute low-frequency noise time series, the average values of the original recordings at successive time intervals of 3000 reports calculated for each station — 1/2 minute time series are obtained for all 23 stations.

Eight of the seismic stations - PLOR, PLOR1, PLOR2, PLOR3, PLOR4, PLOR5, PLOR6 and PLOR7 (Local Ploeschina network), located in the epicentral region (average 20 km from the epicentres of the two earthquakes) of the Vrancea seismic zone, VRI and DRGR stations are located at distances of 30 and 450 km respectively from the earthquake epicentres. All ten listed seismic stations are part of the seismic network of Romania. The seismic stations PRD, AVR, BOZ, DOB, NEF, and ROIA, are part of the Prova-

Table 1. Seismic stations used in the study. The last 3 columns represent the time intervals and the number of 24-hour seismic records, used in the research.

Seismic stations	Digitizer	Latitude (°N)	Longitude (°E)	Sensors	Period 01.08.16 – 23.09.16	Period 24.09.16 – 30.12.16	Period 06.09.18 – 30.10.18
					Number of 24 hour records	Number of 24 hour records	Number of 24 hour records
AVR	DAS 9AF3	43,1178	27,6685	GEOPHON	54	98	53
BOZ	DAS 98B6	43,1044	27,4786	GEOPHON	54	98	53
DOB	DAS 9C9D	43,1790	27,4628	GEOPHON	54	98	53
PRD	DAS 990A	43,1602	27,4099	GURALP	54	98	53
NEF	DAS 986E	43,2644	27,2753	S13	54	98	53
ROIA	DAS 9913	43,0934	27,3778	GEOPHON	54	98	53
PSN	DAS A646	43,6376	28,1359	KS2000/60s	54	98	53
PVL	DAS 990C	43,1227	25,1732	CMG 3ESPC/120	54	98	53
MPE	DAS A625	43,3560	23,7401	S13	54	98	53
SZH	DAS 9901	43,2653	25,9762	CMG 3ESPC/120	54	98	53
ORH	DAS9D18	43,7263	23,9664	S13	54	98	53
VLD	DAS9B2E	43,6899	23,4356	S13	54	98	53
VRI	Altus-K2	45,8665	26,2764	CMG3ESP	54	98	53
DRGR	Altus-K2	46,7917	22,7111	KS54000	54	98	53
PLOR	Q330	26,6498	45,8512	STS2	54	98	53
PLOR1	Q330	45,8520	26,6466	CMG-40T	54	98	53
PLOR2	Q330	45,8502	26,6437	CMG-40T	54	98	53
PLOR3	Q330	45,8539	26,6454	CMG-40T	54	98	53
PLOR4	Q330	45,8512	26,6498	CMG-40T	54	98	53
PLOR5	Q330	45,8455	26,6635	CMG-40T	54	98	53
PLOR6	Q330	45,8419	26,6415	CMG-40T	54	98	53
PLOR7	Q330	45,8603	26,6405	CMG-40T	54	98	53
					1242	2254	1219

dia Local Seismic Network (LSN-Provadia). They are at an average distance of 400 km from the epicenters of the two earthquakes, the PSN, PVL, MPE, SZH, ORH and VLD seismic stations are part of the seismic network of Bulgaria and located at approximately 370 km, 430 km, 470 km, 380 km, 420 km and 460 km from the epicenters, respectively.

With the used methodology, three informative fractal statistics are estimated at consecutive time intervals of 2880 report (1 day) for 1/2-minute time series for each station. The estimation of the values of the noise statistics is made after the separation of the low-frequency trend using an 8th-order polynomial. Trend filtering is required to eliminate the effects of tidal and temperature deformations of the Earth's crust in the seismic noise variations and also represents a necessary procedure for studying the noise's statistical characteristics. The usage of an orthogonal polynomial enables the stability of the

trend evaluations at the reading points. In this case, the order of the polynomial (8th) was chosen as the smallest one after numerical experiments, thus allowing the elimination of the day-to-day variations for the intervals of one-day duration (Lyubushin, A. A. 2007). The question of the regularity of the transition in such a low-frequency domain of seismic signal recordings naturally arises.

It should be noted that the development of seismological apparatus did not consider its use for continuous seismic recording over a more extensive frequency range beyond the earthquake signal frequencies, and is not assumed that seismic sensors could also be used as the usual inclinometer, i.e., to register the change of signal in the tidal band frequencies. Following numerical experiments (Lyubushin AA, 2008), we believe that in solving geophysical monitoring tasks and investigating earthquake preparation processes, there is a theoretical possibility for broader use of seismological equipment that exceeds the formal operating frequency limitations, which is traditionally used to study individual earthquakes. Fig. 2 shows the graphs, illustrating this consideration. Continuous, uninterrupted seismic noise recordings of the taken eight stations and a 1-hour discretization step are made. From the initial recordings at a sampling rate of 100 Hz, the average value was calculated at consecutive time intervals with a length of 360,000 reports, which is 1 hour. In this way, the traditional for gravimetry frequency range is provided. If adhering to the traditional view of such a procedure, the transition to an hourly discretization step seems unacceptable.

Moreover, if we look at the power spectra of the temporal variations of the seismic noise (Oynakov E. et al.2019), recorded with the instrumentation used (Table 1), we see the manifestation of tidal 12 and 24-hour spectral extremum, even separation of different tidal harmonics at sufficient length of time series. This example shows that the signal, recorded with modern seismometers, contains low-frequency components, significantly exceeding the formal limits, specified in their technical passports by the manufacturer. It is these undocumented and poorly understood capabilities of seismometers that could be used in this study.

It should also be pointed out that all of the used noise statistics are dimensionless and do not depend on the scale of the output data. That significantly reduces their dependence on the fact that different seismometers have been installed at the seismic stations.

Results - Hurst exponent

The interest towards the positive value of the Hurst exponent estimate ($H > 0$) is related to the fact that for self-similar processes it is in the interval $0 < H < 1$ (Kantelhardt, Jan W., et al., 2002). Therefore, $H(\tau) > 0$ represents a sign of self-similar fractal behavior of low-frequency seismic noise, indirectly. It is of our interest to separate those time windows, as for all simultaneously analyzed processes, the Hurst exponent is positive, which is a sign of low-frequency synchronization – a possible sign of a future earthquake.

The results obtained show that 2 to 4 days before the earthquake on October 28, 2018, with $M_w = 5.5$ and 2 to 3 days before the earthquake on October 18.2018 with $M_W = 3.7$, the Hurst index has a high value (Fig. 2).

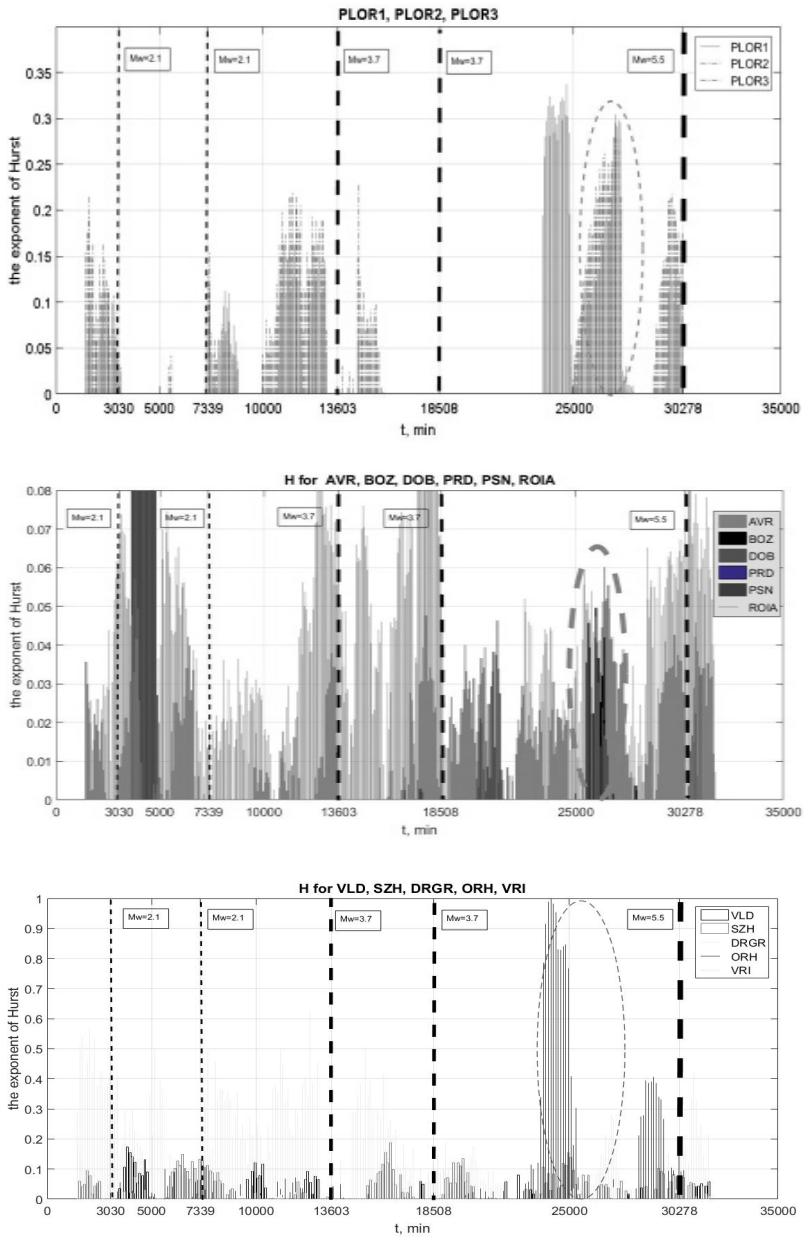


Fig. 2. Graphs of the change in the Hurst (H) metric for different stations combination, calculated in a time window 1 day and 1 hour displacement; the red dotted line shows the moment of the earthquake - 28.10.2018 (Vrancea, $T_0=00:38:15$; $45.7 / 26.4$; $M = 5.5$) and the earthquakes that occurred in the analysed area.

To verify that before earthquakes of magnitude higher than $M_w = 5.5$ in the seismogenic zone of Vrancea, the Hurst (H) exponent increases, both significant earthquakes in 2016 were examined. Fig. 3 shows a graph of the synchronous maximum of H in the period 01.08-30.12.2016, for the stations of the Local Ploeschina network. From the graph, we can summarize that 12 days before the earthquake on September 23, 2016, and 8 days before the earthquake of December 27, 2016, the values of H have increased.

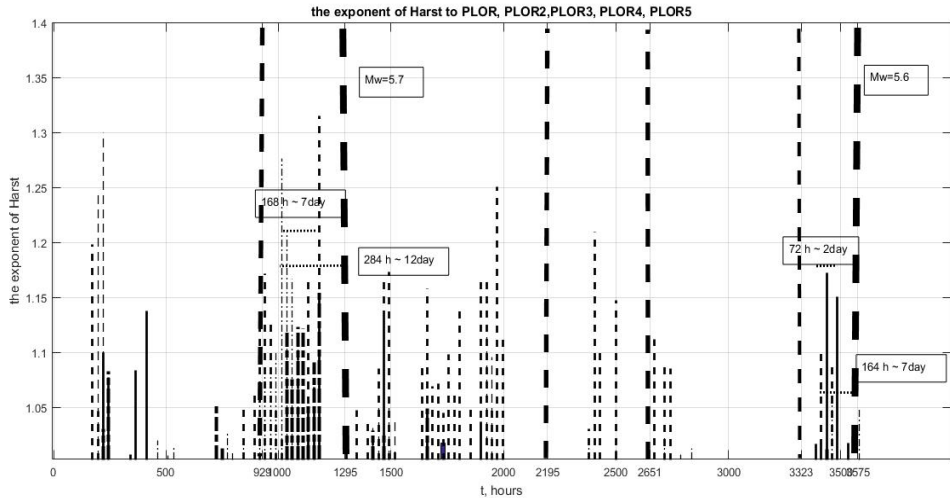


Fig. 3. Graph of the change of $H > 0$ for PLOR, PLOR2, PLOR3, PLOR4, PLOR5 stations; the red dashed lines show the moments of the earthquakes that occurred in the analysed area in the period 01.08-30.12.2016 – 08.09.2016 ($M_w = 4.1$); 09.23.2016 ($M = 5.7$); 10.31.2016 ($M_w = 4$); 11.19.2016 ($M_w = 4.1$); 11.30.2016 ($M_w = 3.5$); 12.17.2016 ($M_w = 3.9$) and 12.27.2016 (Vrancea, $T_0=00:38:15$; $45.7N$, $26.4E$; $M_w = 5.6$). The text boxes show the time from H maxima to the earthquake moments in minutes and days.

Fig. 4 presents in detail the graphs of the Hurst exponent evaluations for DRG, MPEP, VRI stations in the period 23.09-30.12.2016 before the earthquake of December 27, 2016 (Vrancea, $M_w = 5.6$). The zero of the time axis corresponds to $T_0 = 00:00:00$ (GMT) on 23.09.2016. It can be noted that the maximum of the Hurst exponent is present not only before the earthquake of 27.12.2016 but also ~ 9 days before the earthquake of 17.12.2016, $T_0=11: 16: 05$ (GMT) with coordinates $45.5^{\circ}N$, $26.47^{\circ}E$ and $M_w = 3.8$.

Fig. 5 shows in detail the graphs of the Hurst indicator evaluations for stations AVR, DRGR, MPEP, NEF, ORH, PRD, PSN, ROIA, SZH, VRI before the earthquake of 23.09.2016. (Vrancea, $M_w = 5.7$). The zero of the time axis corresponds to 23.08.2016, 00h00m (GMT). Three more seismic events occur in the analysed period (01.09.2016; $T_0=07: 49: 21$; $45.67^{\circ}N$, $26.33^{\circ}E$ ($M_w = 3.9$); 08.09.16; $T_0= 17: 03: 02$; $45.67^{\circ}N$, $26.53^{\circ}E$

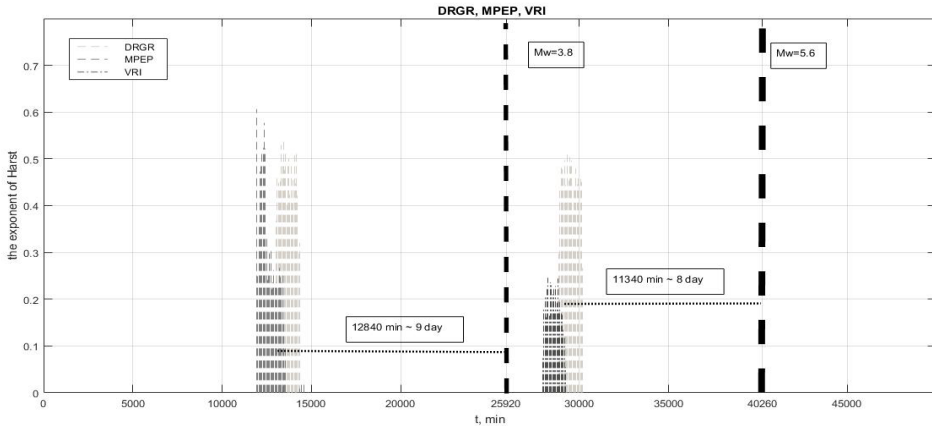


Fig. 4. Graph of the change of $H > 0$ for DRGR, MPEP, VRI stations in the period 24.09-30.12.2016. The red dashed lines show the moment of the earthquakes that occurred in the analysed area - 17.12.16; $T_0 = 11: 16: 05$; $45.50^{\circ}N$, $26.47^{\circ}E$ ($M_w = 3.9$); and 27.12.2016 (Vrancea, $T_0 = 12:38:15$; $45.7^{\circ}N$, $26.4^{\circ}N$; $M_w = 5.5$). The text boxes show the time from H maxima to the earthquake moments in minutes and days.

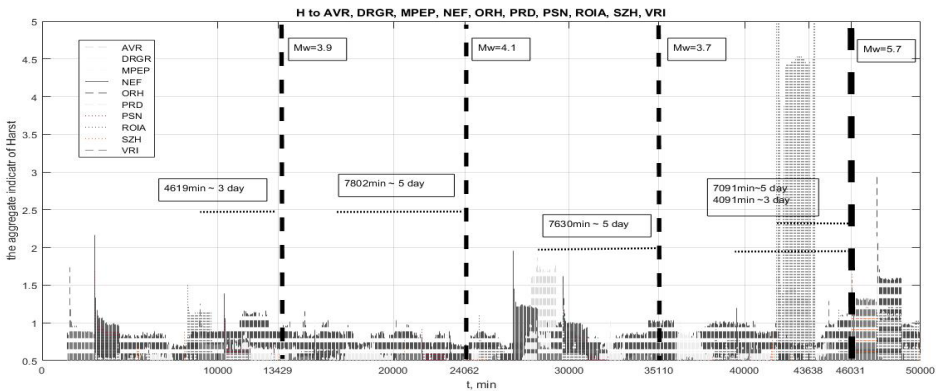


Fig. 5. Graph of the change of $H > 0$ for AVR, DRGR, MPEP, NEF, ORH, PRD, PSN, ROIA, SZH and VRI stations in the period 23.08-23.09.2016. The red dashed lines indicate the time of the earthquakes that occurred in the analysed area - 01.09.2016; $T_0 = 07: 49: 21$ (GMT); $45.67^{\circ}N$, $26.33^{\circ}E$ ($M_w = 3.9$); 08.09.2016; $T_0 = 17: 03: 02$; $45.67^{\circ}N$, $26.53^{\circ}E$ ($M_w = 4.1$); 16.09.2016; $T_0 = 09: 10: 57$; $45.65^{\circ}N$, $26.59^{\circ}E$ ($M_w = 3.7$) and 23.09.2016 (Vrancea, $T_0 = 23:11:20$; $45.71^{\circ}N$, $26.62^{\circ}E$; $M_w = 5.7$). The text boxes show the time from H maxima to the earthquake moments in minutes and days.

($M_w = 4.1$)); 16.09.2016; $T_0 = 09: 10: 57$; $45.65^{\circ}N$, $26.59^{\circ}E$ ($M_w = 3.7$)) and it can be noted that 3 to 5 days before each event there is a synchronous maximum of H for all stations. The figure also shows that the Hurst indicator for all stations is $H > 0$.

Results- Singularity spectrum width

The parameter $\Delta\alpha = \alpha_{max} - \alpha_{min}$ (Feder E., 1991), also called the width of the singularity spectrum, represents one of the important multifractal characteristics and assessments for the variety of random signal behavior. The statistically significant decrease in the average value of $\Delta\alpha$ reflects the decrease in the degrees of system's freedom, generating a signal and thus enables the determination of the time of preparation of an earthquake.

Fig. 6 presents a graph of the overall assessment of the parameter $\Delta\alpha$ for all stations on the PLOR LAN (i.e., the average value of $\Delta\alpha$). For each station, $\Delta\alpha$ is calculated in consecutive non-intersecting windows with a length of 24 hours and a shift of 1 hour over the entire time interval (06.09-30.10.2018, 52 days), after which the average value for the local area network is obtained. One feature of the smoothed $\Delta\alpha$ schedule are the minimums 4 days before the earthquakes on 28.10.2018, respectively, which, as we have indicated above, measures the number of hidden degrees of freedom of the stochastic systems. The other earthquakes in the analyzed time interval are preceded by a minimum of the width index of the singularity spectrum from 1 to 4 days.

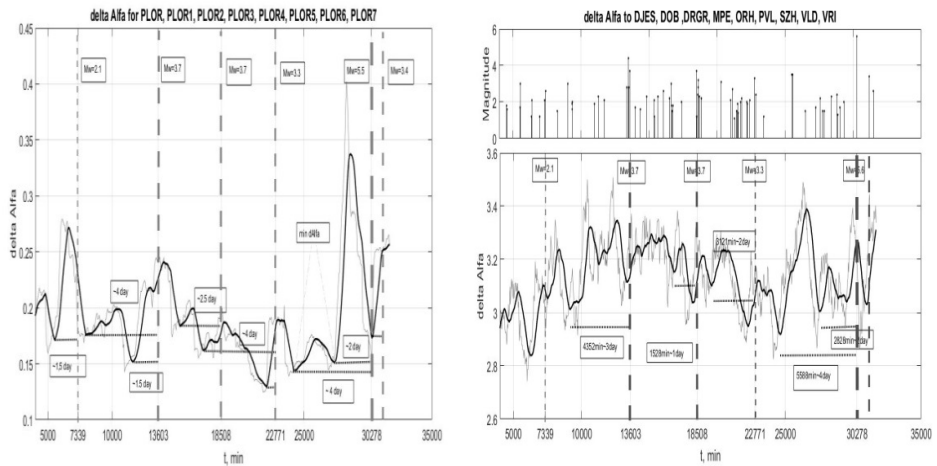


Fig. 6. Diagram of the mean values of parameter $\Delta\alpha$, for stations - DOB, DRGR, MPE, ORH, PVL, SZH, VLD, VRI, between 06.09 and 28.10.2018. Combined with the graphs of all the earthquakes that occurred in the Balkan Peninsula in the period 06.10 - 28.10.2018.

Fig. 7 presents a graph of the overall assessment of the parameter $\Delta\alpha$ for all stations on the PLOR LAN (i.e., the average value of $\Delta\alpha$). For each station, $\Delta\alpha$ is calculated in consecutive non-intersecting windows with a length of 24 hours and a shift of 1 hour over the entire time interval (01.08-30.12.2016, 22 days), after which the average value for the local area network is obtained. One feature of the smoothed $\Delta\alpha$ schedule are the minimums in the 59400 and 199700 minutes, 13 and 10 days before the earthquakes on 23.09.2016 and 27.12.2016. The other earthquakes in the analyzed time interval are

preceded by a minimum of the width index of the singularity spectrum from 6 to 7 days. We may also note a large minimum of $\Delta\alpha$ at 95040 minutes, which precedes the earthquakes at 109796, 119710, and 131759 minutes, and can be assumed to be related to them.

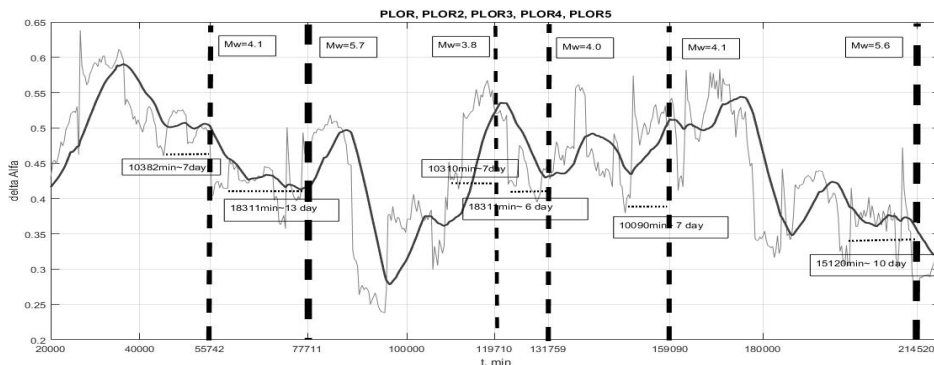


Fig. 7. Graph of the average values of the parameter $\Delta\alpha$, for stations from the local area network Ploeschina. The dashed line indicates all earthquakes, occurrences in the analyzed area for the period. The beginning of the abscissa is 06.10.2018 – 00:00 hours (GMT).

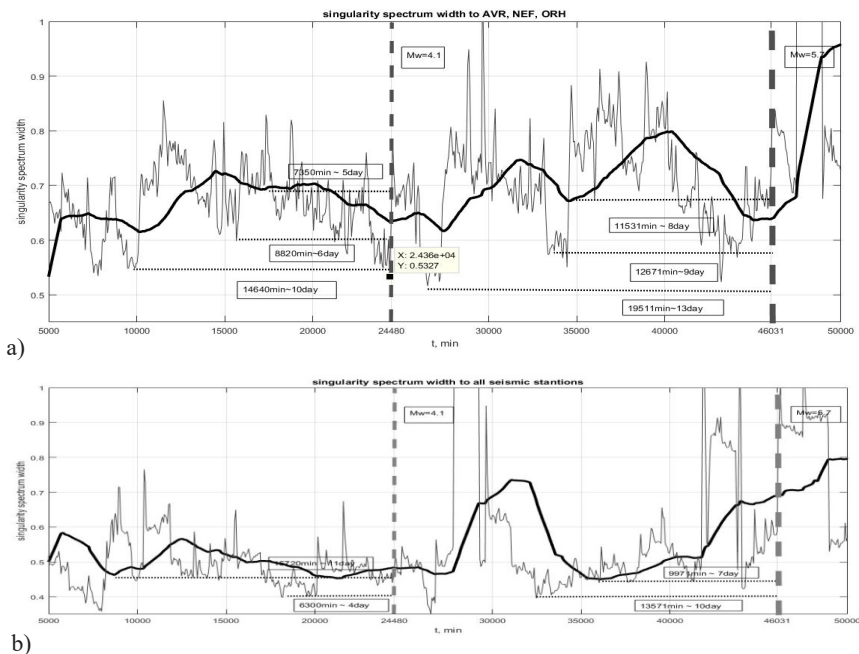


Fig. 8. Graph of the average values of the parameter $\Delta\alpha$ **a)** for stations - AVR, NEF, ORH in the interval 01.08 to 24.09.2016. **b)** for stations - DRGR, PRD, PSN, VRI in the interval 01.08 to 24.09.2016. The red dashed lines mark the moments of the earthquakes

Fig. 8 a), b) shows the evolution of the width parameter of the spectrum of singularity $\Delta\alpha$ for the interval 23.08-23.09.2016 for different station combinations. The $\Delta\alpha$ parameter for each station is calculated for the same length of the time window (24 hours = 2880 reports) and the same displacement (1 hour = 120 reports). Minima of $\Delta\alpha$ can be determined both 6-7 days before the earthquake with $M_w = 5.7$ (23.09.2016) and 3-5 days before the earthquakes, falling within the studied time interval. It should be added that a study on the evolution of the width of the spectrum of singularity before the earthquake of December 27, 2016, was also conducted. ($M_w = 5.6$) in the period 23.08-23.09.16 and the results are identical, i.e., 6-10 days before the earthquake, there is a minimum of $\Delta\alpha$, and 3-4 days before the weaker earthquakes, falling within the analyzed interval.

Results - Spectral Coherence Assessment

For assessing the synchronization effects of the results, measuring of the low-frequency microseismic background for several seismic stations, is used the spectral measure of coherence, proposed by Lyubushin (1998). It is constructed as a module of the product of the component canonical coherence.

$$\lambda(\tau, \omega) = \prod_{j=1}^m |v_j(\tau, \omega)|,$$

where $m \geq 2$ is the total number of jointly analyzed time series (the dimension of the multidimensional time series), ω is the frequency, τ is the time coordinate of the right edge of the scandent time window, $v_j(\tau, \omega)$ is the canonical coherence of the j th scalar time row that describes the relationship between that row and the other ones. The inequality $0 \leq |v_j(\tau, \omega)| \leq 1$ is satisfied. The closer the value of $|v_j(\tau, \omega)|$ is to one, the higher linearly are connected the variations of the j th order of frequency ω in the time window with coordinate τ to the similar variations in other lines studied. Accordingly, measure $0 \leq \lambda(\tau, \omega) \leq 1$ describes the effect of the overall coherent (synchronous, collective) behavior of all signals.

Fig. 9 a) shows the behaviour of the spectral measure of coherent behaviour $\lambda(\tau, \omega)$ of the seismic signal for stations PLOR1-PLOR7, in a time window 20160 half minute reports (7 days) with 720 reports (6 hours) shift for the time interval 06.09.2018 – 30.10.2018 (the abscissa timestamps indicate the right end of the time window). From the result we can conclude that the signal synchronization of all stations has a maximum of all frequencies in 24000 minutes, which is ~ 5 days before the earthquake which is in 30278 minutes (28.10.18, $M_w = 5.5$) and b) shows the behaviour of the spectral measure of coherent behaviour $\lambda(\tau, \omega)$ of the seismic signal for stations MPE; NEF; ORH; PSN; PVL; ROIA; SZH ; VLD. From the result we can conclude that the signal synchronization of all stations has a maximum from 19000 to 21000 minutes, which is ~ 9 to 7 days before the earthquake.

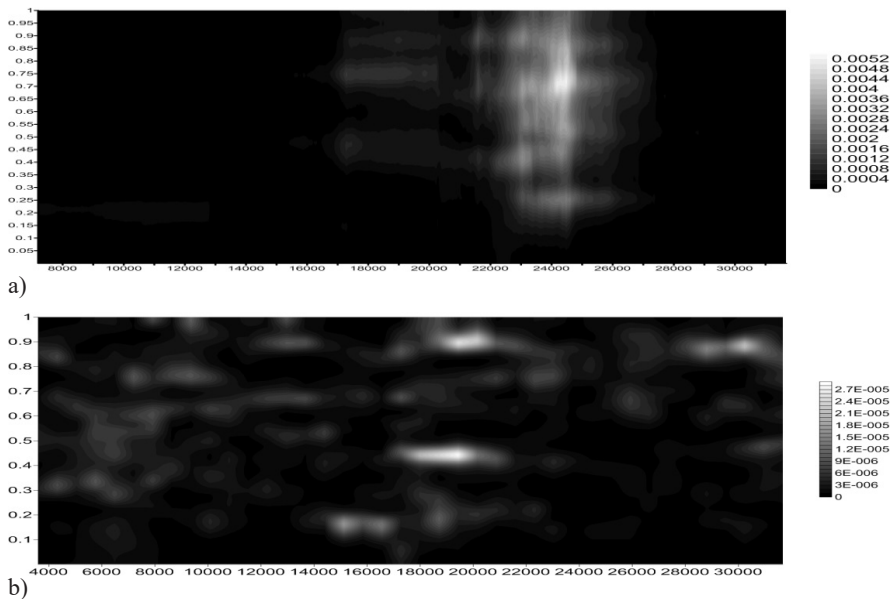


Fig. 9. Frequency-time diagram of the evolution of $\lambda(\tau, \omega)$ (spectral measure of coherent behaviour) for PLOR1-PLOR7 stations **a**); end MPE; NEF; ORH; PSN; PVL; ROIA; SZH; VLD stations **b**).

Fig. 10 shows the behaviour of the spectral measure of coherent behaviour $\lambda(\tau, \omega)$ of the seismic signal for stations PLOR1-PLOR7, in a time window 20160 half minute reports (7 days) with 720 reports (6 hours) shift for the time interval 01.08.2016 – 30.12.2016 (the abscissa timestamps indicate the right end of the time window). From the result we can conclude that the signal synchronization of all stations has a maximum of all frequencies in 30000 minutes, which is ~ 40 days before the earthquake which is in 77711 minutes (23.09.16, Mw = 5.7) and maximum in 14000 minutes - ~ 50 days before the earthquake in 214520 minutes (December 27, 2016, Mw = 5.6).

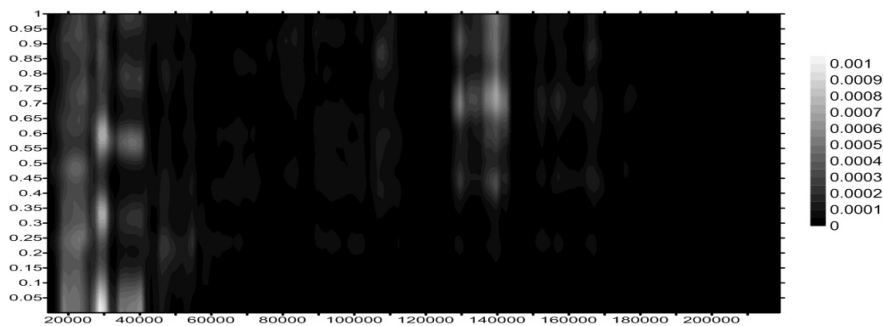


Fig. 10. Frequency-time diagram of the behavior of $\lambda(\tau, \omega)$ for PLOR1-PLOR7 stations. The beginning of the time axis corresponds to 00:00 (GMT) on 01.08.2016 (analyzed time interval from 01.08 to 30.12.2016)

Fig. 11 shows the behaviour of the spectral measure of coherent behaviour $\lambda(\tau, \omega)$ of the seismic signal for; MPE; NEF; ORH; PSN; PRD; ROIA; SZH; VLD; VRI stations, in time window 20160 half minute reports (7 days) with 720 reports (6 hours) shift for the time interval 23.09 - 30.12.2016 (abscissa timestamps indicate the right end of the time window). The signal synchronizations of all stations start from 20000 minutes and reach a maximum of 24000 minutes, which is ~ 15 days before the earthquake on December 27, 2016 ($M_w = 5.6$).

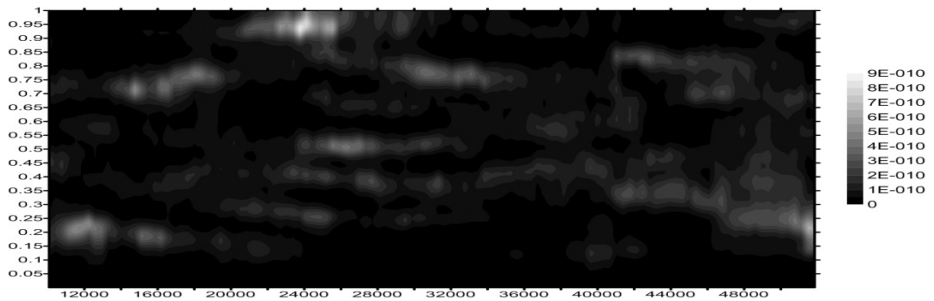


Fig. 11. Frequency-time diagram of the behavior of $\lambda(\tau, \omega)$ for MPE; NEF; ORH; PSN; PRD; ROIA; SZH; VLD; VRI stations, for the time interval 23.09.-30.12.2019. The moment of the earthquake of 27.12.2016 shown with an arrow.

Fig. 12 shows the behaviour of the spectral measure of coherent behaviour $\lambda(\tau, \omega)$ of the seismic signal for MPE; NEF; ORH; PSN; PRD; ROIA; SZH; VLD; VRI stations, in time window 20160 half minute reports (7 days) with 720 reports (6 hours) shift for the interval time 23.08 - 23.09.2016 (abscissa timestamps indicate the right end of the time window). The signal synchronizations of all stations start from 30,000 minutes and reach a maximum of 36,000 minutes, which is ~ 6 days before the earthquake on September 23, 2016 ($M_w = 5.7$).

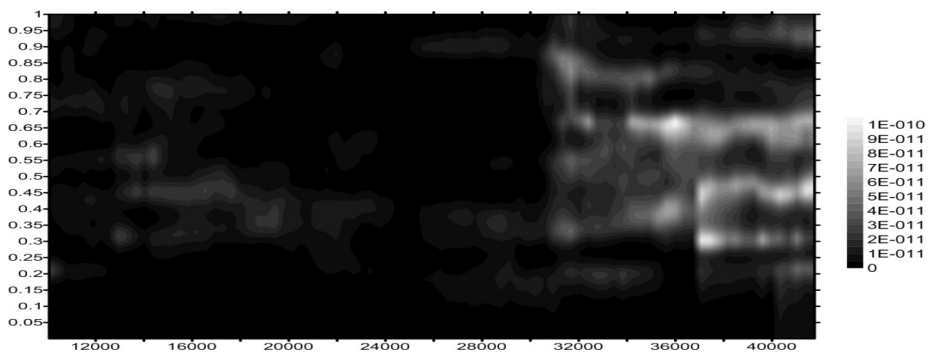


Fig. 12. Frequency-time diagram of the behavior of $\lambda(\tau, \omega)$ for MPE; NEF; ORH; PSN; PRD; ROIA; SZH; VLD; VRI stations, for the time interval 23.08.-23.09.2019. The moment of the 23.09.2016 earthquake is shown above with an arrow.

Conclusions

The study of the Hurst exponent shows that it increases about 7-8 days before earthquakes with $M_w > 5.5$. High H values were indicated 3 to 5 days before other smaller magnitude seismic events ($3.5 \leq M_w \leq 5$).

The analysis of the development of the width of the spectrum of singularity $\Delta\alpha$ shows that earthquakes with $M_w > 5.5$ in the analyzed time interval are preceded by minimums from 10 to 13 days and minimums of 2 to 7 days before earthquakes with smaller magnitude ($3.5 \leq M_w \leq 5$).

The spectral time diagram of the spectral measure of coherent behaviour of the seismic signal for epicentral stations, estimated in a time window of 10080 minutes (7 days), with a 360 minutes (6 hours) shift, for the time interval 01.08 - 30.12.2016, shows synchronization of the stations from 40 to 50 days prior to the earthquakes in Vrancea with $M_w > 5.5$. For stations at a greater distance – from 6 to 15 days before the earthquakes (time window 2880 reports, 120 reports shift).

We can conclude that the analysis of the fractal and multifractal parameters of the microseismic field in the minute time range of discretization can provide valuable information about the process of earthquake preparation and the effects, leading to the accumulation of stress in the lithosphere.

Acknowledgements.

This study has been carried out within the framework of the National Scientific Program “Young Scientists and Postdoctoral Fellows”, approved by Council of Ministers Decision No 11 / 17.08.2018 and supported by the Ministry of Education and Science (MES) of Bulgaria and of the National Science Program “Environmental Protection and Reduction of Risks of Adverse Events and Natural Disasters”, approved by the Resolution of the Council of Ministers № 577/17.08.2018 and supported by the Ministry of Education and Science (MES) of Bulgaria (Agreement № ДЮ-230/06-12-2018).

References

- Berger J., Davis P., Ekström G. Ambient earth noise: a survey of the global seismographic network //Journal of Geophysical Research: Solid Earth. – 2004. – T. 109. – №. B11
- Feder E. Fractals. - M.: Mir, 1991. –254 p.(Ru)
- Friedrich R., Zeller J., Peinke J. A note on three-point statistics of velocity increments in turbulence //EPL (Europhysics Letters). – 1998. – T. 41. – №. 2. – C. 153
- Kantelhardt, Jan W., et al. „Multifractal detrended fluctuation analysis of nonstationary time series.“ Physica A: Statistical Mechanics and its Applications 316.1-4 (2002): 87-114
- McNamara D. E., Buland R. P. Ambient noise levels in the continental United States //Bulletin of the seismological society of America. – 2004. – T. 94. – №. 4. – C. 1517-1527
- Lyubushin A. A. Analysis of canonical coherences in the problems of geophysical monitoring // IZVESTIIA PHYSICS OF THE SOLID EARTH C/C OF FIZIKA ZEMLI-ROSSIISKAIA AKADEMIIA NAUK. – 1998. – T. 34. – C. 52-58

- Lyubushin, A. A. and Sobolev, G. A., Multifractal Measures of Synchronization of Microseismic Oscillations in a Minute Range of Periods, *Fiz. Zemli*, 2006, no. 9, pp. 18–28 [*Izv. Phys. Earth (Engl. Transl.)*, 2006, vol. 42, no. 9, pp. 734–744].
- Lyubushin, A. A. Data analysis of geophysical and environmental monitoring systems (*Geophysical and Ecological Monitoring Data Analysis*), Moscow: Nauka, 2007. (Ru)
- Lyubushin, A. A., Microseismic Noise in the Low-Frequency Range (Periods of 1–300 min): Properties and Possible Prognostic Features, *Fiz. Zemli*, 2008, no. 4, pp. 17–34 [*Izv. Phys. Earth (Engl. Transl.)*, 2008, vol. 44, no. 4, pp. 275–290].
- Oynakov E., I. Aleksandrova Seismic characteristics of the earthquake of 10/28/2019 that occurred in the seismogenic region of Vrancea, Romania. *BULGARIAN ACADEMY OF SCIENCES, Problems of Geography*, 2019, Sofia, no 1, pp. 18-28.
- Stehly L., Campillo M., Shapiro N. M. A study of the seismic noise from its long-range correlation-properties // *Journal of Geophysical Research: Solid Earth*. – 2006. – Т. 111. – №. B10
- Samarov A., Taqqu M. S. On the efficiency of the sample mean in long-memory noise // *Journal of Time Series Analysis*. – 1988. – Т. 9. – №. 2. – С. 191-200
- Oynakov E., Fractal characteristics of random fluctuations of seismic records, *Problems of Geography*, 2019, in print

Вариация на параметрите на фоновия сеизмичен шум в етапа на подготовката на силни земетресения в сеизмична зона вранча

Е. Ойнаков, И. Александрова, Д. Солаков

Резюме: Глобалните въздействия на атмосферни и океански процеси, приливни деформации на земната кора, глобалният сеизмичен процес, както и по-слабо проучените процеси в земната кора са свързани с натрупване и бавно разсейване на тектоничната енергия в литосферата. Тези процеси са „участниците“ във формирането на случайния процес, за който изследването с традиционният апарат за спектрален анализ се оказва слабо ефективен.

Използването на фрактален анализ за дешифриране на структурата на сеизмичния шум е достатъчно добра алтернатива. От началото на 90-те години на миналия век методът се използва както в анализа на турбулентността, така и във финансовите и медицинските изследвания на времевите серии.

Разработването на нови методи за прогнозиране на земетресенията, основани на данни от геофизичен и в частност сеизмичен мониторинг, е един от приоритетните цели на науката за Земята. Анализирани са сеизмичните записи на двадесет и три сеизмични станции разположени на територията на Балканския полуостров на разстояния от 1 до 500 км от земетресенията от 23.09.2016 г., 27.12.2016 г. и 28.10.2018 г., с магнитуди повече от 5,5 в сеизмичната зона Вранча. За анализа се използва методът на Любушин за фрактален анализ на скаларните времеви серии.

Научна цел е да се открият общи сигнали, игнориращи „индивидуалното“ поведение на елементите на системите за мониторинг.

Ключови думи: индикатори на земетресения, сеизмичен шум, фрактален анализ на сеизмичен шум

Благодарности: Това проучване е проведено в рамките на Националната научна програма „Млади учени и докторанти“, одобрена с Решение на Министерския съвет № 11 / 17.08.2018 г. и подкрепено от Министерството на образованието и науката (МОН) на България, както и в рамките на Националната научна програма „Опазване на околната среда и намаляване на рисковете от нежелани събития и природни бедствия“, одобрена с Решение на Министерския съвет № 577 / 17.08.2018 г. и подкрепено от Министерството на образованието и науката (МОН) на България (Споразумение № ДО-230 / 06-12-2018 г.).

INVESTIGATION OF THE IMPACT OF ATMOSPHERIC REFRACTION ON PRECISION LEVELING MEASUREMENTS

N. Dimitrov¹, P. Danchev², I. Georgiev³

National Institute of Geophysics, Geodesy and Geography, Bulgarian Academy of Sciences, Acad. G. Bonchev Str., bl3, Sofia1113, Bulgaria, e-mail: ndimitrov@geophys.bas.bg

DOI: 10.34975/bgj-2019.42.3

Abstract. The effect of atmospheric refraction on the results of precise leveling measurements is investigated. This study is based on level measurements for 30 km line provided by Geodesy, Cartography and Cadastre Agency. The results show that refraction's impact is not eliminated with one and the same positive and negative differences of elevation. The correction must be applied for each instrument set-up. Largest values of refraction are observed in the leveling distances with highest terrain slope. The error caused by refraction is a significant systematic error in the leveling measurements and it is mandatory to be applied.

Key words: precise leveling, atmospheric refraction, national leveling network

Introduction

For the last three-four decades the precision of geodetic instruments has made tremendous progress. Modern electronic geodetic instruments allow a high degree of precision and automation but the accuracy and reliability of geodetic measurement is still strongly influenced by atmospheric conditions and by their knowledge. This phenomenon is particularly recognizable and still not fully unsolved in precise geodetic leveling. Atmospheric refraction is the deflection of light or other electromagnetic waves from the straight line due to the change in air density as a function of the height above the ground. As the geodetic measurements are carried out near the ground surface, the results are significantly influenced from the ground atmosphere. In geodetic leveling the horizontal line of sight passes through different isothermal layers of air (Fig. 1). This causes errors in readings on fore and back rods. The error caused by refraction is generally considered to be a significant systematic error in the leveling measurements. Already in the first half of the 20th century, prof. T. J. Kukkamaki (Finnish Geodetic Institute) investigated this phe-

nomenon and develop a mathematical model for correcting (reducing) its impact. He estimated a correction that is proportional to the difference in the measured two temperatures of air at heights of 0.5 m and 2.5 m. Initially only a few countries apply this correction, but now when it is known that it is necessary, the correction is widely used, especially in countries located in the middle and lower latitudes.

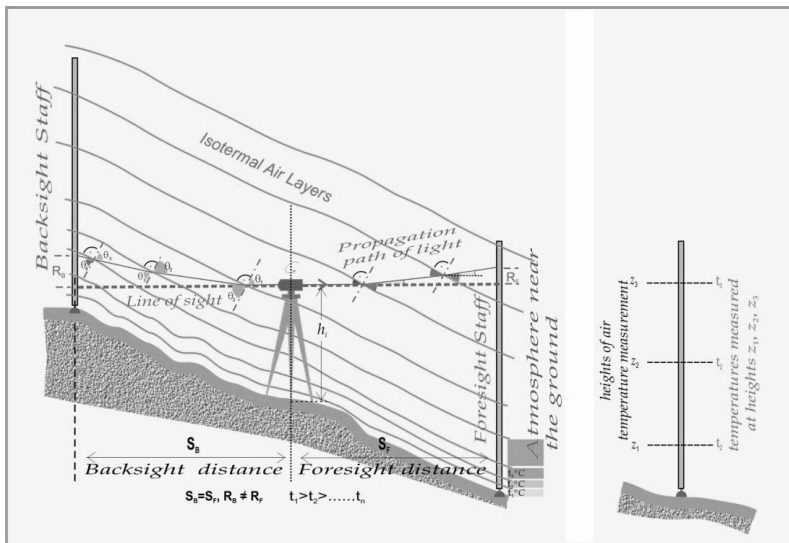


Fig. 1. Refraction

Theoretical model

The refraction correction for geodetic leveling must be applied to each single set-up (Kukkamaki T. J., 1939):

$$R = -2 \times 10^{-6} \alpha \left(\frac{S}{50} \right) \Delta t \Delta h [m], \quad (1)$$

where: S is the average value of the distances between rods in meters (section length); $Dt = t_3 - t_1$ is the temperature difference ($^{\circ}\text{C}$), calculated from the measured temperatures at two heights, for example: t_3 – at a height of 2.5 m and t_1 – at a height of 0.5 m (Fig. 1); Dh – measured difference of elevation in set-up (in meters); a – is a function, dependent on an assumed temperature function:

$$T = a + bz^c, \quad (2)$$

where: T ($^{\circ}\text{C}$) is a temperature at a height z above the ground surface, when z is less than 300cm; a, b and c are constants for any instant and vary with time.

A is sometimes assumed constant (NOAA, 1981), but is rigorously calculated as:

$$\alpha = 5 \cdot \frac{95}{z_3^c - z_1^c} \left[\frac{1}{c+1} (L_F^{c+1} - L_B^{c+1}) - h_i (L_F - L_B) \right], \quad (3)$$

where: z_3 и z_1 are heights of the measurement of air temperature; L_F и L_B are heights of the line of sight on the fore and back rods, respectively; h_i is instrument height, and c is an exponent (Kukkamaki T. J., 1939).

The temperature model (2) and corresponding refraction correction are based on the following assumptions: the refraction coefficient of air depends mainly on temperature; the effect of humidity is negligibly small for optical propagation; isothermal surfaces are parallel to the ground; the ground slope beneath the sightline is uniform in a single set-up of the instrument.

Exponent c can be calculated using temperatures measured by three temperature sensors, located at different heights z_1, z_2, z_3 (Fig. 1) arranged such that $z_1/z_2 = z_2/z_3$. For each measured temperature are drawn three equations of the type of (3). Through the transformations the estimation of the exponent c required to obtain the coefficient α (1), (2) is reached:

$$c = \frac{\ln \left(\frac{\Delta t_2}{\Delta t_1} \right)}{\ln \left(\frac{z_2}{z_1} \right)}. \quad (4)$$

Due to the large air temperature fluctuations direct temperature gradient determination should be performed at every single set-up at the same time as the levelling measurements.

Data processing

For the purpose of this study the level measurements provided by Bulgarian Geodesy, Cartography and Cadastre Agency were used. The measurements were made with a precise electronic digital/barcode levelling system Sokkia SDL 1X with a couple of invar rods. Simultaneously with the leveling, the air temperatures were measured for each set-up at heights of 0.5 m, 1.5 m and 2.5 m. Digital thermometers are used. Their sensors are attached to the back side of the rods and are protected from direct sunlight.

The temperature differences are calculated with the average values of the temperatures measured on the two rods at 2.5m and 0.5m, respectively. Leveling book for one leveling distance is shown at Table 1. The measured temperatures are checked in order to be acceptable, the temperature differences between the upper and lower thermometer of the rods should be between -3.0°C and $+1.0^\circ\text{C}$. Also the difference between the temperature differences of two successive setups should be between -3.0°C and $+3.0^\circ\text{C}$. When the

temperature measurements meet this requirements the average of temperature differences between upper and lower thermometer in back and for rode are used. In several leveling distances one of the thermometers has failed and did not meet the requirements. In this case only temperature differences measured on one rode is used. The refraction correction is calculated for each set-up (Table 1, column 7) and is aggregated for the whole distance and $a = 70$ (Hytonen E.,1967; NOAA, 1981). The measured temperatures are given in Table 2.

Table 1. Levelling book

LEVELING BOOK									
Leveling line		№ 47 - KHP Kazanluk BHP № 86 Haskovo							
Leveling distance		HP1-HP2							
Date	20 may 2016	Observer						
Start	11 h 50 min	Instrument		Sokkia SDL 1X					
End	h min	№		123456					
Destination	north-south	Rod 1		67147					
		Rod 2		67148					
Wheater conditions		clear view		weak wind		sunny			
№	Dist. [m]	reads		Difference (m)		d2 (MM)	R (MM)	diff. (MM)	ΔH (M)
		back 1 fore 2	back 2 fore 2	(back 1) -(fore 1)	(back 2) -(fore 2)				
1	2	3	4	5	6	7	8	9	10
HP1	20.76	0.74420	0.74422						
1	23.38	1.62199	1.62195	-0.87779	-0.87773	0.013	0.005	-0.06	-0.87776
1	26.77	1.21429	1.21429						
2	27.31	1.58203	1.58200	-0.36774	-0.36771	0.043	0.005	-0.03	-0.36773
2	28.65	1.32574	1.32585						
3	28.43	1.52577	1.52579	-0.20003	-0.19994	0.001	0.002	-0.09	-0.19999
3	27.75	1.29577	1.29568						
4	28.41	1.57473	1.57471	-0.27896	-0.27903	-0.002	0.003	0.07	-0.27900
4	29.11	1.36703	1.36701						
---	---	---	---	---	---	---	---	---	---
9	27.86	1.29703	1.29698						
10	29.69	1.79338	1.79336	-0.49635	-0.49638	-0.044	0.005	0.03	-0.49637
10	29.72	1.36363	1.36364						
11	29.61	1.95155	1.95161	-0.58792	-0.58797	0.002	0.004	0.05	-0.58795
11	28.30	1.27017	1.27023						
12	25.91	1.72158	1.72166	-0.45141	-0.45143	-0.038	0.006	0.02	-0.45142
12	29.22	1.36455	1.36449						
13	27.99	1.64569	1.64564	-0.28114	-0.28115	0.027	0.002	0.01	-0.28115
13	27.49	1.20420	1.20411						
HP2	13.40	0.95056	0.95051	0.25364	0.25360	0.050	0.001	0.04	0.25362
		SF [m]		ΣΔH1 [m]	ΣΔH2 [m]	Σ d2[m]	ΣR [m]	Σ [mm]	
		22.75835		-5.49841	-5.49841	0.00011	0.00006	0.000	
S = 0.764 km				d = 0.000 mm					
Ter 20.6 C°				ΔHm = -5.49841 m					
Lcp= 1000 mm				d ₁ = -0.00004 m					
a= 0.000002				d ₂ = 0.00011 m					
				SR = 0.00006 m					
				ΔHcorr.= -5.49853 m					

Table 2. Meteorological book

METEOROLOGICAL BOOK									
Leveling distance		HP1-HP2							
Date		20 may 2016							
st. №	rod	Heights of meas.			mean		Temperatures		
	back	0.5 M	1.5 M	2.5 M	back	fore	Tb-Tet	Tb-Tf	T3-T1
	fore	T1	T2	T3	Tb	Tf			
1	2	3	4	5	6	7	8	9	10
1	rod №1	23.5	23.4	23.4	23.4		2.8		-0.2
	rod №2	23.4	23.3	23.1		23.3		-0.2	
2	rod №2	23.9	23.8	23.7	23.8		3.2		-0.3
	rod №1	23.1	22.9	22.7		22.9		-0.9	
3	rod №1	23.5	23.4	23.3	23.4		2.8		-0.2
	rod №2	23.5	23.4	23.3		23.4		0.0	
4	rod №2	23.2	23.0	22.9	23.0		2.4		-0.3
	rod №1	23.2	23.1	23.0		23.1		0.1	
5	rod №1	22.5	22.4	22.2	22.4		1.8		-0.3
	rod №2	22.8	22.7	22.6		22.7		0.3	
6	rod №2	22.9	22.8	22.7	22.8		2.2		-0.2
	rod №1	22.3	22.2	22.1		22.2		-0.6	
7	rod №1	23.4	23.3	23.1	23.3		2.7		-0.2
	rod №2	24.0	23.9	23.8		23.9		0.6	
8	rod №2	24.5	24.3	24.2	24.3		3.7		-0.4
	rod №1	24.0	23.8	23.6		23.8		-0.5	
9	rod №1	23.6	23.4	23.3	23.4		2.8		-0.3
	rod №2	22.8	22.7	22.6		22.7		-0.7	
10	rod №2	22.5	22.4	22.4	22.4		1.8		-0.2
	rod №1	23.6	23.4	23.3		23.4		1.0	
11	rod №1	23.5	23.4	23.3	23.4		2.8		-0.1
	rod №2	23.5	23.4	23.4		23.4		0.0	
12	rod №2	23.7	23.5	23.3	23.5		2.9		-0.3
	rod №1	24.5	24.4	24.3		24.4		0.9	
13	rod №1	23.1	23.1	23.0	23.1		2.5		-0.2
	rod №2	22.6	22.5	22.4		22.5		-0.6	
14	rod №2	23.8	23.6	23.4	23.6		3.0		-0.3
	rod №1	22.6	22.5	22.5		22.5		-1.1	

Analysis

An adjustment of a leveling line was performed. The leveling line consists of 22 leveling distances. For the purposes of this study a section (part of whole leveling line) was analysed. The section lies between two Fundamental benchmarks and is 30 km long. On Fig. 2 and Fig. 3 the values of refraction correction for every set-up along the line in fore and back leveling are shown along with cross section of the leveling line. The values of refraction correction for the whole length of the line is 0.6 mm. On Fig. 4 and Fig. 5 the refraction correction values for every levelling distance are given for fore and back levelling respectively. Refraction correction, calculated for each leveling distance, varies from 0 mm to 1.5 mm. The largest values of the refraction correction are observed in the leveling distances with highest terrain slope. In case of leveling successive distances with positive and negative difference of elevation, the refractive error is not compensated. For example, in the segment between the benchmark at 6.8 km and the benchmark at 19.7 km the value of refraction correction is 0.6 mm, although the difference of elevation between the endpoints is almost zero, and line going through sequential climb and descent.

The precision of measured temperatures give a significant impact on the value of the systematic refractive error (correction respectively). Numerous meteorological publications show that in the night the ground is colder than the air just above it. Soon after the sunrise temperature of the air is decreasing with the height and the temperature of the ground becomes higher than the temperature of the air just above it. For this reason the temperature gradient is negative at day and positive at night. The absolute values of the vertical gradient are greater in the clear sky, day or night (Kukkamaki T. J., 1978).

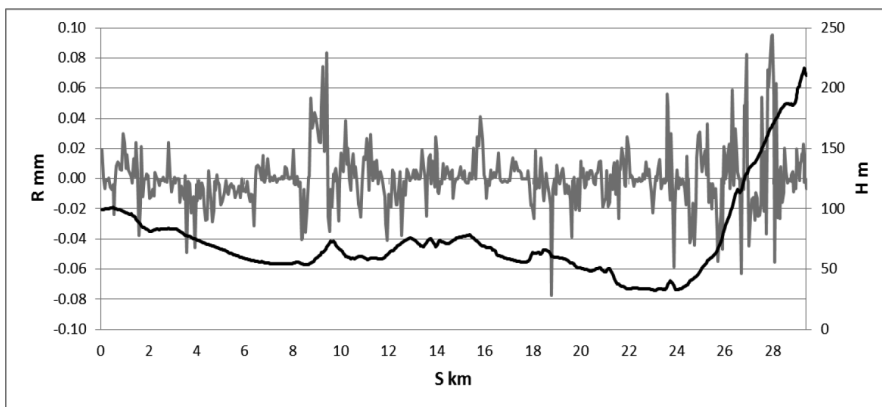


Fig. 2. Refraction correction calculated for every set-up in fore leveling in grey and cross section of the leveling line in black.

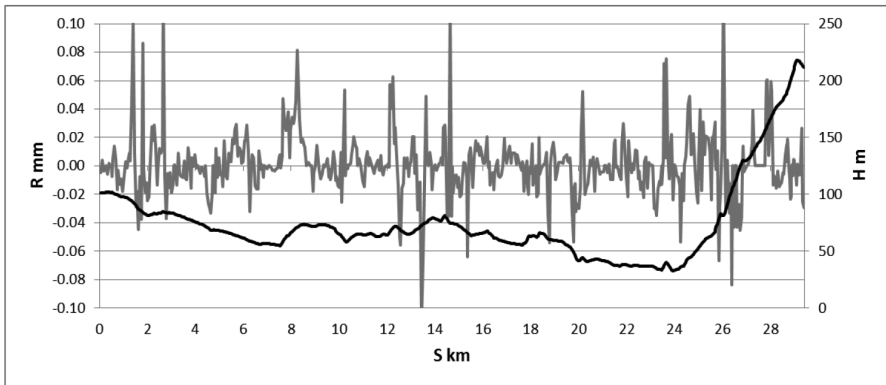


Fig. 3. Refraction correction calculated for every set-up in back leveling in grey and cross section of the leveling line in black

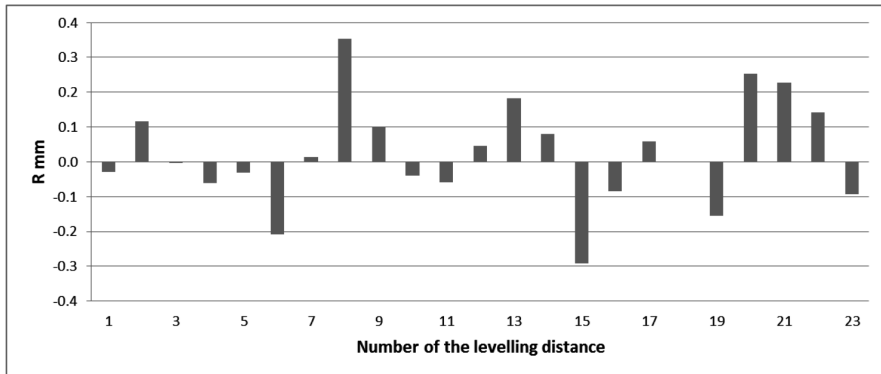


Fig. 4. Refraction correction values for every leveling distance in fore leveling

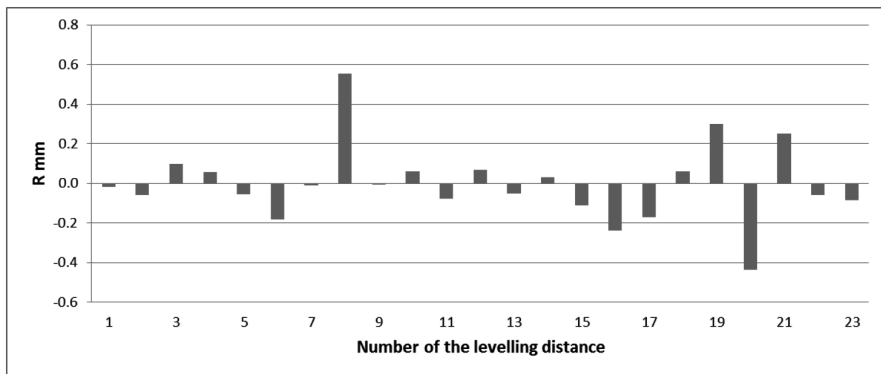


Fig. 5. Refraction correction values for every leveling distance in back leveling.

Measurements of the temperature should be done simultaneously with leveling by aspiration thermometers (with forced air flow) to obtain maximum reliable temperature gradient values. Thermometer readings should be monitored and evaluated. In order to be acceptable, the temperature differences between the upper and lower thermometer of the rods should be between -3.0°C and $+1.0^{\circ}\text{C}$. Also the difference between the temperature differences of two successive setups should be between -3.0°C и $+3.0^{\circ}\text{C}$ (NOAA, 1999).

In case of slope, the refraction is greater on sight close to surface, so the rod reading on that sight that is close to the terrain is more affected than other. This effect is more noticeable on long gentle slopes, when long sight lines are used (Angus-Leppan P.V., 1884).

If the measured temperatures are outside these limits, it is recommended not to conduct leveling measurements until the cause is eliminated or the weather conditions are improved. In processing and analyzing measurements in the test section, the temperatures that do not meet the above conditions are excluded from processing. Instead, only the thermometers of one rod are used or temperatures are interpolated from previous and next set-up.

Conclusions

The results show that the refraction correction is commensurable with the correction for the difference between the average of the rod meter and the reference one. This correction must be applied for each set-up and it is not eliminated with the same positive and negative differences of elevation. The largest values of refraction correction are observed in the leveling distances with highest terrain slope. Refraction error will eliminate almost exactly if back-sight and foresight are well balanced and the terrain is flat.

Measurements of the temperatures should be done with aspiration thermometers, simultaneously with measurements of the leveling. Incorrectly measured temperatures have a negative impact and they can lead to wrong calculated correction and contaminated final results.

Applying this correction does not eliminate error caused by the atmospheric refraction, but it can be reduced by applying various measuring procedures associated with balancing of the length of sights, limiting the length of sight, not reading the portion of level staff close to ground and choice proper weather conditions.

It is recommended to perform experimental research and develop a model for the vertical refraction which is suitable for the territory of Bulgaria.

Acknowledgments. Presentation of this work is supported by Contract No D01-161/28.08.2018 (Project “National Geo Information Center (NGIC)” financed by the National Roadmap for Scientific Infrastructure 2017-2023).

References

- Angus-Leppan P. V. (1884). Refraction in Geodetic Leveling, Geodetic Refraction, Springer, 1984
- Hytonen E. (1967). Measuring of the refraction in the second leveling of Finland. Finnish, Geodetic Institute Publication No. 63, Helsinki.
- Kukkamaki T. J. (1939). Formulas and tables for computation of leveling refraction. Publication of Geodetic Institute, No. 27, Helsinki, Finland.
- Kukkamaki T. J. (1978). Leveling refraction research, its present state and future possibilities. International Astronomical Union, Symposium No 89, pp293-299.
- NOAA Digital leveling user's guide (1999).
- NOAA Technical Memorandum NOS NGS 31 (1981). A model of temperature stratification for correction of leveling refraction.

Изследване на влиянието на атмосферната рефракция върху прецизните нивелачни измервания

Н. Димитров, П. Данчев, Ив. Георгиев

Резюме: Изследвани са някои проблеми при прилагане на корекцията заради вертикалната рефракция в приземния въздушен слой към измерените превишения при прецизна нивелация. Получените резултати показват, че корекцията трябва да се въвежда за всяка станция и не се нулира при преминаване на едни и същи положителни и отрицателни превишения. Неточно измерените температури имат негативно влияние, могат до доведат до грешно изчислена корекция и да повлияят на крайните резултати. По тази причина е важно температурите да се измерват едновременно с нивелацията, посредством аспирационен термометър, с точност не по-малка от $\pm 0.1^\circ\text{C}$. Препоръчително е да се направят експериментални изследвания и да се приеме подходящ за територията на България модел за отчитане на вертикалната рефракция.

WHAT THE NATIONAL GEOINFORMATION CENTER IS GOING TO CHANGE?

N. Miloshev, P. Trifonova

National Institute of Geophysics, Geodesy and Geography, Bulgarian Academy of Sciences, Acad. G. Bonchev Str., bl. 3, Sofia 1113, Bulgaria,, ptrifonova@geophys.bas.bg

DOI: 10.34975/bgj-2019.42.4

Abstract. The NATIONAL GEOINFORMATION CENTER (NGIC) is a newly established scientific infrastructure for integration of data, data products, and facilities from all Earth observation research institutions in Bulgaria. NGIC will bring together scientists, research infrastructures and ICT (Information & Communication Technology) experts, to develop new concepts and tools for accurate, durable, and sustainable products and services concerning geo-hazards and geo-resources which are relevant to the environment and human welfare. Our vision is that integration of the existing research infrastructures will increase access and use of the multidisciplinary data from the Earth monitoring networks and laboratory experiments.

NGIC mission is to build on new e-science opportunities to monitor and understand the dynamic and complex Earth System, to provide permanent access to geo information, to deliver reliable data and services and to support the effective prevention from natural and anthropogenic disasters and industrial accidents.

NGIC has federated organization model, which means that the sources of data are owned by their independent entities and there is no absolute authority that may imperatively force rules. The center has adopted conceptual model of system architecture that uses both service and microservice concepts and may be altered according to the specifics of the organization environment and development goals of particular information system. The sustainable result of the work of NGIC will be a solid basis for conducting research on Earth and the processes associated with it, as well as an indispensable tool for managing the risk of natural disasters and accidents

Key words: scientific infrastructure, geoinformation, Earth science, Earth observation, data products and services.

Introduction

The Earth Science community worldwide has already begun to reap the benefits of integrated accessible data. A very good example is the successful progress of the European Plate Observing System project (EPOS) which started its preparation phase in 2008 and recently obtained the legal status of European Research Infrastructure Consortium (ERIC). It is now accepted that the study of the Earth is necessarily multidisciplinary and requires the access to data and products generated by different communities with different data formats and processing procedures. The understanding of Earth dynamics and tectonic processes for example relies on the analysis of seismological data, ground deformations inferred from terrestrial and satellite observations, geological and petro-chemical studies and laboratory experiments to investigate the chemical and physical processes occurring at depth. In this framework, the next generation of researchers must be able to use multidisciplinary data and prepared to collaborate for cross-disciplinary investigations. This is one of the key challenges for future research in all disciplines. Effective prevention from natural and anthropogenic disasters and industrial accidents requires as well permanent access to reliable data and products acquired by different Earth observation systems. And those are only parts of the benefits from developing a complete, sustainable, multidisciplinary research platform to provide coordinated access to harmonized and quality controlled data from diverse Earth science disciplines, together with tools for their use in analysis and modelling.

NGIC consortium

The NATIONAL GEO-INFORMATION CENTER (NGIC) is a newly established distributed scientific infrastructure for cooperation and integration of human resources, products and data from monitoring networks and observatories and their integrated analysis. It is part of the National road map for scientific infrastructure (2017-2023), adopted by the Council of Ministers of Bulgaria. The partners joined in the research consortium are four institutes working in the field of Earth observation: the National Institute of Geophysics, Geodesy and Geography (NIGGG), the National Institute of Meteorology and Hydrology (NIMH), the Institute of Oceanology (IO), the Geological Institute (GI), and two institutes competent in ICT: the Institute of Mathematics and Informatics (IMI) and the Institute of Information and Communication Technologies (ICT).

Technical characteristics of the partners

NGIC is a distributed scientific infrastructure with national territorial coverage and integrates monitoring networks, observatories, observation stations, laboratories, computing centers and other specialized equipment of the participating partners. Existing technical resources include unique facilities, scientific equipment and computer networks, the most important of which are as follows (Miloshev et al., 2019):

National Institute of Geophysics, Geodesy and Geography - BAS

(www.niggg.bas.bg)

- National Seismological Network (NOTSSI), consisting of 24 seismic stations (16 main and 8 grouped in two local networks), located on the territory of the whole country and a network of 17 stations located in northern Bulgaria. The network performs continuous monitoring of the seismic events in Bulgaria and the surrounding territories.
- National Accelerometric System (NAS) for registration, analysis and assessment of strong earth motions, consisting of 29 stations with national coverage. The network operates in a permanent registration mode for earth motions caused by seismic events.
- National Permanent GNSS Network, consisting of 21 stations located on the territory of the country. Data are collected, archived and processed in a specialized GNSS Processing Center at NIGGG equipped with modern computers and specialized software.
- National mareograph network for sea level monitoring consisting of 4 stations (Varna, Irakly, Burgas, Ahtopol).
- National Geomagnetic Observatory Panagyurishte, which performs continuous registration of the magnetic field on the territory of the country, as well as field measurements of the field elements. It has modern three-component vector variometers (FGE, DTU Space), two systems for absolute geomagnetic measurements (non-magnetic theodolite + magnetometer) and a field proton magnetometer GSM 19.
- National Geodetic Observatory Plana where a permanent GNSS station, a weather station and a telescope for astronomical observation are installed.
- Palaeomagnetic laboratory equipped with unique scientific equipment for measuring the magnetic properties of natural materials, including various types of magnetometers, kappa-meters, magnetizer and de-magnetization devices, laboratory sample heating furnace, electronic pH meter, centrifuge, separator etc.
- A system for chemical weather prediction working in continuous mode, using three internationally recognized models (CMAQ, MM5, SMOKE).
- Monitoring of Ozone/UV, based on one station for registration of UV radiation and a model for determining the total ozone content, working with satellite data.
- GIS center with computers and specialized software.
- “Ogosta” monitoring network for ecological monitoring of river, ground and soil waters, equipped with piezometers, telemetric apparatus for automatic monitoring of water level and physic-chemical indicators, portable equipment, etc.
- Experimental Laboratory of Karst, equipped with a professional multifunctional system for karst water analysis, microclimatic monitoring systems, speleo-radio-logical monitoring (radon detectors, CO₂, gamma-radiation), dilatometer.

National Institute of Meteorology and Hydrology (www.meteo.bg)

- Ground-based stations: synoptic (37), climatological (77), precipitation (249), agro-meteorological (24), hydrological (170), hydrogeological (347), for precipitation acidity measuring (34), for measuring the components of solar radiation (4), automatic meteorological and hydrological (over 150), experimental polygon for atmospheric boundary layer studies (1).
- Aerological measurements - Central Aerological Observatory Sofia. Daily measurements of vertical profiles of meteorological elements up to a height of 25 km by radiosondes.
- Satellite information
- Information from the meteorological satellites of EUMETSAT is received in “real time” mode, which is used in the operational short-range weather forecasts and in determining the state of the earth surface, for issuing warnings for dangerous meteorological phenomena, for detecting thermal anomalies, etc.
- NIMH maintains a complex information system for transferring, processing and archiving of data, disseminated by the Global Telecommunication System (GTS) and is part of the information flow of the World Weather Information Service of WMO,
- The Regional Telecommunication Center (RTC) in NIMH Sofia is one of the 15 GTS Regional Telecommunication Hubs (RTH) of the WMO. It provides information for the countries from Southeastern Europe and the Middle East. The Regional Telecommunication Center also offers real-time access to the national and international hydro-meteorological data and products. The center is responsible for the processing and selective exchange and dissemination of data: forecasts, aerological, radar, satellite and other information needed in the fields of meteorology, hydrology, agro-meteorology, oceanography and ecology.

Geological Institute – BAS (www.geology.bas.bg)

- National Monitoring Network for monitoring of dangerous geologic processes and phenomena, including monitoring of landslides and active faults on the territory of the country using 3D extensometers and 5 GNSS stations located along the Black Sea coast.
- Extensometric points are installed in a seismically active area of SW Bulgaria (Krupnik-Brezhani region and Kresna gorge) and in deep-seated landslides in the Eastern Rhodopes Mts.
- Modern systems for hydrogeological monitoring and analysis;
- Specialized Geotechnical Laboratory and field research equipment. related to the new BDS EN standards introduced;
- Geochemical equipment. Geolab laboratory for chemical and mineral composition research (ICP, LA-ICP, etc.), physical and mechanical properties of rocks, minerals and soils.
- Database for landslides, maps for geological structure of Bulgaria.

Institute of Oceanology – BAS (www.io-bas.bg)

- National monitoring network according to The Water Framework Directive and the Marine Strategy Framework Directive - 51 sampling stations in the coastal, shelf and open sea zones.
- Coastal observatories providing real time oceanographic and meteorological information and 3 laboratories
- A Research vessel 55.5 m long and a research submarine PC-8B, 6.5 m.

Institute of Mathematics and Informatics – BAS (www.math.bas.bg)

Department Software Engineering and Information Systems – performs scientific research in the fields of mathematical structures, modeling and mathematical informatics, leading to innovative applications in other sciences, in ICT, etc. IMI has premises and infrastructure that allow trainings and other educational initiatives.

Institute of Information and Communication Technologies (www.iict.bas.bg)

Department of Grid Technologies and Applications is in good relations with other leading institutions from Bulgaria and Europe, with interest in Grid, Cloud and HPC computing.

- Dedicated one HP ProLiant SL390s G7 4U server with 8 NVIDIA Tesla M2090 GPU cards (total 4096 GPU cores and 4 TB of disk space for testing of services Big Data analysis)
- Dedicated 4 servers from the Avitohol system, for the purposes of NGIC (HP Cluster SL250S GEN8, each with 2 Intel Xeon E2650v2 processor and 2 Intel Xeon Phi 7120P coprocessors)

Conceptual model of the NGIC system architecture

For the development of the basic system architecture model for NGIC more than 10 national and 5 international sources of Earth observation data and services have been studied (Branzov et al., 2019). The first significant observation is that most of national centers, governed by state organization (state agency, company, research institute) has vertical governance structure. Usually their operations are closely connected with everyday life (such as prognosis, warnings, etc.). The research activities support the main activities. The rest of the national centers are focused to establish a common infrastructure for research and development – federated structures with management team and researchers from the universities and research centers (personally, or institutionally). Further, basically all international centers have federated organization structure.

Analysis of enterprise system architecture models reveals that all of studied geoinformation centers implement service oriented architecture. Some of the centers in their implementation documentation explicitly state as principle usage of distributed services.

Five of centers either use microservice concepts in their architecture or plan their implementation (with at least one (EPOS) – with clear implementation plan).

Based on the findings of the analysis a basic conceptual model of architecture is proposed that uses both service and microservice concepts and may be altered according to the specifics of the organization environment and development goals of the NGIC information system (IS) (Branzov et al., 2019b). The purpose of the model is to be useful in the planning or optimization phases of NGIC information systems (IS) design cycle.

The conceptual model consists of three layers (Figure 1). It is based on the architectural concept for a service, defined as a system component (service provider) that acts to achieve desired end results under a request by another component (service consumer) (He, 2003) and microservice as independent, single purposed and loosely coupled component that supports interoperability through message-based communication (Nadareishvili et al., 2016).

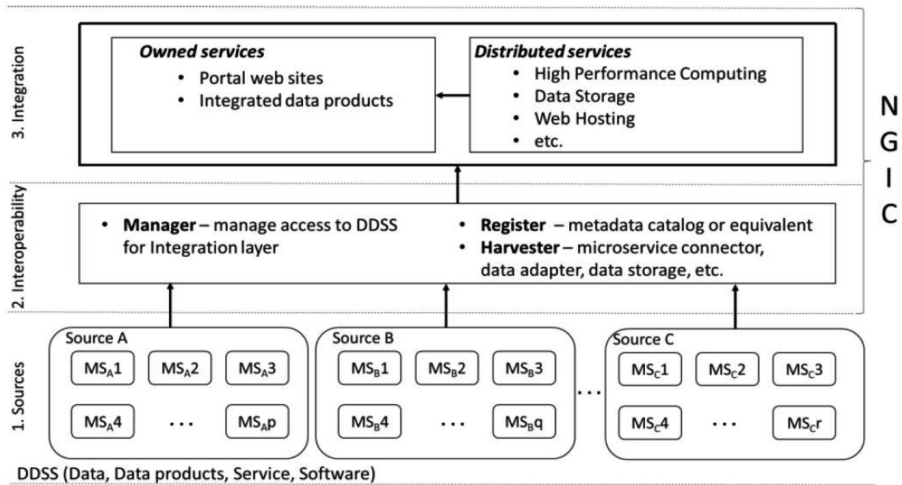


Fig. 1. Conceptual service-microservice model of NGIC (Branzov et al., 2019b).

“Sources” layer contains the providers of Data, Data products, Services and Software (DDSS) that are used by the system to produce advanced integrated products. Providers are presented as sources – collections of microservices. Microservice concept by definition is designed with purpose for providing maximum agility to development of the system, so, its usage provides optimal environment for scaling the systems in the scenarios as – expansion through adding new DDSS by existing source, expansion through adding a new source, shrinking through excluding either DDSS or entire source.

The components in “Interoperability” and “Integration” layers may use either monolithic service or microservice concept. Since they are centrally managed it is possible and convenient to implement the service management framework of choice.

“Interoperability” layer includes components that are mentioned in three abstract categories: “Manager”, which regulate the access to the DDSS in “Sources”

layer; “Register”, which provide automation of discovery and selection of DDSS; and “Harvester”, which includes advanced automated subsystems for data collection from the sources (like data harvesters, data adapters, storages for data buffering, etc.). From these categories only “Manager” is mandatory, but practically in all contemporary geoinformation centered which are reviewed, the two others also exist.

“Integration” layer produces integrated data products (IDP). This is the layer where the value of the GIC is created and delivered. The service architecture is built around two columns – owned services, which provide the access to the IDP. The IDP itself are prepared by owned and distributed services, assured by the ICT support providers or providers that are not partners in NGIC.

Although one of the major characteristic of the “Sources is that they are always passive (i.e. they are designed only to response to requests), the layered nature of the model along with complete authority of NGIC over “Interoperability” and “Integration” layers allow implementation of virtually all other major patterns in manufacturing process of value-added products.

For example, even patterns like “observer” and “publisher-subscriber” that require active side that rises events could be implemented in the top two layer – one approach is to implement a service that regularly pulls DDSS from “Sources” and builds repository that is under authority of NGIC; on the next step that service (or another) may push events on a bus or inform observers that are either services of NGIC or some outside consumers.

Data, data products and services of NGIC

Web site (Figure 2) of the National Geoinformation center (www.ngic.bg) has three main features which are going to be operational: 1) “Risk” section with information about Earthquakes, Air pollution, UV radiation, Magnetic storms, Coastal threats, Landslides and rock falls, etc.; 2) “Thematic” section which will cover all scientific topics of the partners and 3) “Data portal” where the Earth observation data will be organized.

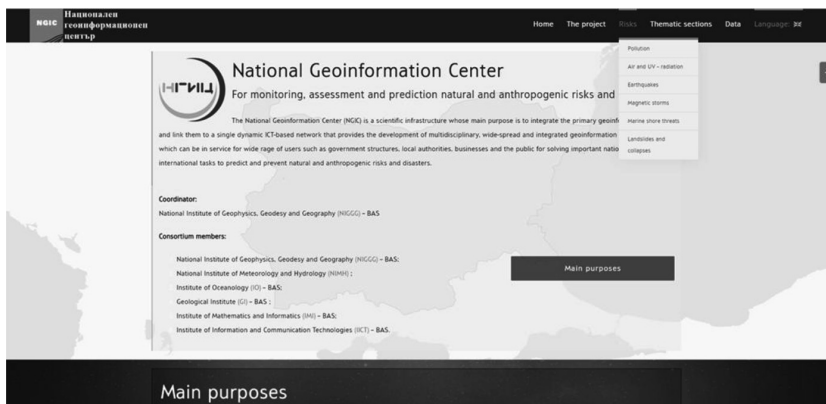


Fig. 2. Features of the National Geoinformation center web page (www.ngic.bg).

Conclusions

Considerable advances in information technology now make an integrated approach possible, easing access to the deluge of data and products available across Earth science and related fields. Accessible datasets will bring novel cross-fertilization of ideas and leads to innovative research that is the key to future success.

From a scientific research perspective, NGIC will provide open access to geophysical, geological and other Earth observational data, while promoting cross disciplinary approaches to Earth science studies. It includes new ways to access data, quality assured metadata and development of new data products and services.

Society needs resources to support home life, industry and business and it needs security in the face of natural hazards. Successful societies depend on the science base to assess the genesis, extent and conservation of natural resources, in order to exploit them and discover new sources without detriment to our environment.

Earth science data can contribute to more effective decision-making in multiple ways. Information can be used to identify emerging problems, trends and changes and monitor ongoing situations. NGIC services will help governmental institutions to make well-informed decisions based on accurate scientific data. Similarly, problems can be anticipated based on forecasts and analysis of future trends.

The overall effect that will be achieved by the establishment of the National Geo-Information Center (NGIC) will be to secure the science effort to understand the Earth system and to increase the quality of life reducing the human and material losses from natural disasters and industrial accidents.

Acknowledgments. Project “National Geoinformation Center (NGIC)” is financed by the National Roadmap for Scientific Infrastructure 2017-2023 under Contract No D01-161/28.08.2018 with the Ministry of Education and Science of Bulgaria.

References

- Miloshev, N., Trifonova, P., Georgiev, I., Marinova, T., Slabakova, V., Dobrev, N., Milusheva V., Guerov, T., 2019. National Geoinformation Center – scientific infrastructure for dissemination of accurate, durable and reliable geodata and products. *Proceedings of the 10th Balkan Geophysical Congress, Albena, 2019*, DOI: 10.3997/2214-4609.201902671
- Branzov T., Kr. Ivanova, Ml. Georgiev, 2019a. Service-microservice Basic System Architecture Model for Geoinformation Centers. *Proc. of the 19th Interdisciplinary Scientific Geo Conference SGEM 2019*, 19, 2.1, 2019, ISBN:978-619-7408-79-9, ISSN:1314-2704, 587-594.
- Branzov T., Kr. Ivanova, Ml. Georgiev, 2019b. Service-Microservice Architecture for Context-Aware Content Delivery in National Geoinformation Center of Bulgaria, *11th International and Interdisciplinary Conference on Modeling and Using Context (CONTEXT 2019)*
- He, H., 2003. What is Service-oriented Architecture?, O’Reilly Media, Inc, www.xml.com/pub/a/ws/2003/09/30/soa.html
- Nadareishvili, I., Mitra, R., McLarty, M., Amundsen, M., 2016. Microservice Architecture Aligning Principles, Practices, and Culture. O’Reilly Media Inc., 126 p.

Какво ще промени създаването на Национален геоинформационен център?

Н. Милошев, П. Трифонова

Резюме: Националният Геоинформационен Център (НГИЦ) е новосъздадена научна инфраструктура за интегриране на данни, услуги и технически капацитет на всички изследователски институти за наблюдение на Земята в България. НГИЦ ще обедини учени, научноизследователски инфраструктури и ИКТ (информационни и комуникационни технологии) експерти, за да разработят нови концепции и инструменти за точни, трайни и устойчиви продукти и услуги, свързани с природните опасности и георесурсите, които са от значение за околната среда и благосъстоянието на хората. Нашата визия е, че интегрирането на съществуващите изследователски инфраструктури ще увеличи достъпа и използването на мултидисциплинарни данни, получавани от мрежите за наблюдение на Земята и лабораторните експерименти.

Мисията на НГИЦ е да създаде нови възможности за наблюдение и изучаване на динамичната и сложна Земна система, за осигуряване на постоянен достъп до гео информация, за предоставяне на надеждни данни и услуги, и за подпомагане на ефективната превенция от природни и антропогенни бедствия и промишлени аварии.

НГИЦ има федерален модел на организация, което означава, че източниците на данни са собственост на институциите, които ги добиват и не се предвижда императивно прилагане на правила в това отношение. Центърът е приел концептуален модел на системна архитектура, която е съобразена със съвременните тенденции в системните архитектури, вкл. в областта на геоинформационните центрове и може да бъде използвана за развитие на НГИЦ.

Дългосрочният резултат от работата на НГИЦ ще бъде солидна база за провеждане на научни изследвания на Земята и процесите, свързани с нея, както и незаменимо средство за управление на риска от природни бедствия и аварии.

DIGITAL DATA RECORDS IN PAG GEOMAGNETIC OBSERVATORY AVAILABLE FOR A 60 YEARS PERIOD

P. Trifonova, M. Metodiev, I. Buchvarov

National Institute of Geophysics, Geodesy and Geography, Bulgarian Academy of Sciences, Acad. G. Bonchev Str., bl. 3, Sofia 1113, Bulgaria, p.trifonova@abv.bg

DOI: 10.34975/bgj-2019.42.5

Abstract. Geomagnetic observatory data are used for investigation of internal Earth structure and processes occurring in the deep interior. In addition, long series of data allow extracting signals related to the Sun, Moon, Earth's motion, etc. To obtain a 60-years long record of the hourly mean values of the geomagnetic field component a lot of efforts have been performed including scan of the old magnetic yearbooks, digitalization of the images and verification of data. As a result, geomagnetic database is created and made available through the institutional web-page and WDC Edinburgh providing basis for scientific research and analysis.

Key words: PAG observatory, geomagnetic records, secular variations, hourly mean values.

History

The Geomagnetic observatory in Panagyurishte (PAG) is established in 1937 – first on the Balkan Peninsula and unique in Bulgaria and during more than 75 years performs the absolute measurements of the geomagnetic field elements and continuous registration of their variations. Until the transfer of the Geomagnetic Observatory from the Military Topographic Service at the Ministry of Defense to the Geophysical Institute of the Bulgarian Academy of Sciences in 1961, and some time afterwards, the diurnal mean, monthly mean, and annual mean values of the elements of the geomagnetic field were obtained from the records on the magnetograms - primarily to reduce field geomagnetic measurements to a common epoch, with no data being published.

The first publication of the data was in 1965, when, under the leadership of Dr. D. Zidarov, head of the “Earth Magnetism and Gravimetry” section of the Geophysical

Institute, the first paper-based Geomagnetic Yearbooks of the Geomagnetic Observatory-Panagyurishte was produced according to the IAGA (International Association of Geomagnetism and Aeronomy) standards. The hourly mean values of the geomagnetic field elements were calculated from the magnetogram's plot by means of a special pallet, and their calculation in the respective magnetic units, as well as the daily mean and annual mean values were obtained on hand. The prepress was done on a typewriter and the printing was performed at the Military Topographic Service unit in Troyan. The production and printing of the Geomagnetic Yearbooks thus continued until 1976, with the yearbooks elaborated back to 1956.

In 1975, Dr. I. Buchvarov developed the first program (for Electronic Computing Machine) for data processing and yearbooks printing. The best machine at that time had 256kB RAM and 4 large (physically large) removable disks of 100 - 200 MB each. All input information: value from the analog recordings of the magnetograms in *mm*, baseline values, scale factor, temperature coefficients, minimum and maximum values, K and C indices and temperature in the variation house were recorded on the so-called "green coding forms". They were then sent to the perforation center at the Institute for Building Cybernetics and put on punch cards. The geomagnetic yearbooks from 1976 to 1983 were produced again on paper. Copy of the Yearbooks had been overspread to the World Data Center's (WDC) and other interested agencies and geomagnetic observatories.

After 1970, emerged the so-called "Mini ECM" of the PDP-11 type, one of which was then supplied to the National Seismological Center at the Institute. In a laboratory of BAS, which had a factory in Plovdiv, began to produce similar ECMs (but smaller ones, something in between the Mini ECMs and PCs). In 1984, one such machine was purchased for the needs of the PAG Observatory. For several years, attempts were made to put it into action and to process the measurement data on it, but this was unsuccessful. Similar attempts at this time were made on a machine of type IZOT 1002 and at the Mathematical Institute of BAS, but again without a success.

By 1982-1983, it became possible to buy PCs. They were first 8-bit, and later, in 1986-1987, the first 16-bit computer ("Pravets") was purchased along with a relatively good dot matrix printer - STAR NX-15. A TURBO PASCAL 5.5 software package was created on this computer and data processing started with it (Butchvarov, 2006). This was one of the reasons that interrupted the production of geomagnetic Yearbooks using large ECMs.

For insuring continuity and for the convenience of the PAG Observatory staff, it was decided that the format of saving the primary data recorded by the analogue magnetograms should remain the same as that used for the punch cards. Using those data, the first program of the software package was producing the hourly and daily mean values of the elements of the geomagnetic field, recorded in the IAGA format, but in the modification of Fürstfeldbruck colleagues (FÜR). Later on, when the Internet came up geomagnetic data were sent to WDC in the required format. Thereafter, various data products were obtained from these files with a number of programs – hourly means – monthly means, only monthly means, annual means, etc.

This method of data processing continued until 2006, when, with the help of colleagues from the Niemeck Observatory, Germany, digital recording equipment was delivered and installed, and the PAG Observatory was incorporated into the INTERMAGNET. After this year, the data are being sent to WDC using licensed software developed by INTERMAGNET.

Registration equipment for geomagnetic field variations in the period 1956-2015.

Analog systems

Between 1937 and 1956 the registration of the geomagnetic variations were made by a single series of variometers “Askania - Werke-AG”, and a recording system “Edelton” using photo paper (Kostov and Nozharov, 1987).

In 1956 were installed second system “Mating & Wiesenberg” D, H and Z variometers. Variometers were almost the same as the previous “Askania - Werke-AG” apparatuses. Magnets suspended on a quartz thread and oriented along the magnetic meridian were used for registration of the declination and horizontal intensity variations. For registration of the vertical intensity the system was installed perpendicular to the magnetic meridian. By means of a triangular agate prism placed in the center of gravity, the system swings freely in the plane perpendicular to the meridian. It is aligned using three weights, with the center of gravity shifted from the anchor points to compensate for the vertical intensity of the magnetic field. Fluctuations of the magnetic systems were recorded through a light beam on the photo paper of the recording block using a system of mirrors and lenses. The system recordings were highly dependent on temperature.

The recording block had two independent recording drums on which variations of the magnetic field of the three variometers could be recorded on photo paper simultaneously. The first one was working with the widely accepted speed of 20mm/hour whereas the other has option for 20, 60 and 240 mm/hour. In addition, the recording block had a special device for visual monitoring of geomagnetic variations.

The sensitivity of the variometers was 0.5'/mm for D, and 2 nT/mm for H and Z.

In 1959 the “Mating & Wiesenberg” and “Askania-Werke-AG” variometers for vertical recordings was replaced by “Bobrov” Z-variometer. The system consists of a quartz frame and a magnet attached to a quartz thread. It is enclosed in a hermetically sealed box. Variometers detect the respective component of the magnetic field depending on how the magnet and the quartz frame are oriented in the airtight box.

In 1971 was installed two quartz F-variometers “Bobrov” for the both systems. They were used for quality control by simultaneous registration of F, H and Z components. The performance of D and H variometers remain very unstable and temperature dependent.

In 1981-1982 old variometers were replaced by “Bobrov” systems. There were two series of variometers in the variation house – western (main one) and eastern. Four quartz

type “BOBROV” variometers were used in each of the series for the registration of the D, H, Z and F. The sensitivity of the variometers was 2 nT/mm for all components and remained constant during the whole year. The variations were registered on photo paper: standard 48 x 20 cm, i.e. 20 mm/h. The recording instrument in the eastern series had two drums. The first one was with a normal speed of 20 mm/h while the second one had additional options for 60 mm/h and 240 mm/h. The fast registration was used only at the time of absolute measurements.

Digital systems

In 2006 with the support of GeoForschung Centrum (GFZ)-Potsdam and Niemegk (NGK) Observatory the analog systems were replaced by another two : 1) 3-axis Fluxgate Magnetometer Model FGM-FGE, suspended version (DTU Space) and 2) Fluxgate Magnetometer MAGSON provided by NGK Observatory + two Overhauser Magnetometers GSM 90 (GEM Systems) provided by NGK as well.

The well-known Danish magnetometer has demonstrated baseline stability in many observatories. In order to avoid drift due to tilt of the instrument pier, which is often the main cause of baseline drift, this FGE version has the sensors suspended by two crossed bronze bands to compensate for pier tilt.

The FGE has analog outputs enabling users to adapt the instrument to their own data logging systems. As an AD-converter is used the MAGDALOG system constructed and provided by GFZ-Potsdam and NGK Observatory.

The main features of this variometer system are:

- Three linear core fluxgate sensors mounted on a marble cube for good mechanical stability.
- Bias and feedback coils on quartz tube for high temperature stability.
- Highly stable digitally controlled compensation of main field.
- Magnetically very clean electronics which may be placed rather close to the sensor head, temperature sensors in the FGE-sensor head and the electronics.

In 2017, the MAGSON Magnetometer was replaced by a second 3-axis Fluxgate Magnetometer Model FGM-FGE, non-suspended version (DTU Space) which is used as a backup system of the main variometer.

Database structure

As it was mentioned above, processing and organization of geomagnetic data in PAG observatory has several periods:

Table 1. Organization of geomagnetic data during the years

	Period	Recording	Processing	Yearbooks preparation	Archiving
1.	1956 – 1975	photographic paper	manual	Manual calculation, typewriting	Paper copy
2.	1976 – 1983	photographic paper	manual	IBM 360	Paper copy
3.	1984 – 2004	photographic paper	manual	PC	Digital Database
4.	2005 – now		PC	PC	Digital Database

To obtain a 60 years long period of the geomagnetic elements records the old printed yearbooks were scanned and digitized. Afterwards they were converted to the accepted IAGA formats, put into a local database which is public available at <http://www.niggg.bas.bg/observatories-bg/geomagnetic-observatory-pag/данни-1956-2015/> and transferred to the Edinburgh WDC (<http://www.wdc.bgs.ac.uk/dataportal/>).

Structure of the local geomagnetic database is presented in Fig. 1 and the folder and file description is given in Table 2.

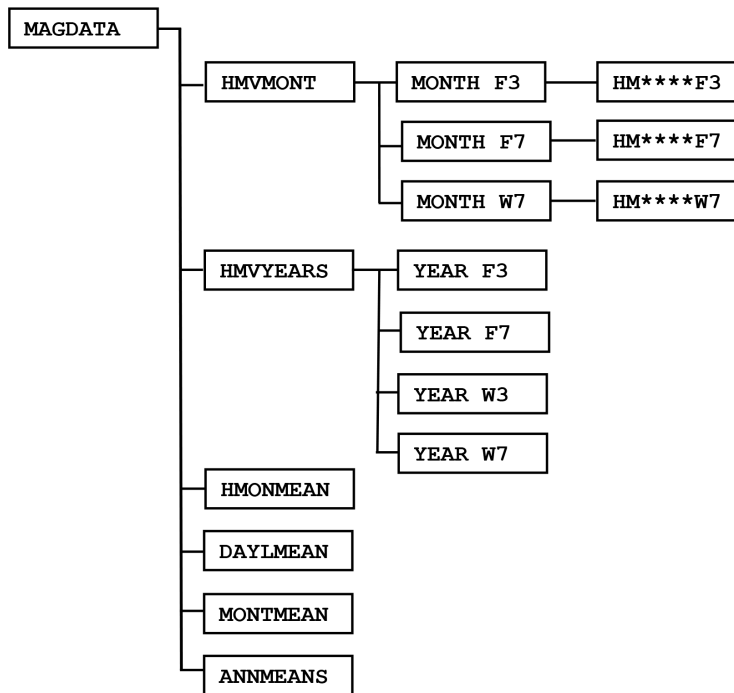


Fig. 1. Structure of the local geomagnetic database available at <http://www.niggg.bas.bg/observatories-bg/geomagnetic-observatory-pag/данни-1956-2015/>

Table 2. Folder and file description of the geomagnetic database, where **** - stands for the YEAR, e.g. 1999, 2000 and so on, and +++ -stands for the month, e.g. JAN, FEB,..., DEC)

FOLDER	DESCRIPTION
MAGDATA	<i>Main folder. Contains all other folders.</i>
HMVMONTH	<i>Contains folders:</i> 1. MONTH_F3. 2. MONTH_F7. 3. MONTH_W7.
1. MONTH_F3	<i>Contains folders:</i> 1.1. HM****F3.
1.1. HM****F3	<i>Contains files ****+++3.FUR with hourly mean values and daily mean value for all days for each month of the year separately (D, H and Z) in the FÜR format.</i>
2. MONTH_F7	<i>Contains folders</i> 2.1. HM****F7.
2.1. HM****F7	<i>Contain files ***+++7.FUR with hourly mean values and daily mean value for all days for each month of the year separately (D, F, H, I, X, Y and Z) in the FÜR format.</i>
3. MONTH_W7	<i>Contains folders</i> 3.1. HM****W7.
3.1. HM****W7	<i>Contains files ****+++7.WDC with hourly mean values and daily mean value for all days for each month of the year separately (D, F, H, I, X, Y and Z) in the WDC format.</i>
HMVYEARS	<i>Contains folders:</i> 1. YEAR_F3. 2. YEAR_F7. 3. YEAR_W3. 4. YEAR_W7.
1. YEAR_F3	<i>Contains files PAG****3.FUR with hourly mean values and daily mean value for all days of the year (D, H and Z) in the FÜR format.</i>
2. YEAR_F7	<i>Contains files PAG****7.FUR with hourly mean values and daily mean value for all days of the year (D, F, H, I, X, Y and Z) in the FÜR format.</i>
3. YEAR_W3	<i>Contains files PAG****3.WDC with hourly mean values and daily mean value for all days of the year (D, H and Z) in the WDC format.</i>
4. YEAR_W7	<i>Contains files PAG****7.WDC with hourly mean values and daily mean value for all days of the year (D, F, H, I, X, Y and Z) in the WDC format.</i>
HMONMEAN	<i>Contains files HMMV****.PAG with hourly mean monthly mean values for each year separately.</i>
DAYLMEAN	<i>Contains files DM****.PAG with daily mean values for each year separately.</i>
MONTMEAN	<i>Contains file MONTMEAN.PAG with monthly mean values.</i>
ANNMEANS	<i>Contains file ANNMEANS.PAG with annual mean values.</i>

The Annual Mean values of the geomagnetic field elements observed in PAG Observatory between 1956 and 2015 are given in Table 3.

Table 3. Annual Mean Values of the geomagnetic field elements calculate from 1) all days “A”, 2) disturbed days “D” and 3) quiet days “Q” in PAG Observatory between 1956 and 2015

Data Report: Observatory Annual Means								
Date: 8-Nov-2019								
Station Name: Panagyurishte			IAGA Code: PAG			Country: Bulgaria (BG)		
Sponsoring Institution: Geophysical Institute, BAS								
Latitude: 42°30.9' N			Longitude: 24°10.6' E			Elevation [m]: 556		
Elements Measured: DHZ								
Year	Type	D	F	H	I	X	Y	Z
1956.5	A	0°54.7'	45659	23477	59°03.4'	23474	374	39161
1956.5	D	0°55.4'	45653	23455	59°05.1'	23451	378	39167
1956.5	Q	0°54.1'	45663	23491	59°02.4'	23488	370	39157
1957.5	A	0°58.1'	45682	23471	59°05.0'	23468	397	39192
1957.5	D	0°59.3'	45674	23444	59°07.0'	23440	404	39199
1957.5	Q	0°57.5'	45686	23486	59°03.8'	23482	393	39186
1958.5	A	1°01.2'	45719	23476	59°06.2'	23472	418	39232
1958.5	D	1°02.5'	45712	23448	59°08.1'	23437	427	39240
1958.5	Q	1°00.5'	45722	23490	59°05.2'	23486	413	39227
1959.5	A	1°03.9'	45762	23484	59°07.4'	23480	471	39277
1959.5	D	1°05.2'	45755	23454	59°09.8'	23450	479	39287
1959.5	Q	1°03.3'	45766	23500	59°06.2'	23495	467	39272
1960.5	A	1°06.6'	45800	23490	59°08.6'	23486	455	39318
1960.5	D	1°08.0'	45793	23462	59°10.8'	23457	464	39326
1960.5	Q	1°05.9'	45805	23507	59°07.4'	23502	451	39313
1961.5	A	1°08.8'	45839	23511	59°08.6'	23506	470	39351
1961.5	D	1°09.5'	45834	23494	59°09.8'	23489	475	39355
1961.5	Q	1°08.4'	45842	23520	59°08.0'	23515	468	39349
1962.5	A	1°11.1'	45889	23534	59°08.7'	23528	521	39395
1962.5	D	1°11.4'	45887	23527	59°09.3'	23521	523	39397
1962.5	Q	1°10.8'	45890	23540	59°08.4'	23534	519	39393
1963.5	A	1°13.4'	45915	23542	59°09.3'	23536	503	39421
1963.5	D	1°14.1'	45911	23530	59°10.2'	23524	507	39423
1963.5	Q	1°13.1'	45917	23549	59°08.7'	23544	501	39418
1964.5	A	1°14.9'	45936	23554	59°09.1'	23549	513	39437
1964.5	D	1°15.3'	45934	23548	59°09.5'	23543	516	39438
1964.5	Q	1°14.7'	45936	23559	59°08.7'	23553	512	39435
1965.5	A	1°16.6'	45961	23568	59°09.1'	23562	525	39459
1965.5	D	1°16.9'	45959	23559	59°09.7'	23554	527	39461
1965.5	Q	1°16.4'	45962	23570	59°08.9'	23564	524	39458

Table 3.

Year	Type	D	F	H	I	X	Y	Z
1966.5	A	1°18.5'	45982	23570	59°09.7'	23564	538	39481
1966.5	D	1°19.1'	45978	23557	59°10.7'	23551	542	39484
1966.5	Q	1°18.2'	45983	23577	59°09.2'	23571	536	39479
1967.5	A	1°20.2'	45997	23570	59°10.5'	23564	550	39499
1967.5	D	1°21.0'	45992	23555	59°11.6'	23548	555	39502
1967.5	Q	1°19.8'	45999	23578	59°09.8'	23572	548	39496
1968.5	A	1°21.4'	46018	23578	59°10.7'	23572	558	39519
1968.5	D	1°22.1'	46013	23562	59°11.9'	23555	563	39523
1968.5	Q	1°20.9'	46020	23587	59°10.1'	23580	555	39516
1969.5	A	1°22.1'	46033	23595	59°09.9'	23588	563	39526
1969.5	D	1°22.8'	46029	23581	59°10.9'	23574	568	39530
1969.5	Q	1°21.7'	46035	23602	59°09.4'	23595	561	39524
1970.5	A	1°22.8'	46055	23607	59°09.8'	23600	569	39544
1970.5	D	1°23.6'	46050	23588	59°11.2'	23582	574	39549
1970.5	Q	1°22.4'	46057	23616	59°09.1'	23610	566	39541
1971.5	A	1°24.3'	46079	23626	59°09.2'	23619	579	39561
1971.5	D	1°24.9'	46075	23613	59°10.2'	23606	583	39564
1971.5	Q	1°24.0'	46080	23633	59°08.7'	23626	577	39559
1972.5	A	1°25.5'	46108	23642	59°09.1'	23635	588	39585
1972.5	D	1°26.2'	46104	23628	59°10.2'	23620	593	39589
1972.5	Q	1°25.1'	46110	23651	59°08.5'	23644	585	39583
1973.5	A	1°27.3'	46140	23658	59°09.2'	23650	601	39614
1973.5	D	1°28.2'	46136	23644	59°10.3'	23636	606	39617
1973.5	Q	1°26.8'	46142	23666	59°08.6'	23659	597	39611
1974.5	A	1°29.7'	46169	23667	59°09.7'	23659	617	39642
1974.5	D	1°30.4'	46165	23652	59°10.8'	23644	622	39645
1974.5	Q	1°29.2'	46172	23678	59°08.9'	23670	614	39638
1975.5	A	1°32.1'	46198	23688	59°09.2'	23679	635	39664
1975.5	D	1°32.7'	46194	23677	59°10.0'	23668	638	39666
1975.5	Q	1°31.8'	46200	23695	59°08.7'	23686	633	39662
1976.5	A	1°35.3'	46225	23701	59°09.3'	23691	657	39687
1976.5	D	1°36.0'	46220	23685	59°10.4'	23676	661	39690
1976.5	Q	1°34.9'	46227	23709	59°08.7'	23700	654	39684
1977.5	A	1°39.2'	46255	23714	59°09.4'	23704	684	39713
1977.5	D	1°39.9'	46251	23701	59°10.4'	23691	688	39716
1977.5	Q	1°38.8'	46257	23722	59°08.8'	23712	682	39711
1978.5	A	1°43.6'	46279	23709	59°10.9'	23698	714	39744
1978.5	D	1°44.7'	46272	23687	59°12.6'	23676	721	39750
1978.5	Q	1°43.0'	46282	23722	59°09.9'	23712	711	39740

Table 3.

Year	Type	D	F	H	I	X	Y	Z
1979.5	A	1°48.0'	46303	23715	59°11.5'	23703	745	39769
1979.5	D	1°48.8'	46299	23699	59°12.7'	23687	750	39774
1979.5	Q	1°47.5'	46306	23725	59°10.8'	23713	742	39766
1980.5	A	1°52.1'	46318	23721	59°11.7'	23708	773	39784
1980.5	D	1°52.8'	46314	23704	59°12.9'	23691	778	39788
1980.5	Q	1°51.9'	46319	23725	59°11.4'	23712	772	39782
1981.5	A	1°56.4'	46336	23708	59°13.6'	23695	803	39811
1981.5	D	1°57.2'	46330	23688	59°15.0'	23675	808	39817
1981.5	Q	1°55.9'	46339	23720	59°12.6'	23707	799	39808
1982.5	A	2°01.2'	46352	23695	59°15.4'	23680	835	39838
1982.5	D	2°02.2'	46346	23671	59°17.1'	23656	841	39845
1982.5	Q	2°00.5'	46356	23708	59°14.4'	23693	831	39835
1983.5	A	2°05.0'	46371	23695	59°16.2'	23679	861	39860
1983.5	D	2°05.8'	46366	23680	59°17.3'	23664	866	39863
1983.5	Q	2°04.4'	46374	23706	59°15.4'	23690	857	39857
1984.5	A	2°08.9'	46392	23690	59°17.6'	23673	888	39888
1984.5	D	2°09.7'	46388	23675	59°18.7'	23658	893	39892
1984.5	Q	2°08.5'	46395	23699	59°16.9'	23682	886	39886
1985.5	A	2°11.8'	46414	23688	59°18.7'	23671	908	39914
1985.5	D	2°12.5'	46411	23677	59°19.6'	23659	912	39917
1985.5	Q	2°11.4'	46417	23697	59°18.1'	23679	906	39912
1986.5	A	2°14.9'	46437	23681	59°20.3'	23663	929	39945
1986.5	D	2°15.5'	46433	23668	59°21.2'	23650	933	39948
1986.5	Q	2°14.4'	46440	23689	59°19.7'	23671	926	39943
1987.5	A	2°17.2'	46461	23683	59°21.2'	23664	945	39972
1987.5	D	2°17.6'	46458	23672	59°22.0'	23654	947	39975
1987.5	Q	2°16.9'	46463	23689	59°20.8'	23670	943	39970
1988.5	A	2°19.5'	46484	23671	59°23.3'	23651	960	40006
1988.5	D	2°20.1'	46480	23654	59°24.6'	23634	964	40011
1988.5	Q	2°18.9'	46487	23682	59°22.5'	23662	957	40003
1989.5	A	2°22.3'	46505	23657	59°25.4'	23637	979	40038
1989.5	D	2°23.6'	46498	23632	59°27.2'	23611	986	40045
1989.5	Q	2°21.6'	46508	23670	59°24.4'	23651	974	40034
1990.5	A	2°24.0'	46525	23656	59°26.3'	23636	991	40062
1990.5	D	2°24.9'	46520	23638	59°27.6'	23617	996	40067
1990.5	Q	2°23.5'	46528	23667	59°25.5'	23646	987	40059
1991.5	A	2°26.8'	46541	23646	59°27.9'	23624	1009	40087

Table 3.

Year	Type	D	F	H	I	X	Y	Z
1991.5	D	2°28.1'	46534	23619	59°29.9'	23597	1017	40095
1991.5	Q	2°26.1'	46544	23659	59°26.8'	23638	1005	40082
1992.5	A	2°28.9'	46557	23653	59°28.0'	23631	1024	40102
1992.5	D	2°29.6'	46552	23633	59°29.5'	23610	1028	40107
1992.5	Q	2°28.3'	46560	23665	59°27.1'	23643	1021	40098
1993.5	A	2°32.0'	46576	23658	59°28.4'	23635	1046	40121
1993.5	D	2°32.7'	46571	23641	59°29.6'	23618	1050	40124
1993.5	Q	2°31.6'	46579	23667	59°27.7'	23644	1043	40118
1994.5	A	2°35.7'	46596	23655	59°29.6'	23631	1071	40146
1994.5	D	2°36.4'	46592	23641	59°30.5'	23617	1075	40148
1994.5	Q	2°35.1'	46599	23666	59°28.7'	23642	1067	40143
1995.5	A	2°39.5'	46618	23662	59°29.8'	23637	1098	40166
1995.5	D	2°40.2'	46614	23650	59°30.7'	23624	1101	40169
1995.5	Q	2°39.1'	46620	23672	59°29.1'	23647	1095	40163
1996.5	A	2°43.7'	46641	23673	59°29.9'	23647	1127	40187
1996.5	D	2°44.2'	46639	23667	59°30.4'	23640	1130	40188
1996.5	Q	2°43.4'	46643	23679	59°29.5'	23652	1125	40185
1997.5	A	2°48.2'	46667	23672	59°31.2'	23643	1158	40218
1997.5	D	2°48.5'	46665	23665	59°31.6'	23637	1159	40219
1997.5	Q	2°47.9'	46668	23677	59°30.8'	23648	1156	40216
1998.5	A	2°52.8'	46695	23665	59°33.0'	23635	1189	40254
1998.5	D	2°53.6'	46689	23647	59°34.3'	23617	1193	40259
1998.5	Q	2°52.5'	46697	23672	59°32.4'	23642	1187	40252
1999.5	A	2°56.7'	46721	23666	59°34.0'	23634	1216	40284
1999.5	D	2°57.4'	46717	23651	59°35.2'	23619	1220	40288
1999.5	Q	2°56.3'	46724	23674	59°33.4'	23643	1214	40282
2000.5	A	3°00.5'	46749	23664	59°35.4'	23631	1242	40318
2000.5	D	3°01.5'	46744	23645	59°36.8'	23612	1247	40323
2000.5	Q	3°00.0'	46752	23674	59°34.6'	23642	1239	40315
2001.5	A	3°04.2'	46779	23672	59°36.0'	23638	1267	40348
2001.5	D	3°05.2'	46773	23650	59°37.6'	23616	1274	40353
2001.5	Q	3°03.7'	46782	23682	59°35.3'	23648	1265	40345
2002.5	A	3°08.6'	46812	23682	59°36.6'	23646	1299	40380
2002.5	D	3°09.3'	46808	23665	59°37.8'	23629	1303	40385
2002.5	Q	3°08.2'	46814	23692	59°35.8'	23656	1296	40377
2003.5	A	3°13.9'	46847	23680	59°38.3'	23642	1335	40422
2003.5	D	3°15.2'	46841	23658	59°39.8'	23620	1342	40427

Table 3.

Year	Type	D	F	H	I	X	Y	Z
2003.5	Q	3°13.2'	46850	23692	59°37.4'	23654	1331	40418
2004.5	A	3°17.9'	46878	23690	59°38.7'	23651	1363	40452
2004.5	D	3°18.8'	46873	23673	59°40.0'	23633	1368	40456
2004.5	Q	3°17.4'	46880	23699	59°38.0'	23660	1360	40448
2005.5	A	3°22.6'	46906	23695	59°39.5'	23654	1395	40482
2005.5	D	3°23.3'	46902	23680	59°40.6'	23639	1400	40486
2005.5	Q	3°22.2'	46909	23703	59°38.9'	23662	1393	40480
2006.5	A	3°27.1'	46935	23713	59°39.2'	23670	1427	40504
2006.5	D	3°27.6'	46931	23704	59°39.8'	23660	1430	40505
2006.5	Q	3°26.7'	46936	23719	59°38.7'	23677	1426	40501
2007.5	A	3°32.4'	46964	23724	59°39.5'	23679	1465	40532
2007.5	D	3°32.9'	46962	23718	59°39.9'	23673	1468	40533
2007.5	Q	3°32.1'	46966	23729	59°39.2'	23684	1463	40530
2008.5	A	3°38.6'	46994	23738	59°39.6'	23690	1509	40558
2008.5	D	3°38.9'	46992	23733	59°40.0'	23684	1510	40558
2008.5	Q	3°38.4'	46995	23742	59°39.3'	23694	1507	40556
2009.5	A	3°45.0'	47023	23748	59°40.0'	23697	1553	40586
2009.5	D	3°45.2'	47022	23745	59°40.2'	23694	1554	40587
2009.5	Q	3°44.9'	47023	23750	59°39.9'	23699	1552	40585
2010.5	A	3°51.7'	47055	23746	59°41.6'	23692	1599	40624
2010.5	D	3°52.1'	47052	23737	59°42.2'	23683	1602	40626
2010.5	Q	3°51.5'	47056	23750	59°41.3'	23696	1598	40623
2011.5	A	3°58.4'	47088	23744	59°43.1'	23687	1645	40664
2011.5	D	3°58.9'	47085	23735	59°43.8'	23678	1648	40665
2011.5	Q	3°58.1'	47090	23750	59°42.7'	23693	1644	40662
2012.5	A	4°05.3'	47123	23744	59°44.6'	23684	1693	40704
2012.5	D	4°06.0'	47119	23730	59°45.7'	23669	1696	40708
2012.5	Q	4°05.1'	47125	23750	59°44.2'	23690	1692	40703
2013.5	A	4°12.0'	47158	23756	59°45.1'	23692	1740	40738
2013.5	D	4°12.3'	47154	23744	59°45.9'	23680	1741	40739
2013.5	Q	4°11.8'	47160	23762	59°44.7'	23698	1739	40736
2014.5	A	4°18.2'	47194	23768	59°45.6'	23700	1783	40772
2014.5	D	4°18.6'	47192	23760	59°46.2'	23693	1786	40774
2014.5	Q	4°17.9'	47195	23773	59°45.2'	23706	1782	40771
2015.5	A	4°25.0'	47235	23764	59°47.6'	23694	1830	40821
2015.5	D	4°25.9'	47229	23746	59°48.9'	23675	1835	40826
2015.5	Q	4°24.6'	47237	23774	59°46.9'	23704	1828	40818

D and I in degrees and minutes; F, H, X, Y and Z in nT.

Secular trend of the geomagnetic field elements between 1956 and 2015

Having a 60-years long period with digital records of the geomagnetic field elements is a vast wealth of data which can be exploited for observation and analysis of the secular variation of the field (Metodiev, 2014), derivation of indices and phenomena, Fourier coefficients of the solar daily variation, other non-cyclic variations, etc. (Malin et al., 1996).

In this paper we are not going to present the results of such harmonic analysis but to announce and demonstrate the data quality and availability of information acquired in the PAG Observatory.

Annual trend and the secular variation of Declination (D), Inclination (I), North (X), East (Y) and Vertical (Z) components recorder in PAG Observatory is displayed as monthly mean value's plots in Figures 2-5.

Values of D (Fig. 2), the first and very important angular component of the geomagnetic field starts from 52.9' in 1956 and with a positive gradient ranging between 1 and 7 min/year reaches 4°27.8' in 2015.

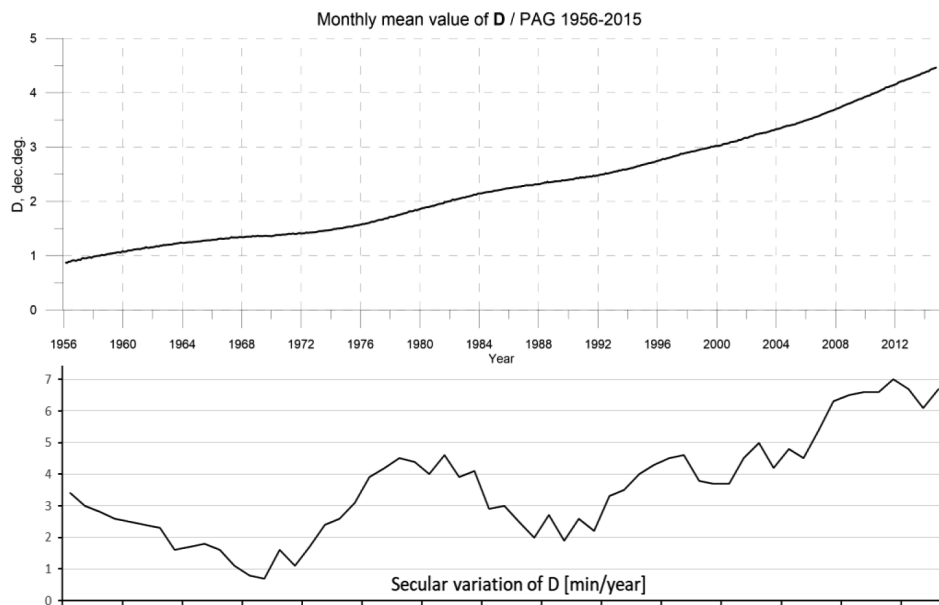


Fig. 2. Plot of the monthly mean values of the Declination [Dec. Degrees] registered in PAG observatory between 1956-2015 and calculated secular variation [min/year].

In contrast, the variation of I (Fig. 3) exhibits more divergent gradients but for the 60-years period its amplitude increase within a smaller range between 59°02' and 59°48'.

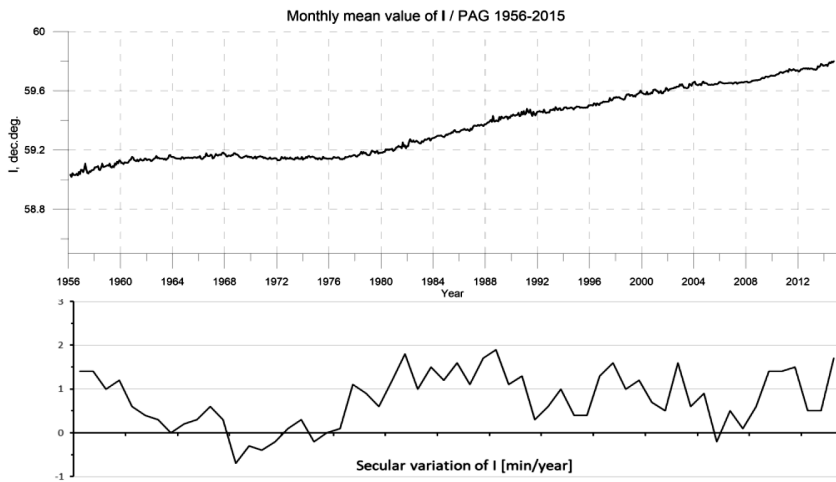


Fig. 3. Plot of the monthly mean values of the Inclination [Dec. Degrees] registered in PAG observatory between 1956-2015 and calculated secular variation [min/year].

North component (Fig. 4) is the only one which has positive as well as negative gradients during the considered time interval. It has a value of 23479 nT in January 1956, reaches its maximum of 23719 nT in 1979 and 1980 and decreases with about 50 nT in the next ten years. Ten more years it is almost constant, then slightly increases again to reach values of 23700 nT in the recent few years.

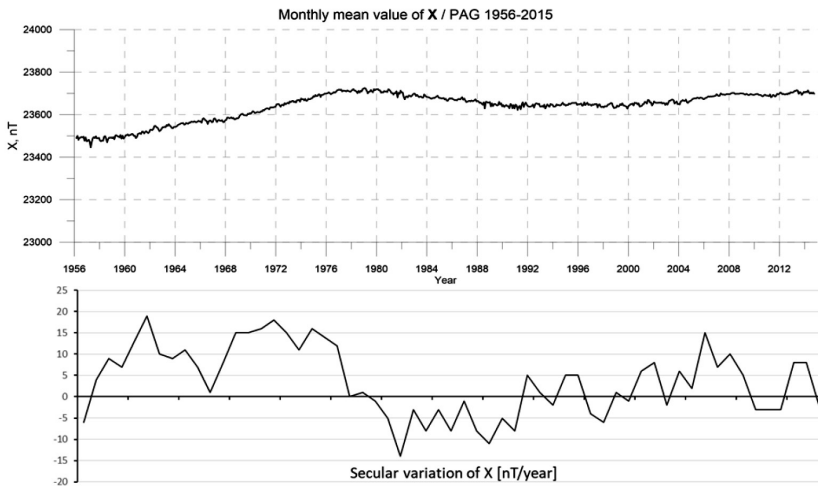


Fig. 4. Plot of the monthly mean values of the North geomagnetic component [nT] registered in PAG observatory between 1956-2015 and its secular variation [nT/year].

East component (Fig. 5) has very similar behavior as D. The 60-years plot of Y smoothly increased from 362 to 1848 nT. It has strongly positive secular variation with smallest value of 5 nT/year between 1969 -1970 and the largest one of 48 nT/year forty years later.

East component (Fig. 5) has very similar behavior as D. The 60-years plot of Y smoothly increased from 362 to 1848 nT. It has strongly positive secular variation with smallest value of 5 nT/year between 1969 -1970 and the largest one of 48 nT/year forty years later.

The East component is probably the most investigated component of the magnetic field due to its relation with the so-called geomagnetic “jerks”. Geomagnetic jerks are still poorly understood phenomena of Earth’s magnetic field. The phenomenon of a geomagnetic jerk was first reported by Courtillot et al. (1978) as an abrupt turning point separating the otherwise linear trends of the Y(East)-component of secular variation prior to and after 1970 at several Northern hemisphere observatories. Until then, several papers had been published analyzing local and global changes of the Y values (e.g. Brown et al., 2013). Calculated secular acceleration of the Y series recorded in PAG observatory point for such changes in 1969, 1981, 1983, 1991, 2002 and 2006.

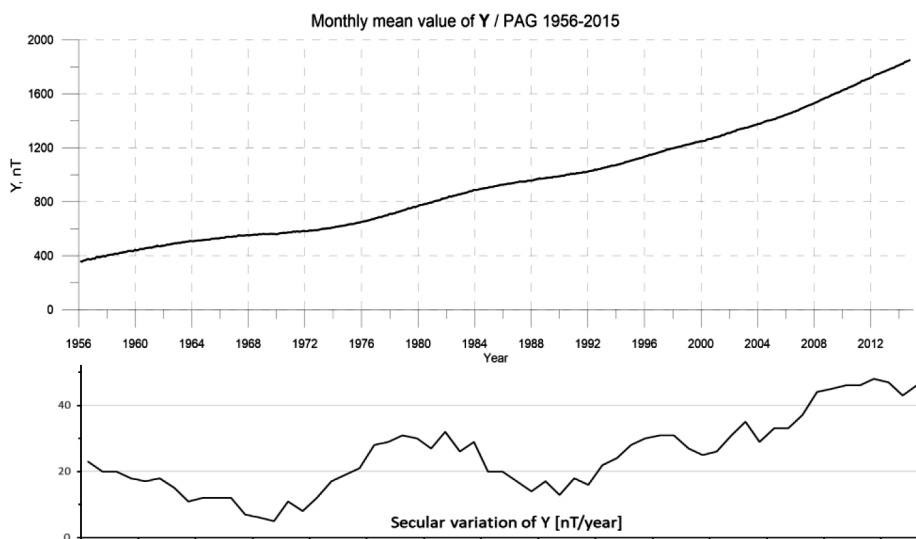


Fig. 5. Plot of the monthly mean values of the East geomagnetic component [nT] registered in PAG observatory between 1956-2015 and its secular variation [nT/year].

Vertical component (Fig. 6) of the geomagnetic field exhibits the smallest variation of 1660 nT for the 60 years period which comprises only 4% of its value. The secular variation of Z is nearly constant between 30 and 40 nT/year. In 2015 the observed annual mean value is 40821 nT.

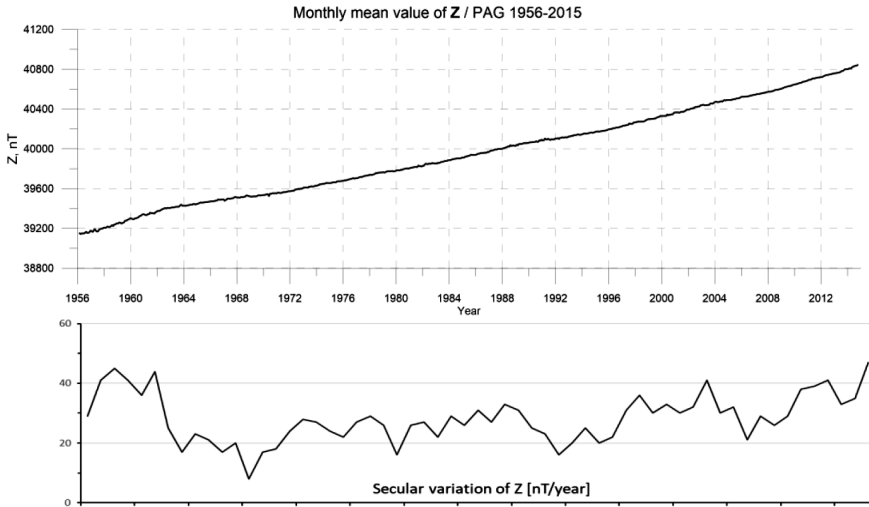


Fig. 6. Plot of the monthly mean values of the Vertical geomagnetic component [nT] registered in PAG observatory between 1956-2015 and its secular variation [nT/year].

Conclusions

The main purpose for the processing of geomagnetic observational data is to find coherent periodic variations, external and internal signals, and their characteristics in long-period records. The presented data for a 60-year period are recorded in the Panagyurishte Geomagnetic Observatory in Bulgaria, part of NIGGG-BAS. This comprehensive database is obtained from scanned and digitized yearbooks and modern digital records. Data are put in a structured database containing hourly mean values in two formats. They are organized in separate monthly files (720 files) and in separate year files (60 files). Additionally, four statistical parameters are calculated and put in single file: hourly-mean monthly-mean values for each year separately, daily-mean values for each year separately, monthly mean values and annual mean values. A detailed analysis of the data will allow the identification of known periods related to the Sun, Moon, Earth's motion, etc., will allow the study of other relationships between the geomagnetic field and processes related to cosmic phenomena, climate parameters, earthquakes etc.

Acknowledgments. The work presented in this paper is supported by the NATIONAL PROGRAM “Young scientists and postdoctoral fellows” of the Ministry of Education and Science of Bulgaria and the Bulgarian Academy of Sciences.

References

- Brown, W., Mound, J. & Livermore, P. Jerks abound: an analysis of geomagnetic observatory data from 1957 to 2008. *Phys. Earth Planet. Int.* **223**, 62–76 (2013).
- Butchvarov I., 2006 Processing and organization of the data obtained from the analog magnetograms of Panagyurishte Geomagnetic Observatory, *Bulgarian Geophys. Journal*, 32, p. 43-54
- Courtillot, V., Ducruix, J., Le Mouél, J.-L.(1978) Sur une acceleration récente de la variation séculaire du champ magnétique terrestre, *C.R. Hedb. Seances Acad. Sci., Ser. D*, Volume 287, Pages 1095-1098
- Kostov K. and P. Nozharov, Absolute magnetic measurements in Bulgaria 1787-1997, Sofia, 1987, pp1.72
- Malin S. R. C., Tunçer M. K. and O. Yazici-Çakin (1996) Systematic analysis of magnetic observatory data – I. A proposed method, *Geophys. Journ. Int.*, 126, p. 635-644
- Metodiev M. (2014) Modelling of declination's secular variation for the purposes of regional topographic mapping, *Bulgarian Geophys. Journal*, vol.40, p. 76-84

Цифрови данни от Геомагнитна Обсерватория Панагюрище налични за 60-годишен период

П. Трифонова, М. Методиев, И. Бъчваров

Резюме: Основна цел на обработката на геомагнитни обсерваторни данни е откриването на кохерентни периодични вариации, явни и неявни зависимости и техните характеристики в дългопериодични записи. Представените данни за 60 годишен период от време са записани в Геомагнитна обсерватория Панагюрище, част от НИГГТ-БАН. Подробният анализ на данните ще даде възможност за идентифициране на периодичности, свързани със Слънцето, Луната, движението на Земята и ще позволи изследването на други зависимости между геомагнитното поле и процеси, свързани с космически явления, параметри на климата, земетресения и др.

ANNUAL REPORT OF THE OBSERVED GEOMAGNETIC ACTIVITY IN PANAGYURISHTE OBSERVATORY FOR 2014

M. Metodiev, P. Trifonova

National Institute of Geophysics, Geodesy and Geography, Bulgarian Academy of Sciences, Acad. G. Bonchev Str., bl. 3, Sofia 1113, Bulgaria, p.trifonova@abv.bg

DOI: 10.34975/bgj-2019.42.6

Abstract. Presently, in the era of Internet communication the preliminary time series (INTERMAGNET's reported data) acquired in geomagnetic observatories are available in near-real time, while the final absolute time series (definitive data) are disseminated with many months delay, being subject to many checks. This paper reports the definitive geomagnetic data obtained in Panagyurishte observatory in 2014, prepared in the form of local geomagnetic indices and absolute time-series of daily mean values plots. Verification of data quality is performed according to "IAGA guide for magnetic measurements and observatory practice".

Key words: PAG observatory, geomagnetic variations, geomagnetic activity, local geomagnetic indices, daily mean values.

Introduction

The Geomagnetic observatory in Panagyurishte (PAG) is established in 1937 – first on the Balkan Peninsula and unique in Bulgaria and during more than 80 years performs absolute measurements of the geomagnetic field elements and continuous registration of their variations (Buchvarov, 2006). In 2007 PAG observatory was equipped with digital systems for the recording of geomagnetic field element's variations. Thus, the observatory implemented the technical requirements and was joined to the INTERMAGNET (International Real-time Magnetic Observatory Network), which establishes a global network of cooperating digital magnetic observatories, and facilitate data exchanges and geomagnetic products in close to real time. Preliminary recorded time series and local geomagnetic k-indices are published on the NIGGG web page (http://data.niggg.bas.bg/magn_data1/dailymag_bg.php) and automatically reported to INTERMAGNET. The present paper provides quasi-definitive geomagnetic data which are checked and processed to comply with the IAGA standards for observatory practices.

Local geomagnetic indices (K , A_K , ΣK) calculated at PAG observatory.

The K-index is often used as a quantitative measure of local magnetic activity. It is a 3-hour quasi-logarithmic scale developed to measure magnetic activity ranging from 0 to 9, with 0 indicating completely quiet conditions and 9, representing extreme magnetic activity. It is intended to measure geomagnetic disturbances outside the normal diurnal quiet time variations. In order to have a somewhat consistent scale of magnetic activity between observatories at high latitudes, where field variations can be quite large in amplitude, and those at low latitudes, each observatory is assigned its own set of amplitude ranges corresponding to the various K-index levels. Thus, for example, a K-index of 5 at College (TCO) observatory (212.4°E, 64.87°N) corresponds to a lower limit of magnetic activity range of 350 nT over the 3-hour interval, while at San Juan (SJG) observatory (293.85°E, 18.117°N) this same K-index level corresponds to a lower limit of magnetic activity of 40 nT. The idea is to have K-index compensation for the influence of latitude on magnetic activity, so that a K-index of 7 at College and San Juan would represent the same magnetic storm intensity despite the actual differences in the range of magnetic fluctuation amplitudes at the two latitudes.

The ranges of the individual K numbers in PAG observatory (24.177°EN, 42.515°N) are defined as follows:

Deviation from the normal Sq variation [nT]	<5	5 -10	10 - 20	20 - 40	40 - 70	70 - 120	120 -200	200-330	330-500	> 500
K	0	1	2	3	4	5	6	7	8	9

The eight three-hourly K numbers (after Bartels) are calculated by a computer code (FMI method, Sucksdorff et al., 1991) from the digital recordings of three component flux-gate variometer FGE.

A_K [nT] is the local equivalent daily amplitude index which is determined by converting K –indices into eight 3-hour equivalent linear amplitudes a_K , and calculating the mean value. The 3-hour equivalent amplitude a_K is assigned for each K value using the following table:

K	0	1	2	3	4	5	6	7	8	9
$a_{K[nT]}$	0	3	7	15	27	48	80	140	240	400

ΣK is the daily sum of the eight K numbers.

The calculated local geomagnetic indices (K, AK, ΣK) at PAG observatory for 2014 are presented in Table 1.

Table 1. Local geomagnetic indices (K, A_K , ΣK) calculated at PAG observatory in 2014.

Activity indices										
PAG Observatory									2014	
Day	K								Ak[nT]	ΣK
01-Jan-14	1	1	2	2	4	4	3	4	15	21
02-Jan-14	3	3	3	2	3	3	5	2	17	24
03-Jan-14	1	1	2	2	3	3	3	1	9	16
04-Jan-14	1	1	2	2	2	1	2	1	5	12
05-Jan-14	1	1	2	1	1	0	0	1	3	7
06-Jan-14	0	1	1	1	1	0	1	1	2	6
07-Jan-14	1	1	1	2	1	3	2	3	7	14
08-Jan-14	3	2	1	1	1	1	2	2	6	13
09-Jan-14	3	2	1	2	1	1	3	2	8	15
10-Jan-14	2	2	2	1	1	2	2	1	6	13
11-Jan-14	1	1	1	2	1	1	3	2	6	12
12-Jan-14	2	1	1	1	1	1	3	3	7	13
13-Jan-14	2	3	2	1	1	1	0	2	6	12
14-Jan-14	3	2	2	1	3	3	2	2	10	18
15-Jan-14	2	1	1	2	1	1	0	1	4	9
16-Jan-14	0	0	1	1	0	0	0	0	1	2
17-Jan-14	0	0	1	1	1	1	1	3	4	8
18-Jan-14	1	0	1	0	0	0	1	0	1	3
19-Jan-14	1	1	2	1	1	0	0	0	2	6
20-Jan-14	0	0	1	1	1	1	1	1	2	6
21-Jan-14	3	1	2	2	2	3	2	2	9	17
22-Jan-14	2	2	2	3	3	2	2	3	10	19
23-Jan-14	2	2	2	2	1	1	2	2	6	14
24-Jan-14	3	1	1	1	1	1	0	0	4	8
25-Jan-14	2	2	2	1	1	2	2	4	9	16
26-Jan-14	3	2	1	1	1	2	2	2	7	14
27-Jan-14	1	1	1	0	1	1	1	2	3	8
28-Jan-14	0	0	2	1	1	2	3	3	6	12
29-Jan-14	1	2	2	2	1	2	2	2	6	14
30-Jan-14	2	2	1	0	0	0	1	0	3	6
31-Jan-14	1	1	1	1	0	0	0	0	2	4
01-Feb-14	-	-	-	-	-	-	-	-	-	0
02-Feb-14	-	-	-	-	-	-	-	-	-	0

Table 1.

03-Feb-14	-	-	-	-	-	-	-	-	-	0
04-Feb-14	-	-	-	-	-	-	-	-	-	0
05-Feb-14	-	-	-	-	-	-	-	-	-	0
06-Feb-14	-	-	-	-	-	-	-	-	-	0
07-Feb-14	-	-	-	-	-	-	-	-	-	0
08-Feb-14	-	-	-	-	-	-	-	-	-	0
09-Feb-14	-	-	-	-	-	-	-	-	-	0
10-Feb-14	-	-	-	-	-	-	-	-	-	0
11-Feb-14	-	-	-	-	-	-	-	-	-	0
12-Feb-14	-	-	-	-	-	-	-	-	-	0
13-Feb-14	-	-	-	-	-	-	-	-	-	0
14-Feb-14	-	-	-	-	-	-	-	-	-	0
15-Feb-14	-	-	-	-	-	-	-	-	-	0
16-Feb-14	-	-	-	-	-	-	-	-	-	0
17-Feb-14	-	-	-	-	-	-	-	-	-	0
18-Feb-14	-	-	-	-	-	-	-	-	-	0
19-Feb-14	-	-	-	-	-	-	-	-	-	0
20-Feb-14	-	-	-	-	-	-	-	-	-	0
21-Feb-14	-	-	-	-	-	-	-	-	-	0
22-Feb-14	-	-	-	-	-	-	-	-	-	0
23-Feb-14	-	-	-	-	-	-	-	-	-	0
24-Feb-14	-	-	-	-	-	-	-	-	-	0
25-Feb-14	-	-	-	-	-	-	-	-	-	0
26-Feb-14	-	-	-	-	-	-	-	-	-	0
27-Feb-14	-	-	-	-	-	-	-	-	-	0
28-Feb-14	-	-	-	-	-	-	-	-	-	0
01-Mar-14	2	1	2	2	2	2	3	3	9	17
02-Mar-14	3	1	2	2	1	1	0	0	5	10
03-Mar-14	2	2	2	1	2	1	0	2	5	12
04-Mar-14	-	-	-	-	-	-	-	-	-	0
05-Mar-14	-	-	-	-	-	2	2	3	-	7
06-Mar-14	1	1	1	2	2	2	3	2	7	14
07-Mar-14	0	1	0	1	1	1	1	1	2	6
08-Mar-14	1	0	2	2	1	1	0	2	4	9
09-Mar-14	2	-	2	1	0	1	2	1	-	9
10-Mar-14	1	1	1	2	1	1	1	1	4	9
11-Mar-14	0	0	0	1	2	1	2	1	3	7
12-Mar-14	2	1	1	1	1	1	2	3	6	12
13-Mar-14	4	3	3	2	2	1	2	1	11	18
14-Mar-14	1	1	2	1	2	2	1	1	5	11

Table 1.

15-Mar-14	2	1	1	2	1	1	2	1	5	11
16-Mar-14	0	0	1	0	1	1	0	0	1	3
17-Mar-14	0	0	2	1	1	1	1	2	3	8
18-Mar-14	1	2	2	1	2	2	2	1	6	13
19-Mar-14	2	1	1	1	2	2	2	1	5	12
20-Mar-14	1	2	2	3	2	1	2	2	7	15
21-Mar-14	2	1	2	3	3	3	2	2	10	18
22-Mar-14	2	1	1	2	3	2	1	2	7	14
23-Mar-14	1	1	2	1	1	2	2	2	5	12
24-Mar-14	2	1	2	3	2	1	1	0	6	12
25-Mar-14	1	1	1	2	2	2	4	4	11	17
26-Mar-14	4	2	3	2	1	1	2	2	10	17
27-Mar-14	1	2	2	2	2	2	2	1	6	14
28-Mar-14	1	2	2	2	3	1	3	3	9	17
29-Mar-14	3	2	1	2	1	1	0	3	7	13
30-Mar-14	2	1	1	1	1	1	2	1	4	10
31-Mar-14	0	1	2	2	3	3	3	0	8	14
01-Apr-14	0	2	2	2	2	2	2	2	6	14
02-Apr-14	1	1	1	2	2	2	1	1	5	11
03-Apr-14	1	1	2	2	2	1	1	2	5	12
04-Apr-14	1	1	2	2	2	2	2	1	6	13
05-Apr-14	1	1	2	3	3	2	3	3	10	18
06-Apr-14	2	0	0	1	0	0	0	2	2	5
07-Apr-14	2	2	2	2	3	3	2	2	9	18
08-Apr-14	2	1	1	2	3	1	1	0	5	11
09-Apr-14	0	0	1	1	2	2	2	1	4	9
10-Apr-14	0	1	1	1	1	1	1	1	3	7
11-Apr-14	1	2	3	1	1	2	2	4	9	16
12-Apr-14	5	3	3	2	3	1	3	2	16	22
13-Apr-14	3	2	2	3	2	2	3	3	11	20
14-Apr-14	1	2	2	2	1	1	3	2	7	14
15-Apr-14	1	3	3	1	1	1	1	2	7	13
16-Apr-14	0	1	1	2	1	1	1	2	4	9
17-Apr-14	3	2	2	2	2	3	2	2	9	18
18-Apr-14	2	2	2	2	4	2	2	3	11	19
19-Apr-14	3	4	3	3	3	3	3	3	17	25
20-Apr-14	3	2	3	5	5	4	4	3	25	29
21-Apr-14	3	3	3	4	3	4	2	2	16	24
22-Apr-14	1	2	1	2	1	1	1	1	4	10
23-Apr-14	1	1	1	2	2	2	3	2	7	14

Table 1.

24-Apr-14	4	2	2	2	2	2	3	3	12	20
25-Apr-14	3	3	2	2	2	3	3	2	11	20
26-Apr-14	0	2	2	2	1	1	1	2	5	11
27-Apr-14	1	2	1	1	1	1	1	3	5	11
28-Apr-14	1	2	2	1	1	1	0	2	4	10
29-Apr-14	1	1	1	1	1	1	2	3	5	11
30-Apr-14	3	3	3	2	3	3	4	1	14	22
01-May-14	2	2	2	1	1	1	1	0	4	10
02-May-14	1	2	1	2	2	1	1	0	4	10
03-May-14	0	1	0	2	0	3	3	3	7	12
04-May-14	2	3	2	3	3	2	2	2	10	19
05-May-14	1	3	1	2	3	3	3	2	10	18
06-May-14	1	1	1	1	1	0	0	0	2	5
07-May-14	0	1	0	1	1	0	1	2	2	6
08-May-14	2	3	3	4	3	2	3	3	15	23
09-May-14	3	3	2	2	1	1	0	1	7	13
10-May-14	1	2	1	2	1	1	3	3	7	14
11-May-14	4	3	2	3	2	2	2	3	13	21
12-May-14	2	2	1	2	2	2	3	2	8	16
13-May-14	1	2	1	1	0	1	1	2	4	9
14-May-14	1	2	1	1	1	2	1	1	4	10
15-May-14	1	2	2	1	1	1	1	1	4	10
16-May-14	2	2	1	1	1	2	1	1	5	11
17-May-14	2	2	1	2	1	1	1	1	5	11
18-May-14	2	2	1	1	1	2	1	2	5	12
19-May-14	1	2	1	1	1	1	1	2	4	10
20-May-14	1	2	1	1	1	1	1	1	4	9
21-May-14	1	2	1	1	1	1	1	2	4	10
22-May-14	2	2	2	2	2	3	2	4	11	19
23-May-14	3	2	2	1	2	4	4	5	18	23
24-May-14	2	2	2	1	2	2	1	1	6	13
25-May-14	2	2	1	0	0	2	1	0	3	8
26-May-14	1	2	1	1	0	0	0	1	2	6
27-May-14	0	1	1	1	1	2	2	2	4	10
28-May-14	2	2	1	1	1	1	1	1	4	10
29-May-14	1	2	1	2	1	2	2	1	5	12
30-May-14	0	2	1	2	3	3	4	2	10	17
31-May-14	1	2	1	2	1	1	2	1	5	11
01-Jun-14	1	1	2	2	1	1	1	1	4	10
02-Jun-14	1	2	1	2	0	1	1	3	5	11

Table 1.

03-Jun-14	3	3	1	2	1	1	2	2	8	15
04-Jun-14	2	2	2	1	1	2	1	3	7	14
05-Jun-14	2	2	1	3	1	1	2	3	8	15
06-Jun-14	2	2	1	1	2	2	2	2	6	14
07-Jun-14	2	2	2	2	2	4	3	3	12	20
08-Jun-14	3	5	5	5	4	4	3	2	29	31
09-Jun-14	1	2	2	2	1	1	3	1	6	13
10-Jun-14	1	1	2	2	3	3	3	2	9	17
11-Jun-14	2	3	2	2	2	3	2	2	9	18
12-Jun-14	1	-	-	2	0	1	1	1	-	6
13-Jun-14	2	2	2	2	2	2	2	2	7	16
14-Jun-14	2	3	3	3	1	2	2	1	9	17
15-Jun-14	1	2	1	1	2	1	1	0	4	9
16-Jun-14	1	1	1	1	2	2	2	1	5	11
17-Jun-14	2	2	2	2	2	2	3	3	9	18
18-Jun-14	3	2	2	2	2	3	3	4	13	21
19-Jun-14	2	3	2	2	2	2	2	3	9	18
20-Jun-14	1	2	2	2	3	3	2	3	10	18
21-Jun-14	2	3	1	2	1	0	0	1	5	10
22-Jun-14	1	2	1	1	1	1	2	2	5	11
23-Jun-14	1	1	1	1	0	1	1	3	4	9
24-Jun-14	3	2	2	2	1	2	3	1	8	16
25-Jun-14	1	2	1	1	2	3	2	3	8	15
26-Jun-14	1	2	1	1	2	1	1	0	4	9
27-Jun-14	1	1	1	1	1	1	1	1	3	8
28-Jun-14	1	2	1	2	2	2	2	1	6	13
29-Jun-14	3	2	1	2	1	1	2	3	8	15
30-Jun-14	3	2	2	2	1	2	2	1	7	15
01-Jul-14	2	2	1	1	1	0	1	1	4	9
02-Jul-14	0	2	2	2	1	3	1	1	6	12
03-Jul-14	2	2	1	2	1	1	1	1	5	11
04-Jul-14	2	2	2	2	2	1	1	1	6	13
05-Jul-14	0	0	1	2	1	1	2	2	4	9
06-Jul-14	1	1	1	3	2	1	1	2	6	12
07-Jul-14	2	2	1	2	3	2	2	1	7	15
08-Jul-14	2	2	1	3	2	2	2	2	8	16
09-Jul-14	2	3	2	-	1	2	2	3	-	15
10-Jul-14	3	3	1	1	1	2	1	1	7	13
11-Jul-14	2	1	2	2	1	2	2	1	6	13
12-Jul-14	1	2	2	2	2	2	2	0	6	13

Table 1.

13-Jul-14	1	2	1	2	1	1	1	2	5	11
14-Jul-14	1	1	2	2	3	4	3	2	11	18
15-Jul-14	2	2	1	3	2	2	2	2	8	16
16-Jul-14	1	2	1	1	2	1	2	2	5	12
17-Jul-14	1	2	2	2	2	1	1	1	5	12
18-Jul-14	1	2	1	1	0	0	0	0	2	5
19-Jul-14	0	1	1	1	1	0	0	0	2	4
20-Jul-14	1	1	1	0	2	2	0	1	3	8
21-Jul-14	0	1	1	1	2	1	2	2	4	10
22-Jul-14	2	2	1	1	2	1	1	2	5	12
23-Jul-14	1	1	1	1	1	2	3	2	6	12
24-Jul-14	1	2	2	3	2	1	2	1	7	14
25-Jul-14	3	2	2	2	1	1	0	1	6	12
26-Jul-14	2	2	2	2	1	2	2	1	6	14
27-Jul-14	2	2	2	2	1	1	1	2	6	13
28-Jul-14	2	3	3	2	2	3	2	2	10	19
29-Jul-14	1	1	1	1	1	1	1	1	3	8
30-Jul-14	2	1	1	1	0	1	1	1	3	8
31-Jul-14	1	2	2	2	1	1	2	3	7	14
01-Aug-14	2	2	1	2	2	2	3	4	10	18
02-Aug-14	3	3	2	3	3	3	2	2	12	21
03-Aug-14	1	3	2	1	1	1	2	2	6	13
04-Aug-14	3	3	2	2	2	2	3	3	11	20
05-Aug-14	2	2	2	2	2	2	3	2	8	17
06-Aug-14	2	2	2	2	1	2	2	1	6	14
07-Aug-14	1	1	1	2	2	1	2	2	5	12
08-Aug-14	3	3	2	3	2	1	1	0	8	15
09-Aug-14	0	1	1	1	0	1	1	0	2	5
10-Aug-14	1	2	2	2	2	2	4	3	10	18
11-Aug-14	2	2	2	2	2	2	2	3	8	17
12-Aug-14	3	2	2	2	2	3	4	3	13	21
13-Aug-14	2	2	1	2	2	1	2	1	6	13
14-Aug-14	1	1	1	2	1	1	0	2	4	9
15-Aug-14	1	1	1	1	2	1	1	2	4	10
16-Aug-14	0	1	0	0	0	0	1	1	1	3
17-Aug-14	2	1	1	2	3	2	1	2	7	14
18-Aug-14	1	2	2	1	1	1	2	2	5	12
19-Aug-14	1	1	2	3	2	3	4	5	16	21
20-Aug-14	3	2	2	2	1	2	2	3	9	17
21-Aug-14	3	2	1	1	2	2	3	1	8	15

Table 1.

22-Aug-14	1	2	1	0	1	1	1	1	3	8
23-Aug-14	1	2	1	1	0	2	1	1	4	9
24-Aug-14	1	1	1	2	2	1	1	0	4	9
25-Aug-14	0	1	1	1	1	1	1	1	3	7
26-Aug-14	1	1	1	1	2	1	2	1	4	10
27-Aug-14	1	2	3	2	3	3	3	4	13	21
28-Aug-14	3	4	4	2	3	3	3	2	16	24
29-Aug-14	3	3	3	4	2	2	3	4	16	24
30-Aug-14	3	2	2	3	3	2	3	2	11	20
31-Aug-14	2	2	2	3	2	1	4	4	13	20
01-Sep-14	2	2	2	2	2	2	2	3	8	17
02-Sep-14	2	2	2	2	2	2	3	3	9	18
03-Sep-14	2	3	2	2	2	2	1	2	8	16
04-Sep-14	3	2	2	2	1	1	1	2	7	14
05-Sep-14	1	1	2	2	2	2	2	3	7	15
06-Sep-14	2	2	3	2	2	3	3	3	11	20
07-Sep-14	3	2	2	2	1	1	1	1	6	13
08-Sep-14	0	1	2	1	1	2	2	1	4	10
09-Sep-14	2	2	3	3	2	2	3	3	11	20
10-Sep-14	2	1	1	2	1	1	2	4	8	14
11-Sep-14	3	3	2	2	1	1	2	4	11	18
12-Sep-14	5	3	2	2	2	4	5	6	30	29
13-Sep-14	4	2	4	3	2	2	3	2	14	22
14-Sep-14	1	0	1	1	1	1	0	0	2	5
15-Sep-14	0	1	1	2	1	0	0	1	2	6
16-Sep-14	1	2	2	2	2	2	3	3	9	17
17-Sep-14	3	2	1	1	1	2	2	2	7	14
18-Sep-14	2	1	2	1	1	2	4	4	11	17
19-Sep-14	3	3	3	3	3	4	4	2	17	25
20-Sep-14	2	2	1	2	3	1	1	1	6	13
21-Sep-14	1	2	1	1	1	1	2	1	4	10
22-Sep-14	1	1	2	2	3	3	3	3	10	18
23-Sep-14	3	2	1	2	2	3	3	3	11	19
24-Sep-14	3	3	2	3	4	4	4	4	20	27
25-Sep-14	4	2	3	3	2	1	3	3	13	21
26-Sep-14	2	2	2	3	3	3	2	3	11	20
27-Sep-14	4	3	3	3	3	3	2	1	14	22
28-Sep-14	1	2	2	2	2	2	3	1	7	15
29-Sep-14	2	1	2	2	2	1	4	3	10	17
30-Sep-14	2	3	1	3	2	3	3	3	12	20

Table 1.

01-Oct-14	4	3	3	2	2	3	3	3	15	23
02-Oct-14	2	2	2	2	2	3	2	3	9	18
03-Oct-14	3	1	1	0	1	2	1	1	5	10
04-Oct-14	1	1	2	2	1	1	2	2	5	12
05-Oct-14	2	2	2	2	1	1	1	1	5	12
06-Oct-14	2	2	1	2	1	1	1	3	6	13
07-Oct-14	2	2	0	1	0	1	1	2	4	9
08-Oct-14	2	2	2	3	2	2	2	3	9	18
09-Oct-14	3	4	3	2	2	2	3	3	14	22
10-Oct-14	2	3	1	1	1	1	2	2	6	13
11-Oct-14	1	2	2	2	3	2	1	1	7	14
12-Oct-14	0	1	0	2	1	1	2	2	4	9
13-Oct-14	1	1	2	1	2	2	3	3	8	15
14-Oct-14	1	2	2	2	3	5	5	5	23	25
15-Oct-14	4	2	2	1	2	2	1	1	8	15
16-Oct-14	2	2	1	2	2	3	2	4	10	18
17-Oct-14	2	2	1	2	2	1	2	3	7	15
18-Oct-14	3	3	3	2	3	4	3	4	17	25
19-Oct-14	3	3	2	2	2	1	3	2	10	18
20-Oct-14	3	2	3	3	4	5	4	3	21	27
21-Oct-14	3	1	3	2	4	3	4	3	16	23
22-Oct-14	3	2	3	2	2	4	3	2	13	21
23-Oct-14	1	1	2	2	3	3	4	2	11	18
24-Oct-14	3	1	2	2	2	3	3	1	9	17
25-Oct-14	2	2	2	2	2	3	2	2	8	17
26-Oct-14	2	2	2	3	2	2	3	1	9	17
27-Oct-14	3	2	2	3	2	3	3	4	14	22
28-Oct-14	3	2	2	2	3	3	3	1	11	19
29-Oct-14	3	1	2	2	1	2	3	1	8	15
30-Oct-14	1	1	1	2	1	1	1	2	4	10
31-Oct-14	1	2	2	2	2	1	2	2	6	14
01-Nov-14	1	1	2	3	3	2	1	1	7	14
02-Nov-14	2	1	1	2	3	3	3	1	9	16
03-Nov-14	2	2	1	1	1	1	1	2	5	11
04-Nov-14	1	2	2	3	5	5	5	5	28	28
05-Nov-14	3	3	3	4	2	2	2	3	14	22
06-Nov-14	1	2	2	2	2	1	1	3	7	14
07-Nov-14	3	2	1	3	2	2	3	3	11	19
08-Nov-14	2	2	2	2	3	2	1	3	9	17
09-Nov-14	2	2	1	2	1	3	3	3	9	17

Table 1.

10-Nov-14	4	2	3	4	4	5	4	2	23	28
11-Nov-14	2	2	1	3	1	1	2	4	9	16
12-Nov-14	4	2	1	1	1	1	1	3	8	14
13-Nov-14	2	2	1	2	1	0	1	2	5	11
14-Nov-14	3	2	3	1	2	2	4	3	12	20
15-Nov-14	3	2	3	2	2	1	3	4	12	20
16-Nov-14	3	3	3	3	3	3	3	3	15	24
17-Nov-14	2	1	2	2	4	3	4	2	13	20
18-Nov-14	2	2	1	2	3	3	2	2	9	17
19-Nov-14	3	1	2	2	2	2	3	2	9	17
20-Nov-14	3	2	2	2	2	4	4	3	14	22
21-Nov-14	3	2	2	3	2	2	4	3	13	21
22-Nov-14	3	2	2	2	1	2	3	4	11	19
23-Nov-14	2	1	1	2	2	2	3	1	7	14
24-Nov-14	2	1	1	2	2	3	2	2	7	15
25-Nov-14	1	1	2	2	2	2	2	2	6	14
26-Nov-14	1	1	1	1	2	1	0	1	3	8
27-Nov-14	2	3	3	2	2	2	3	3	11	20
28-Nov-14	1	1	1	2	3	2	1	1	6	12
29-Nov-14	1	2	2	2	1	1	1	1	5	11
30-Nov-14	2	2	2	2	2	3	3	3	10	19
01-Dec-14	2	2	2	2	2	2	3	4	11	19
02-Dec-14	3	3	2	2	3	3	4	2	14	22
03-Dec-14	3	2	2	2	2	2	3	2	9	18
04-Dec-14	3	1	1	1	2	3	2	4	10	17
05-Dec-14	2	3	2	2	3	2	2	3	10	19
06-Dec-14	2	1	2	3	2	3	4	3	12	20
07-Dec-14	4	2	2	3	5	4	4	4	23	28
08-Dec-14	3	3	3	2	3	5	4	3	20	26
09-Dec-14	3	2	2	2	3	2	4	4	14	22
10-Dec-14	3	2	2	3	1	1	2	2	8	16
11-Dec-14	1	0	1	1	1	1	2	3	5	10
12-Dec-14	3	1	3	4	5	4	4	4	24	28
13-Dec-14	2	2	2	2	3	2	3	4	12	20
14-Dec-14	2	2	2	2	2	3	4	2	11	19
15-Dec-14	2	2	3	3	2	3	3	4	14	22
16-Dec-14	1	1	1	2	3	2	2	3	8	15
17-Dec-14	3	2	1	1	1	2	2	2	7	14
18-Dec-14	1	1	1	2	1	2	2	2	5	12
19-Dec-14	3	1	3	2	1	3	3	2	10	18

Table 1.

20-Dec-14	3	2	2	2	2	2	1	3	9	17
21-Dec-14	2	2	2	2	2	2	4	4	12	20
22-Dec-14	5	5	3	1	1	3	2	2	18	22
23-Dec-14	1	0	2	4	2	2	3	4	12	18
24-Dec-14	4	2	1	2	4	4	5	3	20	25
25-Dec-14	2	2	1	1	3	3	4	3	12	19
26-Dec-14	3	3	2	2	2	2	4	3	13	21
27-Dec-14	3	2	2	2	1	1	0	1	6	12
28-Dec-14	2	1	1	2	2	2	4	3	10	17
29-Dec-14	1	2	2	3	4	6	4	5	27	27
30-Dec-14	3	3	2	2	3	3	3	3	13	22
31-Dec-14	1	2	1	2	2	3	2	1	7	14

Definitive daily mean values of the Declination (D), Inclination (I), Horizontal (X and Y), and Vertical (Z) field components.

Presently, daily mean values are obtained from the hourly means (HMs) which in turn comes from the minute mean values (MMVs), based on the digital recordings of the three-component fluxgate magnetometer FGE. The baseline of this magnetometer is determined from absolute measurements with a DI-flux theodolite and an Overhauser proton magnetometer.

Positions of the Variation house where the three-component fluxgate magnetometer FGE is installed and the Absolute house where absolute geomagnetic measurements are performed are given in the Fig. 1.

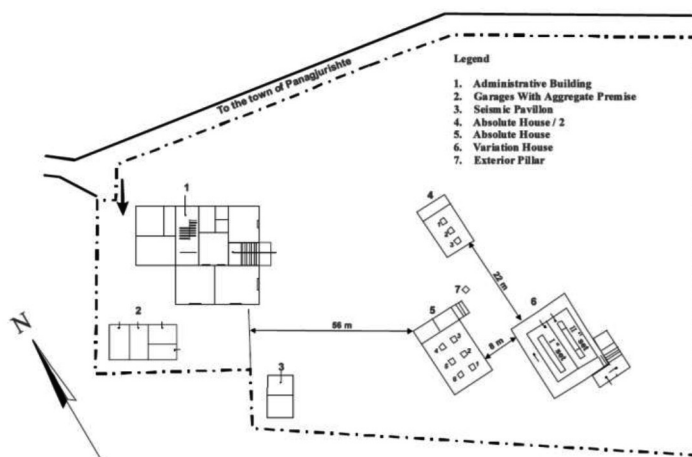


Fig. 1 Ground plan of the Panagyurishte observatory (after Kostov and Nozharov, 1987)

Before calculating of MMVs, inspection and verification of the reported data is performed. The reported data (available in near real time) are usually used in applications where the reliable representation of higher-frequency magnetic field variations is more important rather than absolute levels or secular variation. This concerns, e.g. the forecast of magnetic activity, radio-wave propagation, or space weather. In the case of reported data it is not possible to verify them prior to dissemination. Careful monitoring of the automatically transmitted data and the present-day computer technologies enable us to improve the quality of data and reduce the number of gaps in the records. After the quality control procedures have been applied to the 2014 reported data, we obtained the definitive minute mean values and calculated the HMs and DMVs. Due to technical problems there are gaps in the data records in February and March.

Daily mean values of the Declination (D), Inclination (I), Horizontal (X and Y), and Vertical (Z) field components for 2014 are plotted in the next figures:

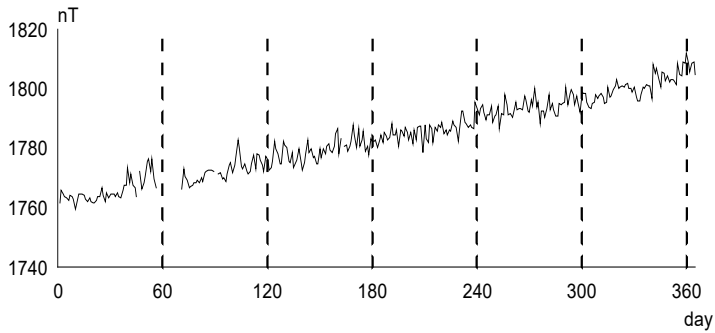


Fig. 2. Plot of the daily mean values of the **Declination (D)** registered in PAG observatory in 2014.

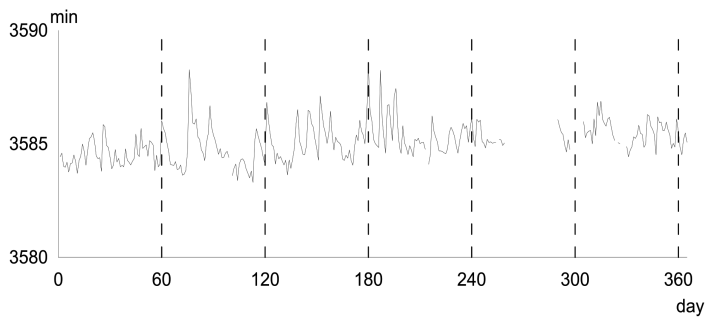


Fig. 3. Plot of the daily mean values of the **Inclination (I)** registered in PAG observatory in 2014.

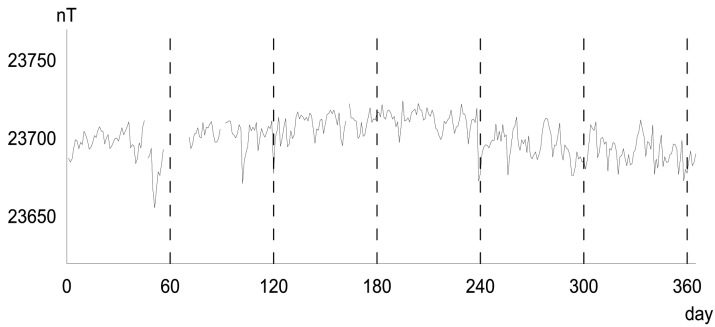


Fig. 4. Plot of the daily mean values of the **North geomagnetic field component (X)** registered in PAG observatory in 2014.

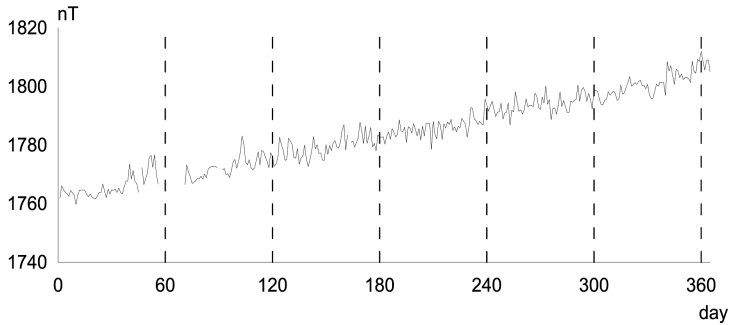


Fig. 5. Plot of the daily mean values of the **East geomagnetic field component (Y)** registered in PAG observatory in 2014.

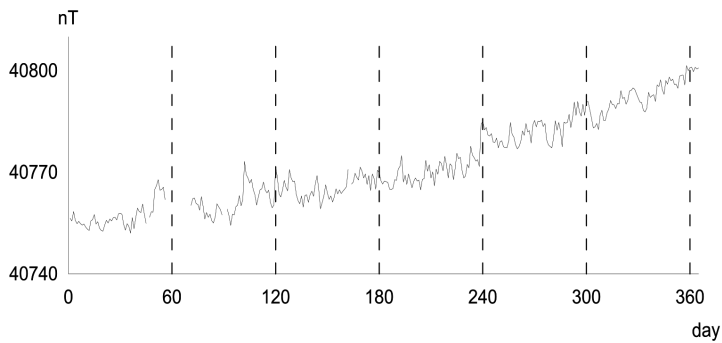


Fig. 6. Plot of the daily mean values of the **Vertical geomagnetic field component (Z)** registered in PAG observatory in 2014

Conclusions

Continuous registration of the geomagnetic field components gives the sum of all field contributions from the internal and external to the Earth sources. A straightforward separation of the individual contributions is impossible and many scientific studies deal with different aspects of this problem (Mandea and Korte, 2010). Approximate description of the strength of different external variations however, are provided by geomagnetic indices. A quantitative measure of 2014 local geomagnetic activity in the form of 3 hour K -index is published here, based upon the range of fluctuations in the PAG observatory records. Table 1 shows that 2014 has relatively quiet geomagnetic field with only 18 disturbed days. The most active period is recorded in December 2014 with 6 days having K -index ≥ 5 and 1 with $K=6$. Annual variations of the geomagnetic field components are plotted in form of daily mean values. Due to technical reasons records are missing for February. Data are checked and verified according to IAGA requirements (Jankowski and Sucksdorff, 1996).

References

- Buchvarov I., 2006. Field and observatory geomagnetic measurements in Bulgaria. in Rasson and Delipetrov (eds.) *Geomagnetics for Aeronautical Safety*, Springer, p.61-62
- Jankowski J., Sucksdorff C., 1996. *Guide for magnetic measurements and observatory practice.*, International Association of Geomagnetism and Aeronomy, Warsaw, Poland.
- Kostov K. and P. Nozharov, Absolute magnetic measurements in Bulgaria 1787-1997, Sofia, 1987, pp.72
- Mandea M., Korte M. (eds), 2010 *Geomagnetic observation and models*, IAGA Special Sopron Book Series 5, Springer.
- Sucksdorff, C., Pirjola, R. and Häkkinen, L., 1991. Computer production of K -values based on linear elimination, *Geophysical Transactions*, 36, 333-345

Годишен доклад за наблюдаваната геомагнитна активност в Обсерватория Панагюрище през 2014

М. Методиев, П. Трифонова

Резюме: Понастоящем, в ерата на интернет комуникациите, записите от геомагнитните обсерватории се предоставят на заинтересованите потребители почти в реално време, докато обработените времеви серии (окончателни данни) са обект на много проверки и се разпространяват с месеци закъснение. Статията представя дефинитивните геомагнитни данни, получени в Обсерватория Панагюрище през 2014 г., дадени под формата на локални геомагнитни индекси и графики на среднодневните стойности на компонентите на магнитното поле.

ANALYSIS OF MONTHLY SEA LEVEL DATA FROM VARNA TIDE GAUGE STATION

A. Ivanov, I. Georgiev, N. Dimitrov

National Institute of Geophysics, Geodesy and Geography, Bulgarian Academy of Sciences, Acad.
G. Bonchev Str., bl. 3, Sofia1113, Bulgaria, e-mail: anton_iv66@abv.bg

DOI: 10.34975/bgj-2019.42.7

Abstract. Climate changes and global warming are assume for main reasons of constant sea level rise. Survey methods such as altimetric measurements are essential for determining global processes related to sea level change, but the regional and local changes are also important. In this paper regional sea level changes at tide gauge station Varna at Black sea coast are analyzed. Single spectrum analysis is use to analyze the monthly sea level data for the period 1929-2019. The sea level trend, long term tidal constituents - amplitudes and phases, are estimated. The results clearly indicate positive mean sea level trend with value of 1.2 ± 0.1 mm/yr.

Key words: mean sea level, tide gauge, radar

Introduction

Climate changes and global warming are the cause of sea level rise during the 20th century of about 2 mm per year. The sea level researches are useful not only to forecast cataclysms and sea level rising, but also in connection with interdisciplinary studies exploring the causes of this change. Climate changes and global warming are supposed to be the main reasons of the constant sea level rise. The regional sea level changes are determine by tide gauge measurements and satellite altimetry is use to investigate global sea level changes. Mean sea level changes are important for geodesy and geophysics. The mean sea level for a long time periods was used in the past to define the height systems. It is an important component in determining the geoid. Tide gauge measurements are important for realizing the worldwide Unified Global Height System (UGHS) of the Global Geodetic Observing System (GGOS) initiative.

Methods and Theory

In this study, monthly sea level data from Varna tide gauge at the Northern Black Sea coast is used. The data period covers the time interval from year 1929 to year 2019 and the daily registrations are aggregate in average monthly sea level values. The methods used to analysis of Time series are Single Spectrum Analysis (SSA), regression and Fourier analysis. The method used for decomposition the time series to trend, periodic components and noise is call Single Spectrum Analysis. The method involves two stages: decomposition and restoration of the time series. The decomposition of the time series involves two sub-stages - the construction of a trajectory matrix and the Singular Value Decomposition (SVD) - the decomposition of single vectors and the restoration of the time series - grouping and diagonal averaging (Golyandina, et al., 2001). Regression analysis is use to solve for the mean sea level and trend and the Fourier analysis - to solve for the periodical constituents.

Data processing

The observations of sea level at tide gauge station Varna has started in 1928. From 1928 until 2013 the tide gauge was of mechanical type - stilling well gauges „A.Ott” Kempten. In 2013 a new radar tide gauge, type Vega Puls S60, is installed above water level in the draw well (Fig. 1). The new radar tide gauge system emits short microwave pulses with frequencies about 18 – 27 GHz in the direction of the surface water, they are reflected and received back. Accuracy of measurements is about 5mm and observations interval is set to one second.



Fig. 1. Radar Tide gauge Vega plus from Varna tide station

Observations are stored in a signal conditioning instrument and can be shown in a web browser in a real time (<http://niggg.bas.bg/wp-content/uploads/2014/02/mare/text.html>). The two data sets are brought to one and the same “zero” point by precise leveling through the Tide Gauge Bench Mark. Data gaps (missing observations) are filled in with the Caterpillar SSA MV software using PI Projection method with sequential filling (Golyandina, and Osipov, 2007).

All data are corrected for the vertical crustal motion obtained by repeated levelling measurements started in 1928. Old data are converted to European Vertical Reference System (EVRS), EVRF2007 (Earth Vertical Reference Frame 2007). The average monthly sea level values are analyzed by the SSA method. The time series are decomposed into separate sub-series, which represent the influence of mean sea level, trend and tidal influences. Significant harmonic constituents are determined by spectrogram analysis. A model comprising the above-mentioned parameters is compiled. The values obtained from the model are compared with the measurements. The residuals of the model are examined for autocorrelation and spectral analysis of the model residuals is performed. The resulting amplitude – Arms, is determined and is used to calculate the Signal to Noise Ratio (SNR). Significant tidal effects are supposed to be these with $SNR > 2$.

The mean sea level and trend are determined by regression analysis of the time series determined by the previous SSA analysis. The Fourier analysis is used to determine the amplitudes and phases of all significant tidal influences from the model determined by SSA analysis. The mean sea level, trend and long term tidal constituents, amplitudes and phases, are estimated. The results clearly indicates positive mean sea level trend with value of 1.2 ± 0.1 mm/yr. Figure 2 shows the mean sea level and the model. Gray curve shows the average monthly sea level values, black curve is shown the model and the trend is represented by the line. The resulting average sea level for the period 1929 - 2019 is 2.8 ± 0.1 cm in EVRF2007.

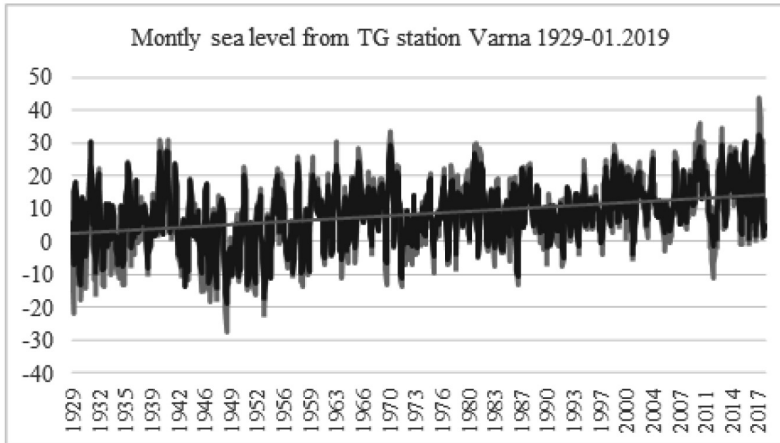


Fig. 2. Monthly seal level data for period 1929-2019 (gray sea level, black model, line is trend)

The model residuals are plotted on Fig. 3. Residual data of the harmonic constituents are analyzed by Fourier analysis. The harmonic influences with major impact at residuals series are given in Table 1. In the table are presented ten of them with the highest amplitudes. The resulting amplitude calculated with the coefficients specified

in the table is 0.7 cm, the mean value of the order of the residuals is 0.45 cm and the standard deviation - 3.4 cm. The resulting amplitudes of the residuals series and Signal to Noise Ratio (SNR) coefficients are computed and shown in Table 2. SNR is computed as a square of amplitudes ratio first from signal and second from noise – Arms. The annual and semi-annual variations, as expected, have the greatest impact with amplitudes of 6.7 cm and 1.4 cm. Table 2 shows also a tide with a periodicity close to 18.6 years with amplitude of 1.3 cm. The value of the tide with period of 14.4 is similar to that of the nodal tide.

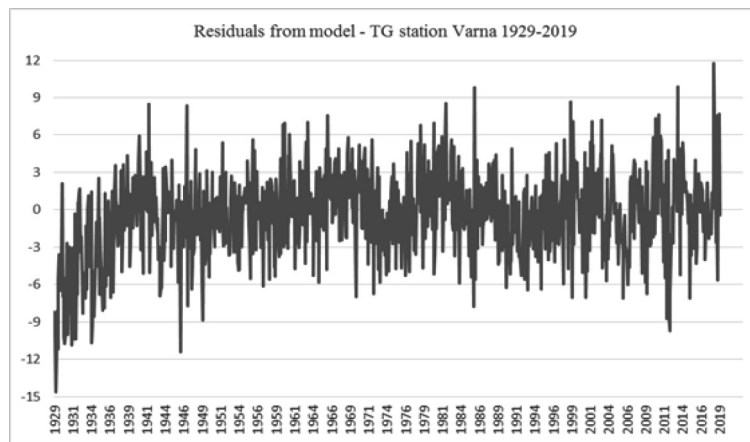


Fig. 3. Residuals from analysis

Table 1. Harmonic influences with major impact at residuals series.

Frequency	Period [mont]	Cosine coef [cm]	Sine coef [cm]	Amplitudes [cm]
0.0009	1080.0	-1.0	0.7	1.23
0.0056	180.0	-0.5	-0.8	0.98
0.0037	270.0	-0.7	-0.1	0.70
0.0639	15.7	-0.4	-0.4	0.58
0.0046	216.0	0.1	-0.5	0.52
0.0306	32.7	0.2	-0.5	0.52
0.0028	360.0	-0.5	-0.1	0.52
0.0120	83.1	-0.3	-0.4	0.47
0.0213	47.0	0.2	-0.4	0.46

Table 2. Solved for parameters from the model.

Frequency	Period [mont]	Cosine coef [cm]	Sine coef [cm]	Amplitudes [cm]	Phases [°]	SNR
0.08333	12.0	-3.42	5.76	6.70	300.67	91.5
0.16667	6.0	1.30	-0.49	1.39	159.42	3.9
0.08426	11.9	-0.75	-0.97	1.22	232.25	3.1
0.02222	45.0	1.30	0.55	1.41	23.01	4.1
0.02315	43.2	-1.31	0.24	1.33	349.64	3.6
0.06944	14.4	-0.92	0.77	1.20	320.32	2.9
0.01667	60.0	-0.94	0.62	1.12	326.65	2.6
0.00429	233.0	-1.26	0.47	1.34	339.37	3.7

Conclusions

The analysis of tide gauge data for 90 years clearly indicates annual, semiannual and decadal variations of the mean sea level. The estimated mean sea level is 2.8 ± 0.1 cm with trend of 1.2 ± 0.1 mm/yr. The SSA analysis is helpful to identify and allocate the mean sea level, trend and harmonic influences in the monthly data. Five long term periodical variations with amplitudes greater than 1 cm are observed in the time series data. The annual and semi-annual variations, as expected, have the greatest impact with amplitudes of 6.7 cm and 1.4 cm. The long period variation of about 233 months (19.4 years) can be associated with the nodal tide with period (18.61 years) in the mean sea level. The tide gauge registration from the radar equipment will give the opportunity to resolve the short term harmonic constituents and the relatively long 90 years data will be valuable contribution for realizing the Unified Global Height System.

Acknowledgments. Presentation of this work is supported by Contract No D01-161/28.08.2018 (Project “National Geoinformation Center (NGIC)” financed by the National Roadmap for Scientific Infrastructure 2017-2023.

References

- Golyandina N., Nekrutkin V., and Zhigljavsky A(2001). Analysis of Time Series Structure: SSA and Related Techniques. London: Chapman & Hall/CRC., 305 p.
- Golyandina, N. and Osipov, E. The “Caterpillar” - SSA method for analysis of time series with missing values. Journal of Statistical Planning and Inference 13. 2007, pp2642 – 2653p.

Анализ на средномесечни стойности на морското ниво от мареографна станция Варна

А. Иванов, И. Георгиев, Н. Димитров

Резюме. Предполага се че климатичните промени и глобалното затопляне са основните причини за покачването на морското ниво. Методи за наблюдения като алтиметричните измервания са от изключително значение за определяне на глобалните процеси свързани с изменението на морското ниво, но регионални и локални изменения също са много важни. В тази статия са анализирани регионални изменения на морското ниво от мареографна станция Варна на Черноморското крайбрежие. Използван е анализ на единичния спектър за средномесечни стойности за периода 1929 – 2019 година. Определени са трендът на морското ниво, сезонни вариации и дългопериодични влияния, амплитуди и фази. Резултатите показват положителен тренд на средното морско ниво със стойност от 1.2 ± 0.1 mm/y.

FORTY YEARS NATIONAL OPERATIVE TELEMETRIC SYSTEM FOR SEISMOLOGICAL INFORMATION

L. Christoskov, L. Dimitrova, D. Solakov, S. Simeonova

National Institute of Geophysics, Geodesy and Geography, Bulgarian Academy of Sciences, Acad. G. Bonchev Str., bl. 3, Sofia 1113, Bulgaria, e-mail: lidim@geophys.bas.bg

DOI: 10.34975/bgj-2019.42.8

Abstract. National Operative Telemetric System for Seismological Information (NOTS-SI) is operating since 1980. At the beginning, the real-time data transfer from the stations to the data center was organized through analog telephone lines and earthquake parameters were evaluated manually. In 2006 both the seismological network and the data center were upgraded with state-of-the-art digital equipment and automatic data processing was organized. More than 12 TB processed and raw data are archived during the last 12 years in PASSCAL, mini SEED continues data formats and in event oriented CSS format. The data completeness exceeds 99% and the rare loss of data is mainly due to communication outages. The maintenance of the network and the data center is organized in such a manner that the upgrade of the equipment and the software updates do not affect the performance of the Operating Center. During the last 12 years the number of seismic stations increased significantly and at the end of 2019 it is 40. Currently the seismic center is upgraded with software for acquisition and automatic data processing SeisComP3 that is widely used in seismological community and data centers.

Key words: National Operative Telemetric System for Seismological Information, Bulgarian Seismological Network, Seismic Data Centre, SeisComP3

Introduction

Bulgaria is an earthquake prone country. Over the past centuries, Bulgaria has experienced strong earthquakes. The first well documented earthquake on the territory of Bulgaria is the 1st c BC quake occurred in the Black Sea near the town of Kavarna. In historical aspect, it is worth to mention the 1818 (8-9 MSK) and the 1858 (MS=6.3, I0=9 MSK) earthquakes occurred near the city of Sofia. Some of the Europe's strongest 20th century earthquakes occurred in Bulgaria (at the beginning of the 20th century from 1901 to 1928 five earthquakes with magnitude larger than or equal to 7.0 occurred on the territory of

Bulgaria) – 30.03.1901 Shabla earthquake with magnitude $M_s=7.2$; 04.04.1904 Kresna earthquakes with M_s magnitudes 7.1 and 7.8, 14.6.1913 G. Orjahovitsa earthquake with magnitude $M_s=7.0$ and two earthquakes near the city of Plovdiv in 1928 - 14.04 with magnitude $M_s=6.8$ and 18.04 with magnitude $M_s=7.0$.

The seismological observations on the territory of Bulgaria have traditions of more than 120 years. The beginning of Bulgarian seismology dates back to 1891. At that time Spas Watzof, the director of Central Meteorological Station in Sofia, organized network of correspondents for observation of felt earthquakes in Bulgaria (Watzof, 1902). Watzof formed a proto-type of macro-seismic bulletin (Christoskov, 2007) containing: time of perceived shaking, locality, direction of impact, observed effects, intensity assessed by Rossi-Forel scale till 1912 and Forel-Mercalli since then. The first bulletin including data for Central Balkan earthquakes occurred in the 19th century was published in 1902 (Watzof, 1902). Afterwards, the bulletins have been published yearly up to 1959.

The period of Bulgarian historical era ends in 1905 when the seismograph of Omori-Boch type was installed in the first Seismological Station in the town of Sofia. The same year four seismoscopes of Agamenonne type were installed in Sofia, Petrohan, Rila monastery and the town of Kazanlak.

In the period 1961-1979, six seismic stations were run. These are stations in Dimitrovgrad, Pavlikeni, Musomishta, Kardjali, Preselentsi and Vitosha (DIM, PVL,MMB, KDZ, PSN and VTS). The strong 1977 Vrancea (Romania) intermediate depth earthquake with seismic moment magnitude $M_w=7.4-7.5$ and its negative impact on the territory of the northern Bulgaria (loss of human lives and destroyed properties) force the development of a new strategy for monitoring and investigation of the seismicity in Bulgaria and surroundings (Samardjiev et al., 1980). At the end of 1980 the National Operative Telemetric System for Seismological Information was put in operation. It was a key point in seismic monitoring in Bulgaria. The major tasks of NOTSSI are:

- To provide reliable continuous recording and transfer of seismological data;
- To ensure rapid notification of the governmental authorities, media and broad public in case of felt or damaging earthquakes on the territory of Bulgaria;
- To provide a modern basis for seismological studies in Bulgaria.

NOTSSI was a part of the Geophysical Institute (GPhI) of the Bulgarian Academy of Science (BAS) up to 2010 and of the National Institute of Geophysics, Geodesy and Geography (NIGGG) of BAS after that.

Analogue Seismological Network and Data Center

At the beginning, NOTSSI operated with 6 seismic stations. Over the next two decades, the seismic network was developed and new stations were run. At the end of the last century NOTSSI consisted of 21 short period one component seismic stations deployed on the territory of the country (Christoskov et al., 2012). The analogue information from all stations was transferred in real time mode by telephone lines to the Seismological Data Center of NOTSSI at the Geophysical Institute. Seismic data were visualized on paper drums with two levels of amplification to achieve larger dynamic range of the

records. An automated processing system based on a PDP 11/34 mini-machine was built at the Data center in 1981. Analog signals were digitized and processed in near real time and an archive of detected and localized seismic events was created.

In routine practice the main parameters of the earthquakes were estimated manually using S minus P time differences. The wave amplitudes and signal duration were used for magnitude evaluation.

Later the DHypo computer code (Solakov and Dobrev, 1987) was involved in the seismological practice. The input information for the calculation of the earthquake parameters are the P and/or S onsets, the maximum amplitude of the P and/or S phases and/or signal duration.

Digital Seismological Network

Modernization and digital upgrading of NOTSSI started in 1996. First, station Vitosha (VTS, since 1979) was included in the MEDNET network (within international project “PLATO-1”) and was updated with VBB seismometer STS-1 and Quanterra 380 DAS (Christoskov et al., 1996).

In the period 2001-2004, with the financial support of the Permanent Commission for Prevention of the Population from Natural Disasters and Catastrophes and in the frame of the European project MEREDIAN-2, two digital stations (Plovdiv (PLD) and Yambol (JMB)) were put in operation. A digital real-time data communication between the three digital stations – VTS, PLD and JMB and the Data Center at the Geophysical Institute in Sofia was created. A real-time data exchange with international (MEDNET, ORFEUS-European Center for Digital Seismological Data, NEIC etc.) and regional seismological centers (Austria, Slovenia, Czech Republic, Romania, etc.) was established. Bulgaria becomes a part of the European and world digital seismological data structures.

At the end of 2005, by the financial support of the former Ministry of Emergency Situations, digital equipment and software were purchased from the company “Refraction Technology” Inc. (<http://reftek.com>). In 2006 the digital seismological equipment was installed at all stations of the network and a data center with real-time automatic and interactive data processing was organized.

During the next 12 years the number of seismic stations increased thanks to several projects with NPP “Kozloduy” PLC, National Scientific Fund and the financial support of the National Institute of Geophysics, Geodesy and Geography. At the end of 2019 the number of the seismic stations of the National Seismic Network and the two Local Seismological Networks - “Provadya” and “Kozloduy” is 25 (Table 1). After 2012 in the frame of trans-regional project “Danube Cross-border system for Earthquakes Alert (DA-CEA)” was installed fifteen stations on the territory of the North Bulgaria and is operated by NOTSSI (Table 2). These stations are part of Bulgarian Romanian trans-border Early Warning System.

In Tables 1 and 2 are presented lists of seismic stations, seismological equipment and data recording information of the Bulgarian seismological network with following parameters:

Table 1. Seismic stations of the National Seismic Network and Local Seismological Network – LSM “Kozloduy” and LSM “Provadya” and their equipment

Station Name	BG Code	INT Code	Lat(°) N	Long(°) E	Elev [m]	Seismometer Accelerometer	Components	Data acquisit. system/ sampling rate
Dimitrovgrad	DIM	DIM	42.04	25.58	144	S-13	3C	Reftek 130-01/ 100 sps
Yambol	JMB	JMB	42.49	26.53	210	GMT-40T/30s <i>131A-02/3</i>	3C	Reftek 130-01/ 100 sps
Kurdzhali	KDZ	KDZ	41.63	25.34	335	3ESPC/120s	3C	Reftek 130-01/ 100 sps
Krupnik	KKB	KKB	41.84	23.13	439	GMT-40T/30s <i>131A-02/3</i>	3C	Reftek 130-01/ 100 sps
Musomishta	MMB	MMB	41.55	23.75	632	STS2 <i>131A-02/3</i>	3C	Reftek 130-01/ 100 sps
Panagyurishte	PGB	PGB	42.51	24.17	574	GMT-40T/30s	3C	Reftek 130-01/ 100 sps
Plovdiv	PLD	PLD	42.15	24.75	198	GMT-40T/30s	3C	Reftek 130-01/ 100 sps
Provadya	PRD	PRD	43.16	27.41	120	GMT-40T/30s	3C	Reftek 130-01/ 100 sps
Preselentsi	PSN	PSN	43.64	28.13	185	KS 2000/60s <i>131A-02/3</i>	3C	Reftek 130-01/ 100 sps
Pavlikeni	PVL	PVL	43.12	25.17	218	3ESPC/120s <i>131A-02/3</i>	3C	Reftek 130-01/ 100 sps
Rozhen	RZN	RZN	41.69	24.74	1735	GMT-40T/30s	3C	Reftek 130-01/ 100 sps
Sofia	SOF	SOF	42.68	23.37	570	S-13	3C	Reftek 130-01/ 100 sps
Strazhitsa	SZH	SZH	43.26	25.98	331	3ESPC/60s <i>131A-02/3</i>	3C	Reftek 130-01/ 100 sps
Vitosha	VTS	VTS	42.61	23.23	1390	3ESPC/120s <i>131A-02/3</i>	3C	Reftek 130-01/ 100 sps
Malo Peshtene	MPE	MPEP	43.36	23.74	344	RefTek 151/120s S13	3C, 1C	Reftek 130-01/ 100 sps
Plana	PLN	PLNA	42.48	23.42	1245	3ESPC/120s <i>131A-02/3</i>	3C	Reftek 130-01/ 100 sps
Tran	TRAN	TRAN	42.83	22.65	706	RefTek 151/30s <i>147-01/3</i>	3C	Reftek 130-01/ 100 sps
Oriahovo	ORH		43.73	23.97	231	S-13	3C	Reftek 130-01/ 100 sps
Valchedram	VLD	VALD	43.69	23.43	93	S-13 -Borehole	1C	Reftek 130-01/ 100 sps
Avren	AVR	AVR	43.12	27.67	306	Geophone GS 11D	3C	Reftek 130-01/ 100 sps
Roiak	ROIA	ROIA	43.09	27.38	356	Geophone GS 11D	3C	Reftek 130-01/ 100 sps
Bozvelijsko	BOZ		43.10	27.48	37	Geophone GS 11D	3C	Reftek 130-01/ 100 sps
Dobrina	DOB		43.18	27.46	230	Geophone GS 11D	3C	Reftek 130-01/ 100 sps
Nevsha	NEF	NEF	43.26	27.27	359	S-13	3C	Reftek 130-01/ 100 sps
Balsha	BLSH	BLSH	42.86	23.28	739	Reftek151B/30s	3C	Reftek 130-01/ 100 sps

Station name – the name of the nearest settlement where the station is located to;

Code – the unique international code of the station;

Lat,N, Long,E, Elev,m – geographic coordinate and elevation of the station;

Seismometer/Accelerometer – the type of sensors installed. Seismometers are installed in several stations, in others – seismometers and accelerometers; and the last 7 stations mentioned in the table 2 are equipped with accelerometers EpiSensor;

Component – the type of data registration – 3 components (Z, NS, EW) or 1 component (Z);

Data acquisition system/ sampling rate – the type of digitizer and the sampling rate of the real-time transferring data;

Real-time data transfer is realized via Virtual Private Network (VPN) of the Bulgarian Telecommunication Company (BTC).

The Bulgarian Seismological Network has international code *BS* and *Digital Object Identifier (DOI)*: 10.7914/SN/BS (<https://doi.org/10.7914/SN/BS>).

Table 2. DACEA seismic stations on the territory of the North Bulgaria and their equipment

Station Name	Code	Lat(° N	Long(° E	Elev [m]	Seismometer Accelerometer	Compo nents	Data acquisit. system/ sampling rate
Belogradchik	BLKB	43.62	22.67	650	KS2000 <i>EpiSensor</i>	3C	Bazalt
Pleven	PLVB	43.39	24.62	199	KS2000 <i>EpiSensor</i>	3C	Bazalt
Loznitsa	LOZB	43.37	26.59	342	KS2000 <i>EpiSensor</i>	3C	Bazalt
Razgrad	RAZG	43.57	26.508	383	KS2000 <i>EpiSensor</i>	3C	Bazalt
Shabla	SHAB	43.54	28.60	430	KS2000 <i>EpiSensor</i>	3C	Bazalt
Elena	ELND	42.93	25.87	334	KS2000 <i>EpiSensor</i>	3C	Bazalt
Kubrat	KUBB	43.80	26.49	261	KS2000 <i>EpiSensor</i>	3C	Bazalt
Balgarevo	KALB	43.40	28.43	121	KS2000 <i>EpiSensor</i>	3C	Bazalt
Dobrich	DOBAM	43.58	27.83	246	<i>EpiSensor</i>	3C	Bazalt
Montana	MNNAM	43.41	23.23	240	<i>EpiSensor</i>	3C	Bazalt
Vidin	PLVAM	43.95	22.85	880	<i>EpiSensor</i>	3C	Bazalt
Belene	RAZAM	43.64	25.12	820	<i>EpiSensor</i>	3C	Bazalt
Ruse	RUSAM	43.85	25.96	100	<i>EpiSensor</i>	3C	Bazalt
Silistra	SILAM	44.10	27.27	840	<i>EpiSensor</i>	3C	Bazalt
Veliko Tarnovo	VETAM	43.08	25.64	224	<i>EpiSensor</i>	3C	Bazalt

The location of all seismic stations of the Bulgarian seismological network is presented in Fig. 1.

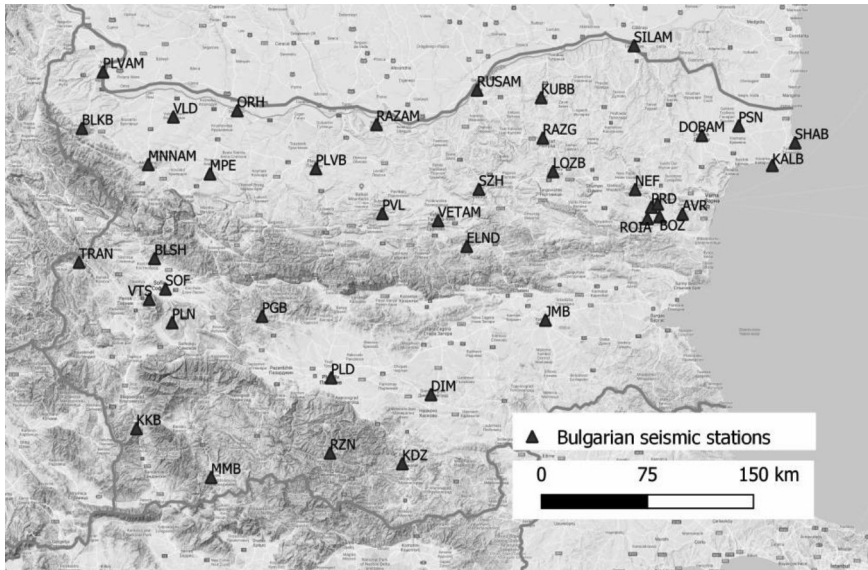


Fig. 1. Map of the seismic stations of Bulgarian Seismological Network

Data Centre

The Data Centre is equipped with Seismic Network Data Processor Software (SNDP) (Haikin and Kushnir, 2005) which provides real-time data acquisition, automatic processing and interactive analysis of the seismological data registered by the stations of National Seismological Network and number of stations from neighbor countries. The SNDP is a set of asynchronous interactions of many processes. The Continuous seismic data receiving process is designed to receive and store the incoming data in a 7-day disk loop buffer. It ensures access to stored data for all client processes working both in automatic and interactive modes. The Real-time detection is carried out independently for each station and determines signal to noise ratio (SNR), frequency band of detection and the onset time. The detection is implemented by adaptive broadband and traditional STA/LTA detectors in several narrow frequency bands. The Estimator process reveals seismic phases of detected signals estimate their parameters and identify their types. The Estimator sends a message to the process of association and location of seismic source. The Associator of phases and locator of seismic sources associate the estimated phases to a seismic source by method of node sorting and minimization of residuals. Daily bulletins with the coordinates and parameters of seismic event, and its associated phases are produced as results from the automatic data processing. The geographic coordinates of the seismic events are drawn on a map and published in real-time.

The real-time seismic data are fed into the automatic data processing by two protocols – RTPD and SeedLink. RTPD protocol acquires the data recorded by the 25-th seismic stations all over the country (Table 1) and the SeedLink – the DACEA seismic stations in the North Bulgaria. SeedLink protocol is used for data exchange with the seismic centers of the neighbor countries and various International Data Centers.

During the last 12 years the seismological equipment and processing software have been periodically upgraded with the latest releases. The upgrade procedures have never affected the performance of the Network and the Data Centre due to both the high professional skill of the maintenance staff and the excellent organized support services.

More than 12 TB processed and raw data have been archived during the last 12 years in PASSCAL and mini SEED continues data formats and in event oriented CSS format. The data completeness exceeds 99% and the loss of data in rare cases was mainly due to communication outages.

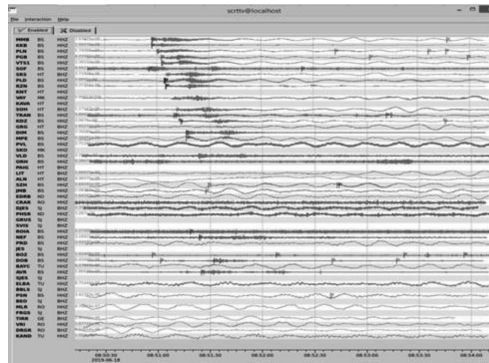
Current state of the Data Centre

Currently, the National Data Centre is upgraded with SeisComPro software for automatic data processing that is widely used in seismological community and data centers. SeisComPro is developed by German company Gempa (<https://gempa.de>). The software is an extension to SeisComP3 community package distributed by GFZ Potsdam. The main features provided by the SeisComp3 package are: *data acquisition, quality control and recording; real-time data processing and exchange; network status monitoring; automatic and interactive event detection and location; event parameter archiving; easy access to relevant information about stations, waveforms and recent earthquakes.*

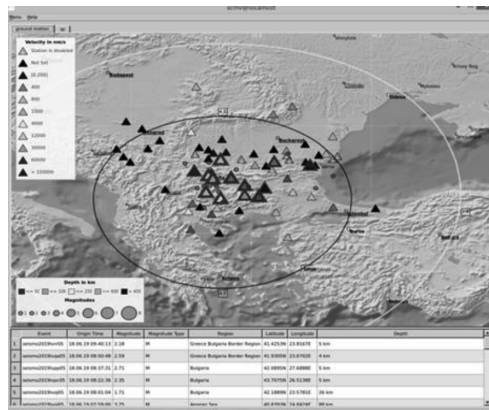
The SeisComPro is developed in order to improve the local earthquake and microseismicity monitoring. To upgrade the National Data Center we have installed free SeisComP3 software package as a base and three commercial modules of the SeisComP Pro.

The module *scanloc* is developed to monitor the natural and induced seismicity within the both small and large seismic networks. The module uses a cluster search algorithm to associate P phase detections to one or many potential earthquake sources. In a second step S-phases are also associated and used for earthquake location. Fig. 2 represents three steps of the execution of the scanloc procedure – real-time automatic P-phase picking (upper left), waveform propagation after event detection (upper right) and automatic event location parameters (down left).

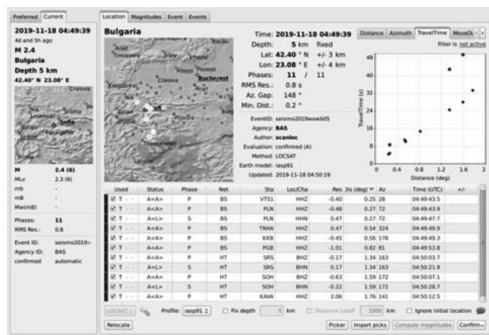
The module *sceval* is designed to evaluate the event locations produced by the scanloc module (fig. 3). It automatically discriminates real earthquakes from fake solutions and marks them even if they are very weak. Such a way the monitoring system can be tuned not to miss small events.



a



b



c

Fig 2. The execution of the scanloc module: a – Upper left picture - Automating P–phase picking; b – Upper right picture - Waveform propagation after event detection; c – Down left picture - Automatic event location

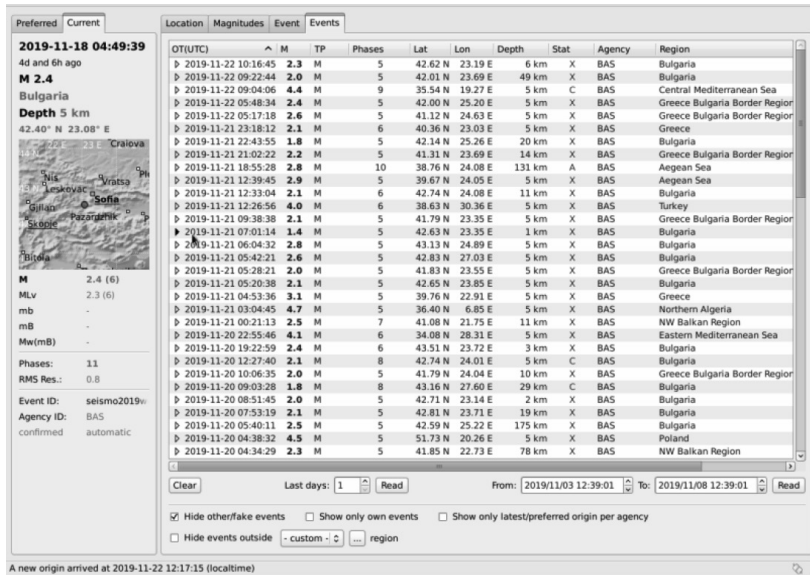
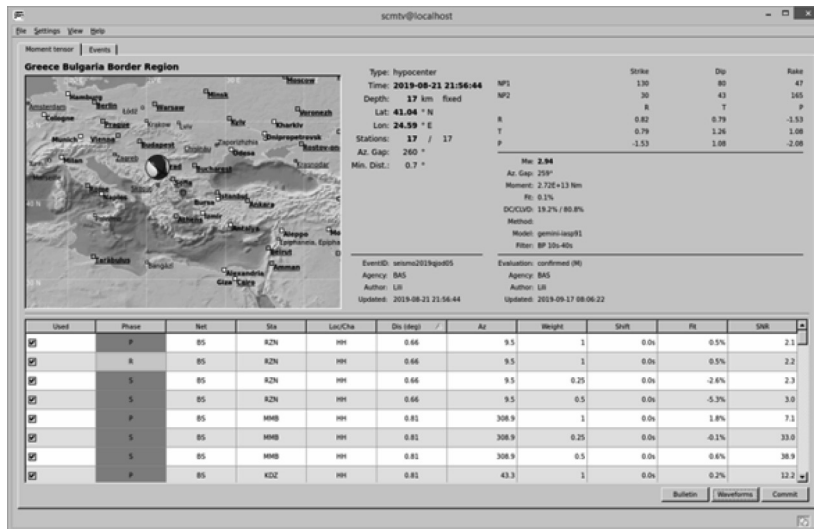
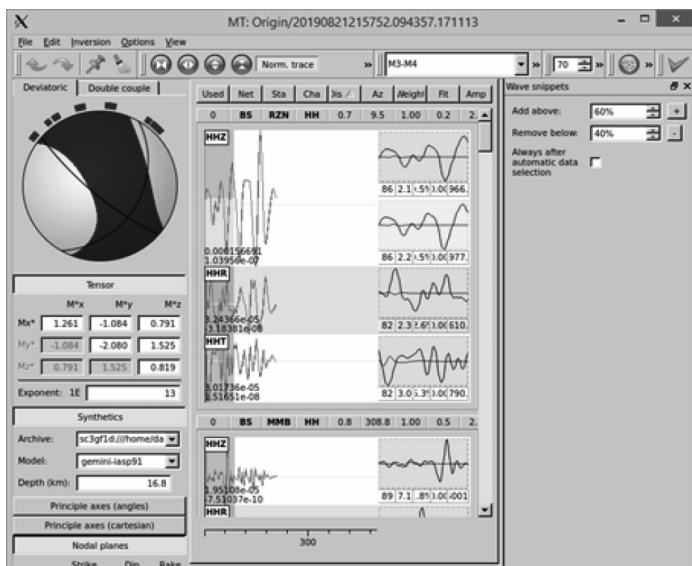


Fig. 3. List of event locations evaluated by the sceval module

The module *mt* computes and analyzes moment tensors (fig. 4). The moment tensor inversion technique uses a combination of several seismic wave types, time windows and frequency bands carefully chosen based on event magnitude and station distance.



a



b

Fig 4. An example of the automatic moment tensor solution produced by the **mt** module for the 21.8.2019 earthquake with parameters $T_0=21:56:44$, coordinates 41.04N, 24.59 E and $M_w=2.94$.

Conclusions

National Operative Telemetric System for Seismological Information is in continuous exploitation during the last 40 years. The hardware and software are maintained at a high and up-to-date level to meet the requirements of a nationally responsible institution: reliable registration and processing of earthquakes on the territory of Bulgaria and surroundings in order to provide reliable information to the authorities, general public and scientific community.

Acknowledgements. The presented paper is supported by the Contract No D01-282/17.12.2019 Project “National Geoinformation Center (NGIC)” financed by the National Roadmap for Scientific Infrastructure 2017-2023

References

- Christoskov, L., A. Morelli, D. Pesaresi, L. Petrov, D. Solakov, M. Tozzi, 1996. Observatory Vitoshka as a MEDNET seismic station of VBB type, *Bulg. Geophys. J.*, **Vol.22, No. 4**, 75-82.
- Christoskov L., 2007. *Seismology, Part I*, 362 pp., Sofia University “St. Kl.Ohridski”, Sofia. (in Bulgarian)

- Christoskov, L., L. Dimitrova, D. Solakov, Simeonova S., 2012. Instrumental seismological monitoring in Bulgaria, *Journal of BAS*, **2**, 19-27 (in Bulgarian).
- Haikin, L.M. and A.F.Kushnir, 2005. Seismic Network Data Processor (Sndp). Comprehensive Software for UNIX Networks. *Introductory Software Manual*. Ver. 5.1.
- Samardjiev, D., L. Christoskov, P. Danev, L. Petrov, C. Georgiev, 1980. National operative telemetric system for seismological information (NOTSSI), *BGJ*, **IV**, **3**, 43-49 (in Bulgarian).
- Solakov, D., Тс. Dobrev, 1987. A computer code for evaluation of earthquake main kinematic parameters for PC "Pravets", *BGJ*, **XIII**, **4**, 100-104 (in Bulgarian)
- Watzof, S., 1902. *Earthquakes in Bulgaria during the XIX century*. С М Ст., Ст..P., 1-93. (In Bulgarian)

Четиридесет години Национална оперативна телеметрична система за сеизмологична информация

Л. Христосков, Л. Димитрова, Д. Солаков, С. Симеонова

Резюме. Българската сеизмологична реално-временна мрежа и Националният център за данни работят от 1980 г. В началото данните от сеизмичните станции са пренасяни в реално време чрез аналогови телефонни линии до центъра за данни, а параметрите на регистрираните сеизмични събития са обработвани ръчно. През 2006 г. както сеизмологичната мрежа, така и информационният център бяха модернизирани със съвременен цифрово оборудване и беше организирана автоматична обработка на данни. През последните 12 години са архивирани повече от 12 TB обработени и сурови данни в PASSCAL, mini SEED и в CSS формати. Пълнотата на архивираните данни надвишава 99%, а загубата на данни се дължи главно на прекъсвания на комуникацията. Поддръжката на мрежата и центъра за данни е организирана по такъв начин, че надграждането на оборудването и обновяването на софтуера не влияят върху оперативната дейност. През последните години броят на сеизмичните станции нараства значително и в края на 2019 г. е 40. В момента сеизмичният център е модернизирани със софтуер SeisComP3 за реално времеви трансфер и автоматична обработка на данни, който се използва широко в сеизмологичната общност и центровете за данни.

SEISMICITY ON THE TERRITORY OF BULGARIA AND THE ADJACENT LANDS RECORDED BY NOTSSI IN 2017

V. Buchakchiev, E. Oynakov, D. Dragomirov, Y. Milkov

National Institute in Geophysics, Geodesy and Geography, Bulgarian Academy of Sciences, Acad. G. Bonchev Str., bl.3, Sofia 1113, Bulgaria, e-mail: valioka12@gmail.com

DOI: 10.34975/bgj-2019.42.9

Abstract. A map of epicenters of 114 earthquakes with magnitude $M_w \geq 2.5$ that occurred during 2017 in Bulgaria and surroundings (sector outlined by latitude $j = 41^\circ - 44.5^\circ N$ and longitude $l = 22^\circ - 29^\circ E$) registered by NOTSSI is presented. Expert generalized analysis is proposed. Catalog of earthquakes is applied.

Key words: Bulgaria, seismicity.

The Balkan Peninsula is one of the active regions in the Alpine-Himalayan seismic belt. High activity is observed in Western Turkey, Greece, and Vrancea region – Romania, Bulgaria, Northern Macedonia, Albania, and Serbia. The depth distribution is very characteristic. There are two highly active levels in the range of 20-40 km and 90-110 km and a less active one in 50-70 km.

Bulgaria is an earthquake prone country. Over the past centuries, Bulgaria has experienced strong earthquakes. Some of the strongest European earthquakes during the 20th century have been occurred in Bulgaria. At the beginning of the 20th century, from 1901 to 1928, five strong earthquakes with magnitude larger than or equal to 7.0 occurred on the territory of Bulgaria – 30.03.1901 $M_s = 7.2$ Shabla earthquake; 04.04.1904 Kresna earthquakes with M_s magnitudes 7.1 and 7.8; 14.6.1913 $M_s = 7.0$ G.Orjahovitsa earthquake and two earthquakes near the city of Plovdiv in 1928 - 14.04 with magnitude $M_s = 6.8$ and 18.04 with magnitude $M_s = 7.0$.

Strong seismic impact on the territory of Northern Bulgaria has the intermediate earthquakes in Vrancea – Romania region. The strongest being the one in 1944 with magnitude of 7.7 and some may remember the one in 1977 with magnitude of 7.4 caused a lot of deaths and destructions.

The present study contains generalized information and analysis of the data about the seismic events recorded by the National Operative Telemetric System for Seismological Information (NOTSSI) during 2017. Seismic data is gathered in real time by 26 Bulgarian stations and a number of stations from neighbouring countries which increases the accuracy of hypocentral locations. Between 2005 and 2010 almost all stations are modernized and equipped with broadband seismometers. A number of stations also are equipped with accelerometers of type RefTek 131A-02/3 of the company “Refraction Technology”. The data from the digitizers DAS 130-01 are collected through the RTPD (Real time protocol demon) module and the data from foreign stations and from Quanterra digital systems are collected with the sl2rptd module.

Data are transferred to the National seismological center in the Geophysical Institute, BAS in real time. Then they are archived in PASSCAL format and additionally in the widely used miniSEED format. The data are processed automatically (relevant signals are recognized and the main parameters of the earthquake are evaluated) by the program Seismic Network Data Processor (SNDP) (Christoskov et al., 2012). The data are later processed manually by an on-duty seismologist and corrections are made if required. At present the body P-wave magnitude M_p is evaluated by formula:

$$M_p = \log\left(\frac{A}{T}\right)_{max} + \sigma_{BB}(\Delta) + S_j, \quad (1)$$

where $-\log(A/T)_{max} = V_{max}/2\pi$, A is the amplitude in μm , T is a period in s , and V_{max} is the peak ground velocity in $\mu m/s$ of P -phase recorded on the broadband seismograph vertical-component at epicenter distances less than 10° ; $\sigma_{BB}(\Delta)$ is the calibration function; and S_j is the j station magnitude correction.

In the present study M_p is transformed into the more reliable and more widely used M_w magnitude, which would allow the creation of a uniform catalogue of earthquakes, needed for reliable evaluation of the seismic hazard on the territory of the country and surroundings. M_p is transformed into M_w through the formula (D. Solakov et al., 2018):

$$M_w = 0.93M_p + 0.31. \quad (2)$$

The high sensitivity of the seismographs allows recording and processing of a great number of local and regional earthquakes. Different magnitude's lower thresholds for reliable determination of local and regional earthquakes are established: $M_w = 2.5$ for the territory of Bulgaria, $M_w = 3.0$ for the central part of the Balkans, $M_w = 5.0$ for regional events. The accuracy of the epicenter location is different; except on the distance it depends also on the epicenter position the position of the epicenter with respect to the recording network. The parameters of seismic events occurring at a distance more than 100-150 km outside the territory of Bulgaria should be accepted only informatively and cannot be used for reliable seismotectonic investigation.

After comprehensive analysis of the digital records and application of the above mentioned calculation procedures it is established that 114 of all registered earthquakes are on the territory of Bulgaria and surroundings outlined by space window 41° – 44.5° N and 22° – 29° E. In the Fig. 1 are plotted the earthquake epicenters using different magnitude levels.

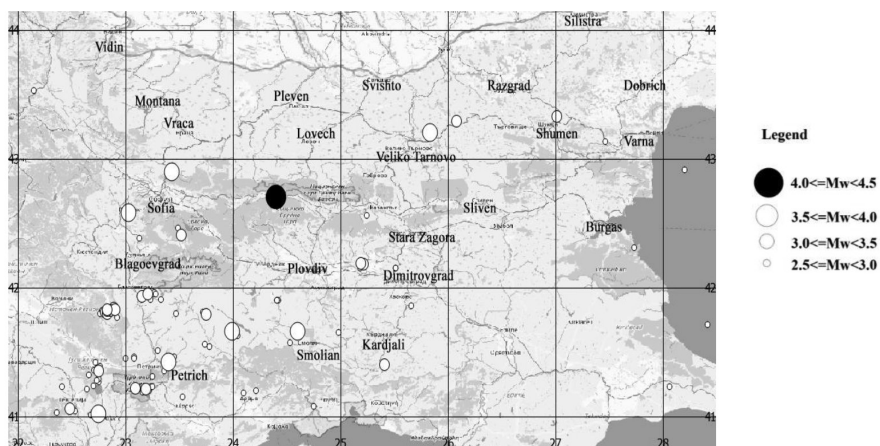


Fig. 1. The earthquake epicenters using different magnitude levels.

The number of the events in the magnitude interval $M_w = 2.5 - 3.0$ is 84, in $M_w = 3.1 - 3.5$ there are 21, in $M_w = 3.6 - 4.0$ there are 8 and in $M_w = 4.1 - 4.5$ there is 1 earthquake, as shown in Fig. 2. Fig. 3 shows that the data fit well with theoretical expectations, meaning that all incoming earthquakes have been detected by the network.

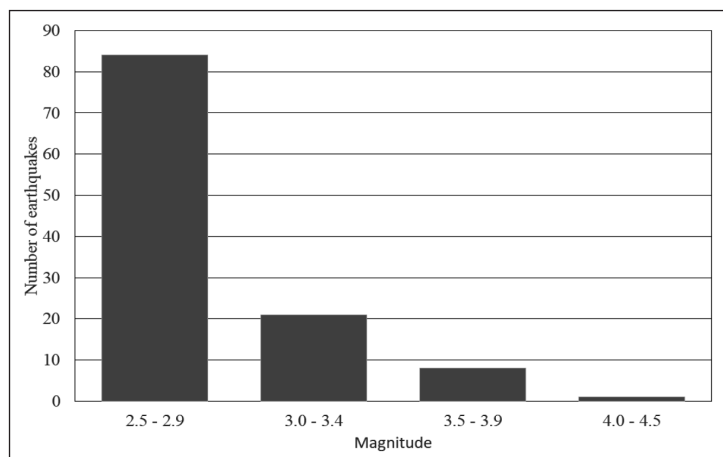


Fig. 2. The number of the events in the magnitude interval $M_w = 2.5 - 3.0$ is 84, in $M_w = 3.1 - 3.5$ there are 21, in $M_w = 3.6 - 4.0$ there are 8 and in $M_w = 4.1 - 4.5$ there is 1 earthquake.

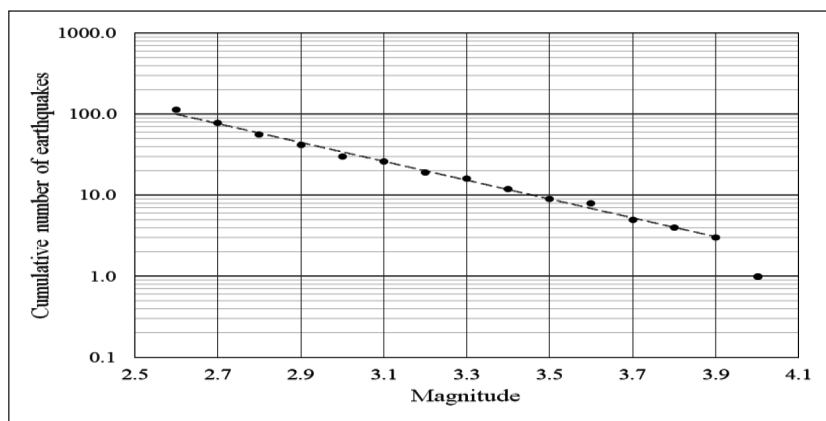


Fig. 3. The number of the events in the magnitude interval $M_w = 2.5 - 3.0$ is 84, in $M_w = 3.1 - 3.5$ there are 21, in $M_w = 3.6 - 4.0$ there are 8 and in $M_w = 4.1 - 4.5$ there is 1 earthquake.

Throughout the year 21 earthquakes in total were felt on the territory of Bulgaria from local and regional sources. The strongest event during the studied period occurred in the Plovdiv region close to Klisura with a magnitude of $M_w = 4.1$. Maximum intensity on

As a whole, events with $M_w < 3.0$ which occur outside Bulgaria are difficult to be localized by the national seismological system.

Table 1. List of earthquakes with $M_w \geq 2.5$ in Bulgaria and surroundings during 2017

Date	Time	Latitude	Longitude	Depth	Magnitude
		[N°]	[E°]	[km]	[Mw]
03.01.2017	22:02:32	43,2	25,83	16	3.8
04.01.2017	4:34:22	42,15	25,18	15	2.9
04.01.2017	9:50:33	44,26	25,26	10	2.7
31.01.2017	1:16:15	41,27	22,75	4	2.6
03.02.2017	2:35:25	41,45	23	6	2.7
03.02.2017	9:12:09	41,54	23,78	7	2.8
04.02.2017	8:20:12	41,46	23,45	10	2.6
06.02.2017	17:05:46	41,29	22,75	13	2.6
21.02.2017	20:59:56	41,4	25,41	16	3.0
26.02.2017	19:59:46	41,28	22,73	10	2.8
27.02.2017	10:16:19	41,93	23,15	20	3.0
05.03.2017	20:17:28	41,18	24,1	11	2.6
10.03.2017	2:07:44	42,18	25,21	15	3.1
12.03.2017	0:09:19	41,95	23,16	14	2.7

Table 1.

15.03.2017	11:20:43	41,95	23,21	17	3.4
16.03.2017	3:44:16	41,01	22,77	3	2.6
16.03.2017	13:40:50	41,01	22,77	10	2.6
18.03.2017	22:01:30	41,9	24,42	20	2.7
20.03.2017	13:19:47	41,96	23,27	14	2.7
22.03.2017	16:54:45	41,86	25,66	16	2.6
22.03.2017	22:01:30	41,9	24,41	20	2.7
24.03.2017	17:26:45	42,41	23,51	13	2.7
24.03.2017	17:40:27	42,41	23,52	13	3.2
24.03.2017	18:34:46	42,41	23,52	13	2.6
02.04.2017	7:59:37	41,51	23,3	15	2.8
08.04.2017	21:10:54	41,96	23,18	14	2.6
09.04.2017	10:14:33	41,95	23,17	16	2.6
10.04.2017	15:11:12	42,46	23,49	12	2.8
15.04.2017	12:41:54	41,38	22,74	3	2.9
21.04.2017	19:35:26	41,15	23,53	4	2.6
26.04.2017	2:53:21	42,18	25,22	10	2.8
29.04.2017	0:07:45	41,35	22,75	5	3.2
03.05.2017	20:42:05	43,53	22,15	2	2.6
04.05.2017	14:31:17	41,46	23,08	12	2.6
04.05.2017	14:44:13	41,45	23,08	13	2.8
09.05.2017	22:42:34	42,38	23,13	13	2.6
11.05.2017	20:33:23	41,9	24,41	20	2.8
26.05.2017	19:58:01	41,57	24,53	20	2.6
07.06.2017	9:43:55	42,31	27,73	2	2.6
26.06.2017	22:36:07	41,91	23,23	11	2.6
28.07.2017	2:58:38	41	22,75	5	2.7
29.07.2017	3:31:39	41,02	22,75	18	3.7
31.07.2017	15:45:08	41,2	23,22	11	2.9
02.08.2017	16:30:02	41,21	22,64	2	2.6
19.08.2017	13:19:36	43,29	26,08	14	3.3
21.08.2017	14:44:26	41,8	23,47	4	2.7
27.08.2017	22:12:48	41,06	22,48	10	3.4
29.08.2017	23:13:51	41,63	24,04	20	2.6
31.08.2017	9:12:04	41,32	22,66	20	2.8
03.09.2017	20:13:31	41,04	22,53	13	2.6
04.09.2017	8:10:05	41,95	23,26	9	2.6
08.09.2017	19:17:44	41,31	23,25	13	2.6
10.09.2017	6:28:02	41,71	28,41	2	2.9
14.09.2017	1:53:18	42,58	23,03	13	3.6

Table 1.

17.09.2017	16:37:00	41,65	24,98	20	2.9
24.09.2017	20:36:07	43,13	27,46	5	2.6
26.09.2017	16:27:59	41,03	22,36	10	2.6
27.09.2017	7:38:15	41,97	23,22	14	2.7
27.09.2017	22:42:00	41,81	22,81	7	3.1
27.09.2017	22:45:07	41,81	22,78	13	2.6
30.09.2017	12:19:51	41,42	22,72	9	2.6
02.10.2017	8:48:24	41,8	22,76	4	2.7
03.10.2017	5:30:44	41,23	23,24	12	2.8
03.10.2017	9:34:05	41,23	23,25	15	2.9
04.10.2017	0:37:42	41,37	22,74	8	2.8
04.10.2017	4:23:27	41,82	22,78	8	2.7
04.10.2017	10:40:17	41,83	22,85	14	2.9
04.10.2017	10:40:17	41.83	22.85	14	3.5
04.10.2017	12:53:24	41.83	22.83	10	2.6
04.10.2017	17:59:59	41.91	23.33	20	2.8
09.10.2017	6:05:14	41,81	22,82	11	2.9
09.10.2017	6:06:28	41,8	22,83	11	2.9
09.10.2017	7:31:33	41,8	22,83	12	3.1
18.10.2017	3:51:34	41,39	22,76	10	2.6
18.10.2017	5:48:29	41,19	23,16	12	2.7
19.10.2017	8:00:47	41,82	22,86	20	3.3
19.10.2017	8:17:15	41,84	22,9	20	2.8
19.10.2017	8:19:33	41,84	22,89	20	3.1
19.10.2017	8:27:21	41,83	22,9	20	3.4
21.10.2017	8:25:19	41,36	22,71	1	2.7
03.11.2017	6:16:07	42,15	25,51	14	2.6
03.11.2017	9:34:02	41,21	23,19	15	3.1
06.11.2017	22:53:32	41,01	22,68	10	2.7
07.11.2017	17:11:57	41,81	23,72	2	2.7
07.11.2017	17:17:05	41,78	23,75	17	2.6
10.11.2017	23:51:05	41,03	22,77	1	3.1
11.11.2017	4:54:05	42,9	23,43	17	3.9
11.11.2017	6:45:48	42,15	25,51	14	2.6
12.11.2017	15:06:52	41,21	23,1	13	2.8
12.11.2017	15:39:45	41,21	23,09	11	2.9
12.11.2017	15:58:18	41,21	23,1	12	2.6
13.11.2017	6:08:51	41,22	23,09	7	3.0
16.11.2017	23:43:59	41,79	23,75	14	3.1

Table 1.

18.11.2017	16:18:18	41.36	22.73	10	2.7
19.11.2017	1:26:26	41.24	22.7	4	2.6
22.11.2017	9:47:15	42,91	28,2	5	2.7
24.11.2017	7:53:48	41,56	23,74	13	2.7
24.11.2017	12:12:59	43,33	27,01	13	3.2
24.11.2017	17:26:50	41,66	24,6	13	3.6
24.11.2017	17:31:43	41,64	24,61	13	3.0
25.11.2017	10:35:44	41,65	24,6	13	2.6
26.11.2017	19:01:31	42,7	24,4	14	4.1
27.11.2017	9:12:51	42,18	25,21	20	2.7
28.11.2017	3:40:16	41,95	23,28	20	2.7
03.12.2017	9:31:06	41,23	22,41	7	2.9
07.12.2017	23:24:34	41,35	23,36	11	2.9
07.12.2017	23:50:14	42,19	25,19	14	3.3
08.12.2017	4:05:57	41,42	23,4	15	3.9
16.12.2017	19:15:57	41,08	24,75	10	2.8
18.12.2017	17:51:11	41,66	23,99	20	3.6
21.12.2017	10:24:02	41,2	24,21	8	2.7
28.12.2017	2:33:18	41,77	22,92	19	2.6
29.12.2017	12:24:10	42,56	25,24	4	2.6
29.12.2017	23:09:19	41,82	22,83	11	3.3

As usual, the largest concentration of the epicenters in the other regions of Bulgarian territory during 2017 is marked in the southwestern part of the investigated region (presented in Fig.1 and Table 1). In 2017 no events of $M_w \geq 4.0$ occurred in this region. The strongest felt earthquake for the south-western part of Bulgarian territory is with magnitude $M_w = 3.5$. It occurred on April 10th in Blagoevgrad region with intensity of III degree on MSK-64 scale.

A detailed analysis of seismicity in the individual seismic zones is hard to be fulfilled because of the insufficient quantity of events and the narrow magnitude range of the earthquakes. The joint statistics of all the events in Fig. 1 characterize predominantly the seismicity parameters of the southwestern part of the territory under investigation.

The depth distributions in Fig. 4 show that the majority of events occur in the range 10-20 km depth. Fig.6 does not show correlation between magnitude and depth, as the majority of the events occurred in the 8-20 km depth range. The number of events does not decrease smoothly with increase of the depth. At the same time the number of events in the interval 10-15 km is bigger. The magnitude distribution of the events in depth (Fig. 5) permits to note some differentiation of depth "floors" with the increase of magnitude - the maximums can be traced out for the depth interval from 5 to 20 km. The stronger events with magnitude of $M_w \geq 3.75$ have depth in the range 10-20 km.

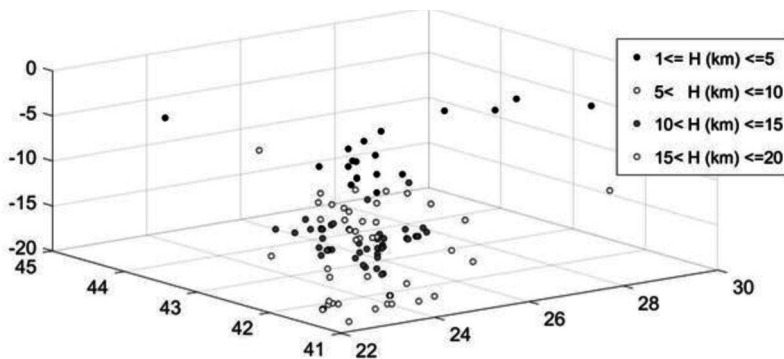


Fig. 4. The depth distributions.

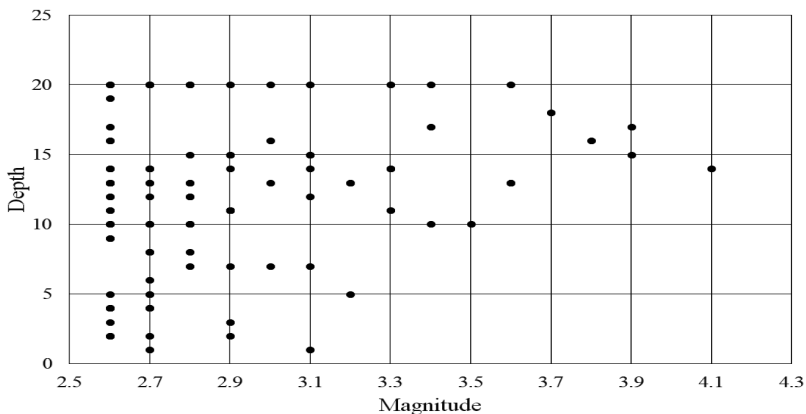


Fig. 5. The magnitude distribution of the events in depth.

Fig. 6 illustrates the distribution of seismicity in time according to the number of events per months. The highest amount of earthquakes is displayed in November, when 24 earthquakes occurred, and it is associated with seismic activity in South-Western Bulgaria – Bulgaria-Greece border and the seismic activity in the North Black sea. The lowest earthquake quantity is in June and July, with 2 and 3 events respectively. Fig. 7 shows that there is no definite distribution of the earthquakes throughout the months for they show no tendency towards an average amount.

The graphs below show the daily distribution of the number of earthquakes each month. We see that the distribution is not spread out equally and there are any more than 6 earthquakes/day.

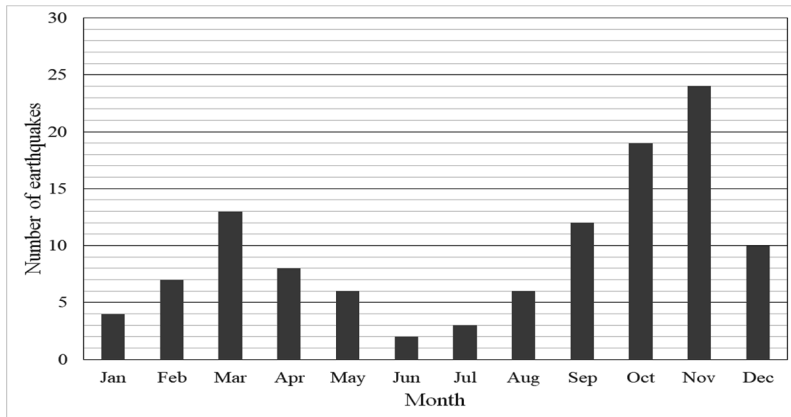
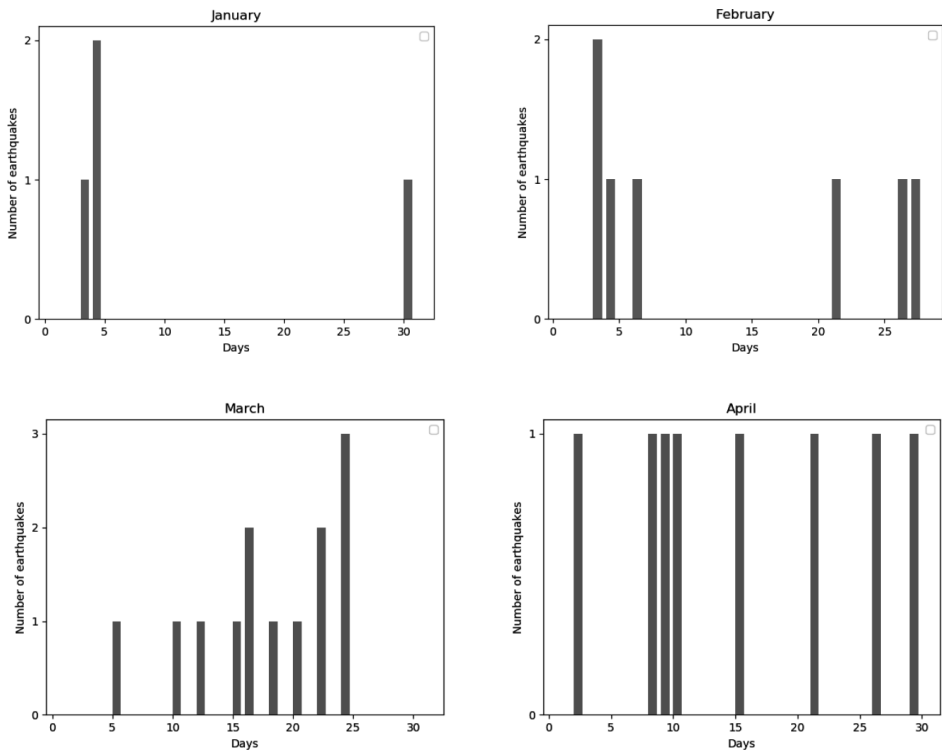


Fig. 6. The distribution of seismicity in time according to the number of events per months.



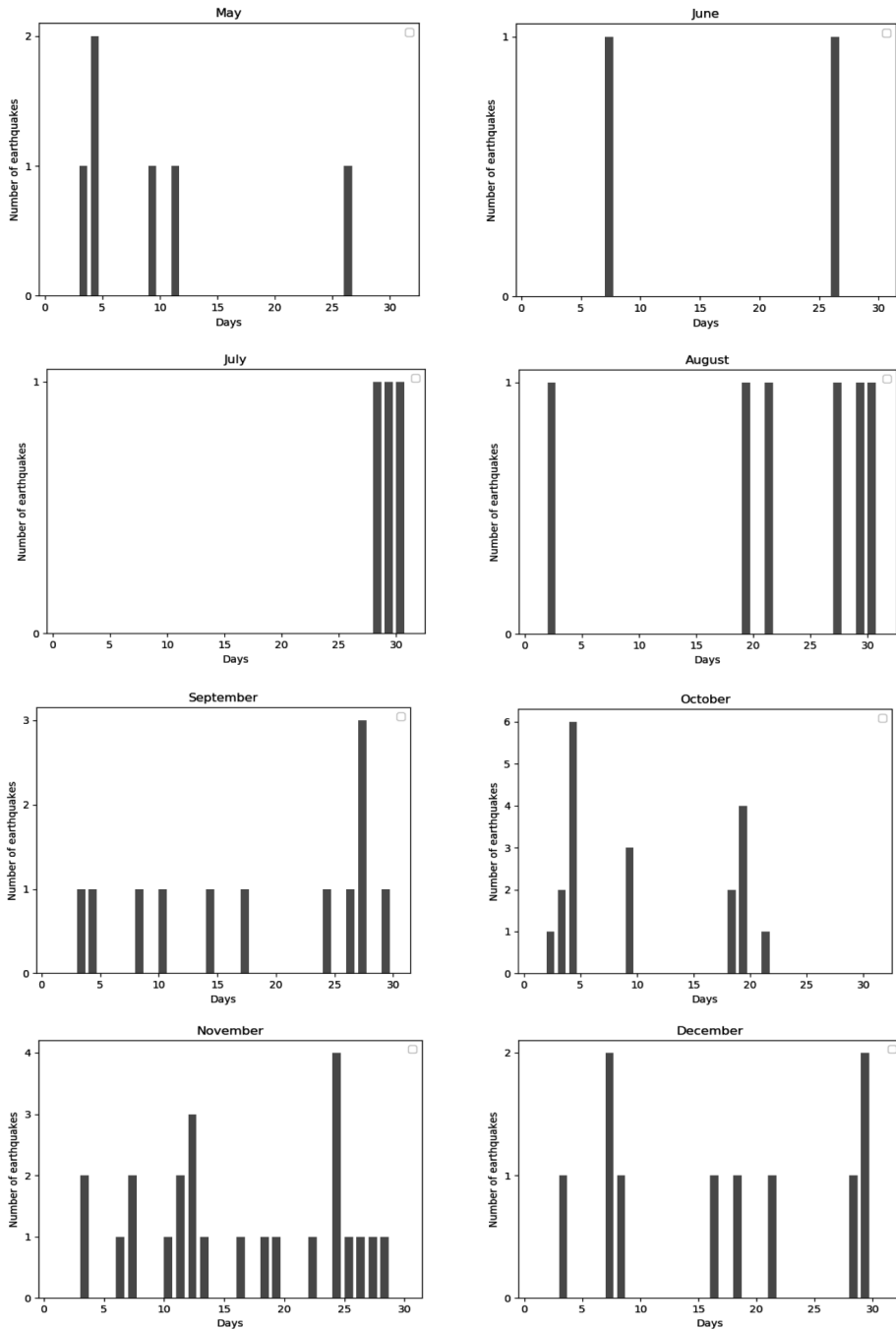


Fig. 7.

Acknowledgments: The authors express their gratitude towards the seismologists who have worked in NOTSSI for the period 01.01.2017 - 31.12.2017.

References

- Christoskov L., L. Dimitrova, D. Solakov, S. Simeonova. 2012. Instrumental seismological observations in Bulgaria. *Journal of BAS*, 2, 19-27 (in Bulgarian)
- D. Solakov, S. Simeonova, P. Raykova, I. Aleksandrova. EMPIRICAL RELATIONS CONVERTING M_d AND M_p MAGNITUDES APPLIED IN BULGARIAN SEISMOLOGICAL ROUTINE PRACTICE TO MOMENT MAGNITUDE. *Comptes rendus de l'Acad'emie bulgare des Sciences*, 71, 8, 2018, DOI:DOI:10.7546/CRABS.2018.08.09, 1076-1085. SJR: 0.21, ISI IF: 0.27

Сеизмичност на територията на България и прилежащите земи по данни от НОТССИ през 2017 г.

В. Бучакчиев, Е. Ойнаков, Д. Драгомиров, Й. Милков

Резюме: Представена е карта с епицентрите на 114 земетресения магнитуд $M_w \geq 2.5$ случили се през 2017 г. в България и околностите (сектор ограничен от географска ширина $\varphi = 41^\circ - 44.5^\circ$ N и географска дължина $\lambda = 22^\circ - 29^\circ$ E) регистрирани от Националната Оперативна Телеметрична Система за Сеизмологична Информация (НОТССИ). Представен е обобщен анализ. Приложен е каталог със земетресенията.

Ключови думи: България, сеизмичност

Благодарности: Авторите изразяват своите благодарности към соизмолозите, които са работили в НОТССИ през периода 01.01.2017 – 31.12.2017.

SEISMICITY ON THE TERRITORY OF BULGARIA AND THE ADJACENT LANDS RECORDED BY NOTSSI IN 2018

D. Dragomirov, E. Oynakov, V. Buchakchiev, Y. Milkov

National Institute of Geophysics, Geodesy and Geography, Bulgarian Academy of Sciences, Acad.
G. Bonchev Str., bl.3, Sofia 1113, Bulgaria, e-mail: drago.n.dragomirov@gmail.com

DOI: 10.34975/bgj-2019.42.10

Abstract. A map of epicenters of 168 earthquakes with magnitude $M \geq 2.5$ that occurred during 2018 in Bulgaria and surroundings (sector outlined by latitude = 41° - 44.5° N and longitude = 22° - 29° E) registered by NOTSSI is presented. Expert generalized analysis is proposed. Catalog of earthquakes is applied.

Key words: Bulgaria, seismicity

Introduction

The Balkan peninsula is one of the active regions in the Alpine-Himalayan seismic belt. High activity is observed in Western Turkey, Greece, Vrancea region – Romania, Bulgaria, Northern Macedonia, Albania, Serbia. The depth distribution is very characteristic. There are two highly active levels in the range of 20-40 km and 90-110 km and a less active one in 50-70 km.

Bulgaria is an earthquake prone country. Over the past centuries, Bulgaria has experienced strong earthquakes. Some of the European strongest earthquakes during the 20th century have been occurred in Bulgaria. At the beginning of the 20th century, from 1901 to 1928, five strong earthquakes with magnitude larger than or equal to 7.0 occurred on the territory of Bulgaria – 30.03.1901 $M_s = 7.2$ Shabla earthquake; 04.04.1904 Kresna earthquakes with M_s magnitudes 7.1 and 7.8; 14.6.1913 $M_s = 7.0$ G.Orjahovitsa earthquake and two earthquakes near the city of Plovdiv in 1928 - 14.04 with magnitude $M_s = 6.8$ and 18.04 with magnitude $M_s = 7.0$.

Strong seismic impact on the territory of Northern Bulgaria have the intermediate earthquakes in Vrancea – Romania region. The strongest being the one in 1944 with magnitude of 7.7 and some may remember the one in 1977 with magnitude of 7.4 caused a lot of deaths and destructions.

The present study contains generalized information and analysis of the data about the seismic events recorded by the National Operative Telemetric System for Seismological Information (NOTSSI) during 2017. Seismic data is gathered in real time by 26 Bulgarian stations and a number of stations from neighbouring countries which increases the accuracy of hypocentral locations. Between 2005 and 2010 almost all stations are modernized and equipped with broadband seismometers. A number of stations also are equipped with accelerometers of type RefTek 131A-02/3 of the company “Refraction Technology”. The data from the digitizers DAS 130-01 are collected through the RTPD (Real time protocol demon) module and the data from foreign stations and Quanterra digital systems are collected with the sl2rptd module.

Data are transferred to the National seismological center in the Geophysical Institute, BAS in real time. Then they are archived in PASSCAL format and additionally in the widely used miniSEED format. The data are processed automatically (relevant signals are recognized and the main parameters of the earthquake are evaluated) by the program Seismic Network Data Processor (SNDP) (Christoskov et al., 2012). The data are later processed manually by an on-duty seismologist and corrections are made if required. At present the body P-wave magnitude M_p is evaluated by:

$$M_p = \log \left(\frac{A}{T} \right)_{max} + \sigma_{BB}(\Delta) + s_j, \quad (1)$$

where $\left(\frac{A}{T} \right)_{max} = \frac{V_{max}}{2\pi}$, A is the amplitude in μm , T is a period in s, and V_{max} is the peak ground velocity in $\mu\text{m/s}$ of P-phase recorded on the broadband seismograph vertical-component at epicentral distances less than 10° ; $\sigma_{BB}(\Delta)$ is the calibration function; and s_j is the j station magnitude correction.

In the present study M_p is transformed into the more reliable and more widely used M_w magnitude, which would allow the creation of a uniform catalogue for earthquakes, needed for reliable evaluation of the seismic hazard on the territory of the country and surroundings. M_p is transformed into M_w through the formula (D. Solakov et al., 2018):

$$M_w = 0.93 * M_p + 0.31. \quad (2)$$

The high sensitivity of the seismographs allows recording and processing of a great number of local and regional earthquakes. Different magnitude's lower thresholds for reliable determination of local and regional earthquakes are established: $M_w=2.5$ for the territory of Bulgaria, $M_w=3.0$ for the central part of the Balkans, $M_w=5.0$ for regional events. The accuracy of the epicenter location is different; except on the distance it depends also on the epicenter position the position of the epicenter with respect to the recording network. The parameters of seismic events occurring at a distance more than 100-150 km outside the territory of Bulgaria should be accepted only informatively and cannot be used for reliable seismotectonic investigation.

After comprehensive analysis of the digital records and application of the above mentioned calculation procedures it is established that 168 of all registered earthquakes

are on the territory of Bulgaria and surroundings outlined by space window $41^{\circ} - 44.5^{\circ}$ N and $22^{\circ} - 29^{\circ}$ E. In the Fig. 1 are plotted the earthquake epicenters using different magnitude levels.

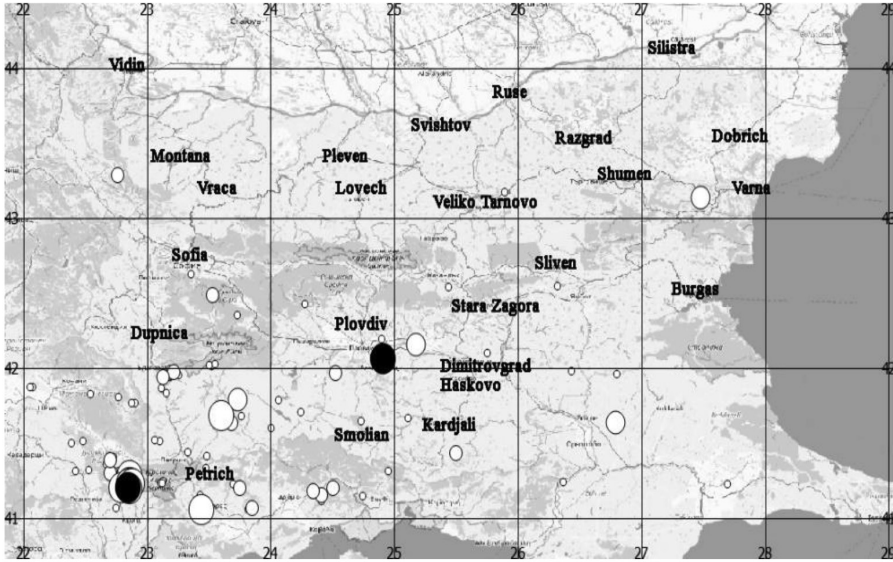


Fig. 1. The number of the events in the magnitude.

The number of the events in the magnitude interval $M_w=2.5-3$ is 115, in $M_w=3.1-3.5$ - 32, in $M_w=3.6-4$ - 11, in $M_w=4.1-4.5$ - 8, $M_w=4.6-5$ is 2 earthquakes (as shown in Fig. 2). Fig. 3 shows that the data fit well with theoretical expectations, meaning that all incoming earthquakes have been detected by the network.

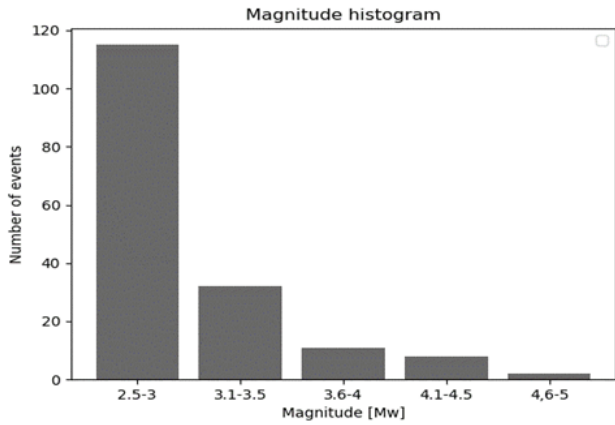


Fig. 2. The number of the events in the magnitude.

Throughout the year 24 earthquakes in total were felt on the territory of Bulgaria from local and regional sources. The strongest event outside Bulgaria during the studied period occurred in the region of Vrancea (Romania) with magnitude $M_w=5.6$. Maximum intensity on the territory of Bulgaria is $I_{max}=V$.

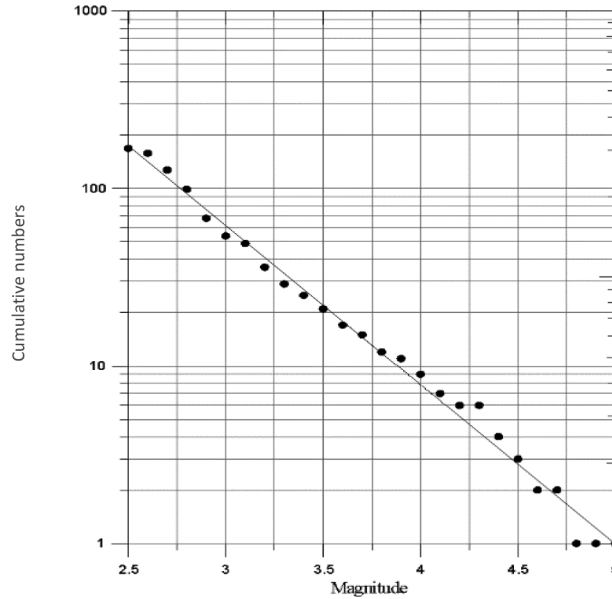


Fig. 3. The data fit well with theoretical expectations

As a whole, events with $M_w < 3.0$ which occur outside Bulgaria are difficult to be localized by the national seismological system.

Table 1. List of earthquakes with $M_w \geq 2.5$ in Bulgaria and surroundings during 2018

Date	Time	Latitude	Longitude	Depth	Magnitude
		[N°]	[E°]	[km]	[Mw]
1.1.2018	18:19:54	41.24	22.89	13	2.8
1.1.2018	18:22:25	41.24	22.90	14	2.8
1.1.2018	22:13:51	41.23	22.85	11	4.3
1.1.2018	22:16:12	41.23	22.87	12	4.0
1.1.2018	22:19:12	41.22	22.86	11	3.7
1.1.2018	22:32:30	41.22	22.88	16	2.9
1.1.2018	22:37:52	42.35	23.73	18	2.8
1.1.2018	22:45:29	41.22	22.87	12	2.9

Table 1.

1.1.2018	23:00:46	41.24	22.86	12	4.0
1.1.2018	23:37:51	41.21	22.84	10	2.6
1.1.2018	23:52:38	41.22	22.87	16	2.9
2.1.2018	4:24:16	41.20	22.85	11	5.0
2.1.2018	4:28:41	41.20	22.79	9	4.0
2.1.2018	6:26:19	41.21	22.84	7	3.0
2.1.2018	9:35:06	41.21	22.86	8	2.6
2.1.2018	10:07:49	41.22	22.87	8	2.8
2.1.2018	15:40:14	41.22	22.84	11	3.4
2.1.2018	17:36:33	41.20	22.86	13	4.5
2.1.2018	17:59:07	41.21	22.85	12	2.6
2.1.2018	18:50:02	41.22	22.83	8	2.6
2.1.2018	19:23:17	41.26	22.88	10	3.2
3.1.2018	5:32:55	41.24	22.87	10	3.1
4.1.2018	0:23:07	41.25	22.88	11	2.6
4.1.2018	19:03:51	41.25	22.85	15	2.8
5.1.2018	3:06:13	41.29	22.86	7	4.0
5.1.2018	3:26:39	41.24	22.84	15	2.6
5.1.2018	9:50:54	41.23	22.87	20	3.5
6.1.2018	0:27:22	41.25	22.86	8	2.5
7.1.2018	12:32:11	41.23	22.86	2	3.2
7.1.2018	22:57:08	41.23	22.87	12	3.5
11.1.2018	15:09:19	41.23	22.85	11	3.1
12.1.2018	2:16:13	41.23	22.88	11	2.7
13.1.2018	12:07:49	41.21	22.86	11	2.9
13.1.2018	20:11:35	41.23	22.88	10	2.9
13.1.2018	23:11:08	41.23	22.88	10	2.6
14.1.2018	19:40:43	41.23	22.89	13	2.7
15.1.2018	3:36:13	41.23	22.86	9	2.8
16.1.2018	3:47:55	41.25	22.86	20	3.3
17.1.2018	23:35:18	41.77	22.88	20	2.7
21.1.2018	1:25:52	41.24	22.88	7	2.8
24.1.2018	11:50:05	41.23	22.87	9	2.9
25.1.2018	20:16:37	41.81	22.77	20	2.6
29.1.2018	20:36:10	41.24	22.87	9	2.7
4.2.2018	1:17:04	42.16	25.16	9	2.7

Table 1.

4.2.2018	23:53:59	41.24	22.87	11	2.6
5.2.2018	9:13:07	41.23	22.88	13	4.4
5.2.2018	10:14:03	41.24	22.89	10	2.5
5.2.2018	11:24:19	41.22	22.85	20	2.7
5.2.2018	11:25:44	41.24	22.88	13	2.7
5.2.2018	11:30:47	41.23	22.88	20	2.7
5.2.2018	19:22:18	41.25	22.92	16	2.6
5.2.2018	20:26:27	41.24	22.90	9	2.7
5.2.2018	20:28:46	41.24	22.90	7	2.8
6.2.2018	0:38:25	41.24	22.90	13	2.8
6.2.2018	0:41:51	41.24	22.89	11	2.8
6.2.2018	0:50:59	41.23	22.90	10	2.7
6.2.2018	13:47:10	41.23	22.88	14	2.8
7.2.2018	23:06:46	41.24	22.88	10	3.2
8.2.2018	13:44:59	41.31	22.77	4	2.6
9.2.2018	15:22:03	42.16	25.20	11	3.0
14.2.2018	8:23:53	41.25	23.13	10	2.7
15.2.2018	22:11:05	41.23	22.87	20	3.1
16.2.2018	16:08:14	41.31	22.42	15	2.6
17.2.2018	9:45:21	41.44	25.50	14	3.1
19.2.2018	16:21:11	41.96	26.80	8	2.6
19.2.2018	16:23:30	41.25	22.86	13	2.7
21.2.2018	4:33:23	41.06	23.82	7	2.6
21.2.2018	23:41:58	42.07	24.91	14	4.7
22.2.2018	0:01:11	42.04	24.89	14	2.6
22.2.2018	1:10:23	42.04	24.89	15	2.6
22.2.2018	8:03:42	41.24	22.89	10	3.2
22.2.2018	15:05:06	42.06	24.90	14	3.1
22.2.2018	23:15:04	42.05	24.89	14	3.8
2.3.2018	8:24:35	41.88	22.05	3	2.8
4.3.2018	10:18:13	41.60	24.00	15	2.5
5.3.2018	13:25:44	43.18	25.89	9	2.8
7.3.2018	19:12:42	41.88	22.07	19	2.7
7.3.2018	22:13:38	43.14	27.48	9	3.7

Table 1.

9.3.2018	21:21:30	43.37	29.52	28	2.9
15.3.2018	18:28:40	41.25	22.90	14	2.8
18.3.2018	15:42:46	41.77	22.90	13	2.6
24.3.2018	0:20:41	41.18	24.34	16	3.1
25.3.2018	15:01:59	41.64	26.79	16	3.7
29.3.2018	4:21:28	41.52	22.48	3	2.9
29.3.2018	16:18:27	41.25	22.75	10	2.6
29.3.2018	16:55:30	41.27	22.75	10	2.8
31.3.2018	18:13:04	41.26	22.84	14	2.6
2.4.2018	19:23:22	41.20	23.75	12	3.4
3.4.2018	6:04:32	41.79	24.07	20	2.8
4.4.2018	22:09:11	41.96	23.26	10	2.5
9.4.2018	18:50:04	42.63	23.36	10	2.7
11.4.2018	5:09:32	41.04	29.62	18	3.3
12.4.2018	16:55:29	41.51	23.11	20	2.5
13.4.2018	12:34:25	42.43	24.28	2	2.8
14.4.2018	17:50:58	42.55	26.32	8	2.8
20.4.2018	15:45:45	42.10	25.76	17	2.8
22.4.2018	1:59:57	41.98	26.44	3	2.6
23.4.2018	13:38:15	41.42	23.49	20	2.6
25.4.2018	10:53:27	41.63	23.69	16	2.6
26.4.2018	0:45:02	42.75	29.88	20	3.6
30.4.2018	14:25:08	41.94	23.19	17	2.7
10.4.2018	9:49:19	42.07	29.35	17	3.6
4.5.2018	15:11:26	41.50	22.39	15	2.6
6.5.2018	22:27:44	41.83	22.54	2	2.6
8.5.2018	3:05:05	41.24	26.37	11	2.5
8.5.2018	4:43:55	43.29	22.76	18	3.1
11.5.2018	7:26:54	43.15	27.48	6	3.4
12.5.2018	6:30:51	42.16	25.17	15	3.5
14.5.2018	18:38:37	41.23	22.83	20	2.7
17.5.2018	11:42:21	42.54	25.44	2	2.8
25.5.2018	22:48:30	41.22	22.86	10	2.6

Table 1.

29.5.2018	9:10:13	42.73	29.09	13	2.7
6.6.2018	7:38:40	41.63	23.68	15	3.2
9.6.2018	12:47:01	41.78	23.72	19	2.7
10.6.2018	8:40:24	41.79	23.74	17	3.1
17.6.2018	2:39:32	42.03	23.55	2	2.9
18.6.2018	9:00:29	41.79	23.74	18	3.5
26.6.2018	18:44:20	41.80	23.76	20	2.8
2.7.2018	15:15:28	41.97	23.22	15	3.1
5.7.2018	4:24:48	41.15	23.43	13	2.8
9.7.2018	0:40:39	41.23	23.11	9	2.5
9.7.2018	0:42:01	41.23	23.12	10	2.9
11.7.2018	14:56:28	41.32	22.53	6	2.5
16.7.2018	14:00:01	41.67	25.11	12	2.7
18.7.2018	6:21:42	42.00	23.18	10	2.7
19.7.2018	20:46:14	42.02	23.51	11	2.9
22.7.2018	1:45:05	41.30	22.74	11	2.5
29.7.2018	19:38:30	41.07	22.75	8	2.8
2.8.2018	14:17:37	41.69	23.60	19	4.3
2.8.2018	15:02:58	41.68	23.62	7	3.3
3.8.2018	0:33:38	41.32	24.95	16	2.7
11.8.2018	15:04:31	41.52	23.07	20	2.8
14.8.2018	12:34:42	41.23	27.70	12	2.8
25.8.2018	10:03:33	41.94	23.13	15	3.2
30.8.2018	0:10:40	41.39	22.70	10	3.4
30.8.2018	0:15:28	41.39	22.72	9	2.7
30.8.2018	4:24:36	41.36	22.67	1	2.8
30.8.2018	4:34:37	41.40	22.72	5	2.8
31.8.2018	16:01:39	41.82	23.76	2	2.9
17.9.2018	9:28:26	41.41	22.73	20	2.6
24.9.2018	7:56:46	41.71	24.24	11	2.8
2.10.2018	12:00:34	41.65	24.73	17	2.7
5.10.2018	11:05:19	41.44	23.33	16	2.8
9.10.2018	20:39:59	41.20	24.51	12	3.1

Table 1.

12.10.2018	6:48:07	41.07	23.85	10	3.1
13.10.2018	20:06:49	41.23	23.69	20	2.5
17.10.2018	13:24:41	41.30	22.70	13	3.1
27.10.2018	0:23:37	41.15	24.75	7	2.6
28.10.2018	20:53:05	41.34	23.48	20	2.7
1.11.2018	5:39:16	41.31	22.73	20	2.9
1.11.2018	5:58:52	42.01	23.53	20	2.6
3.11.2018	0:18:37	41.79	23.76	20	2.7
5.11.2018	15:22:09	41.68	23.77	18	2.7
5.11.2018	23:19:13	42.20	24.90	2	2.6
9.11.2018	22:13:52	41.79	23.75	20	2.8
16.11.2018	15:07:42	41.05	23.46	10	3.0
16.11.2018	15:10:17	41.06	23.46	10	3.0
17.11.2018	5:22:04	41.04	23.43	15	2.7
17.11.2018	12:09:27	41.05	23.44	11	4.1
17.11.2018	14:34:41	41.84	23.15	15	2.7
19.11.2018	2:09:03	41.94	23.20	17	2.9
19.11.2018	14:35:20	42.49	23.53	15	3.3
30.11.2018	13:18:43	41.03	23.46	9	3.2
2.12.2018	22:03:20	41.86	23.12	13	2.6
13.12.2018	4:47:33	41.05	23.43	8	2.6
17.12.2018	21:28:20	41.97	24.53	14	3.1
30.12.2018	3:05:27	41.16	24.41	10	3.0
30.12.2018	3:09:57	41.11	24.41	9	2.8

As usual, the largest concentration of the epicenters in the other regions of Bulgarian territory during 2018 is marked in the southwestern part of the investigated region (presented in Fig. 1 and Table 1). In 2018 only 3 events of $M_w \geq 4.0$ occurred in this region. The strongest felt earthquake for the south-western part of Bulgarian territory is with magnitude $M_w=4.7$, it was felt on the 21th of February in Asenovgrad region with intensity of V degree on MSK-64 scale.

A detailed analysis of seismicity in the individual seismic zones is hard to be fulfilled because of the insufficient quantity of events and the narrow magnitude range of the earthquakes. The joint statistics of all the events in Fig. 1 characterize predominantly the seismicity parameters of the southwestern part of the territory under investigation.

The graph of the depth distribution in Fig. 4, Fig. 5 Fig. 6 shows that the majority of events occur in range 5-20 km depth. Fig.6 does not show correlation between magnitude and depth, as the majority of the events occurred in the 5-20 km depth range. The number of events does not decrease smoothly with increase of the depth. In the same time the number of events in the interval 10-15 km is the largest. The magnitude distribution of the events in depth (Fig. 6) permits to note some differentiation of depth “floors” with the increase of magnitude - the maximums can be traced out for the depth interval from 5 to 20 km. The stronger events with magnitude $M_w \geq 4$ have depth in the range 10-20 km.

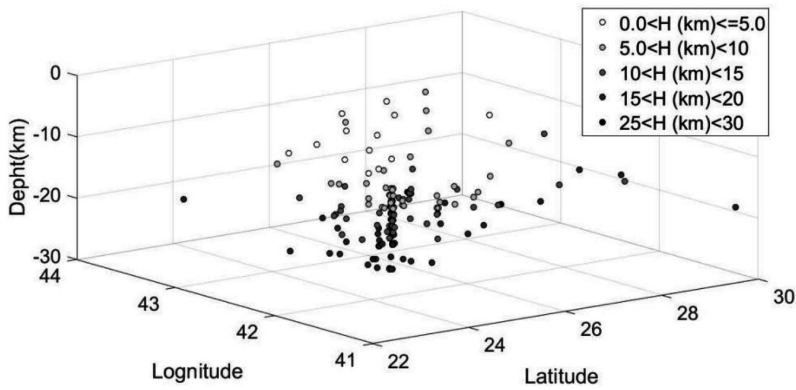


Fig. 4. The depth distribution

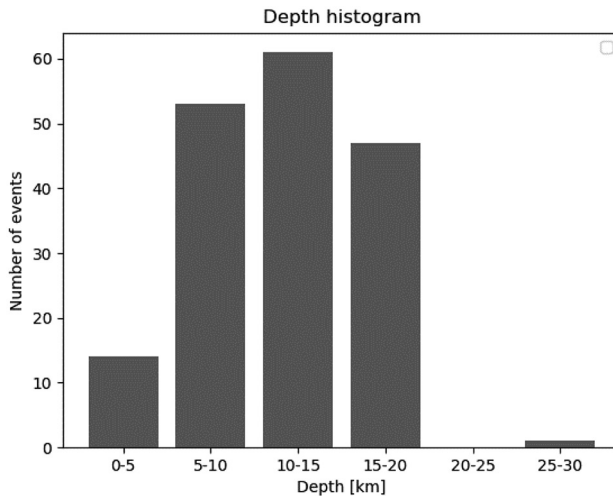


Fig. 5. The depth distribution

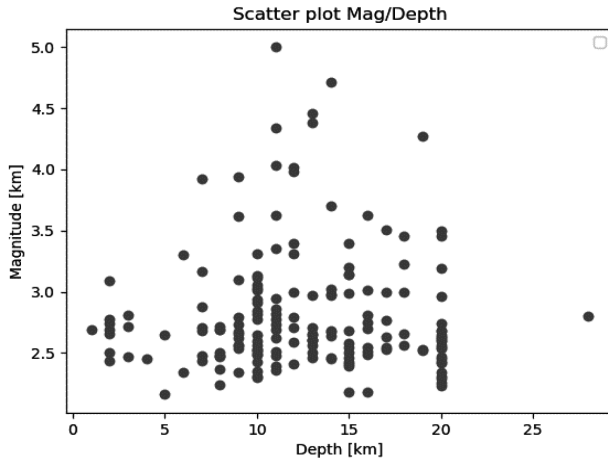


Fig. 6. The magnitude-depth distribution

Fig. 7, 8 illustrates the distribution of seismicity in time according to the number of events per months. The highest amount of earthquakes is displayed in January, when 43 earthquakes occurred, and it is associated with seismic activity in South-Western Bulgaria – Bulgaria-Greece border. The lowest earthquake quantity is in September, when only two vents with magnitude larger than 2.5 occurred. Fig.7 shows that there is no definite distribution of the earthquakes throughout the months.

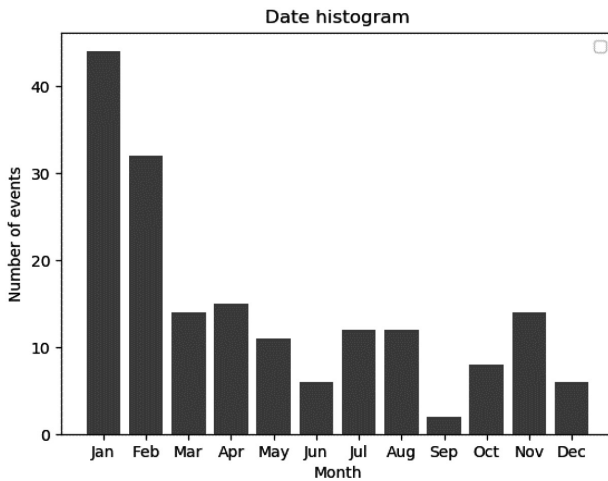
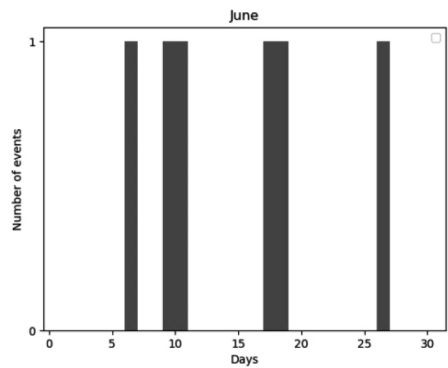
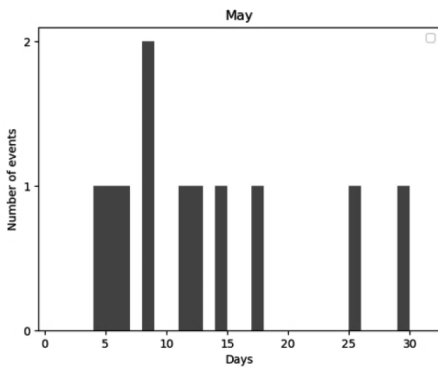
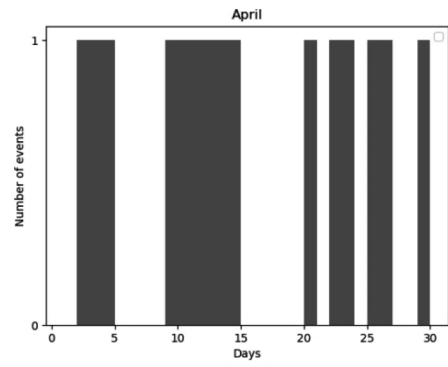
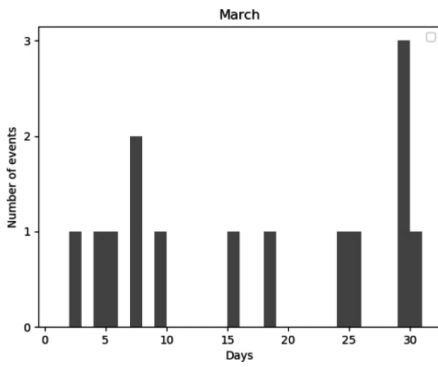
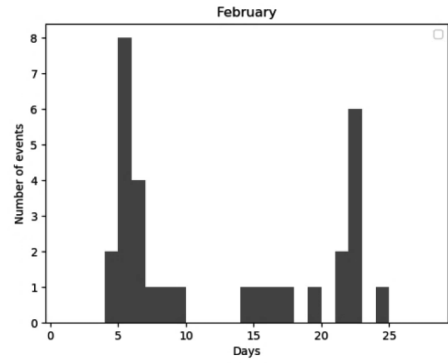
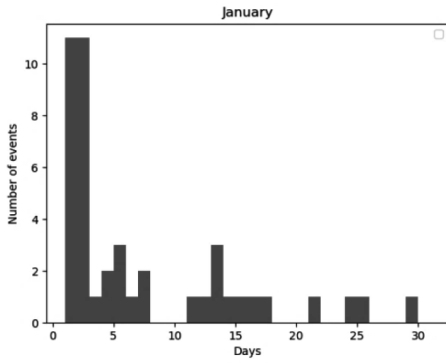


Fig.7. The distribution of seismicity in time according to the number of events per months



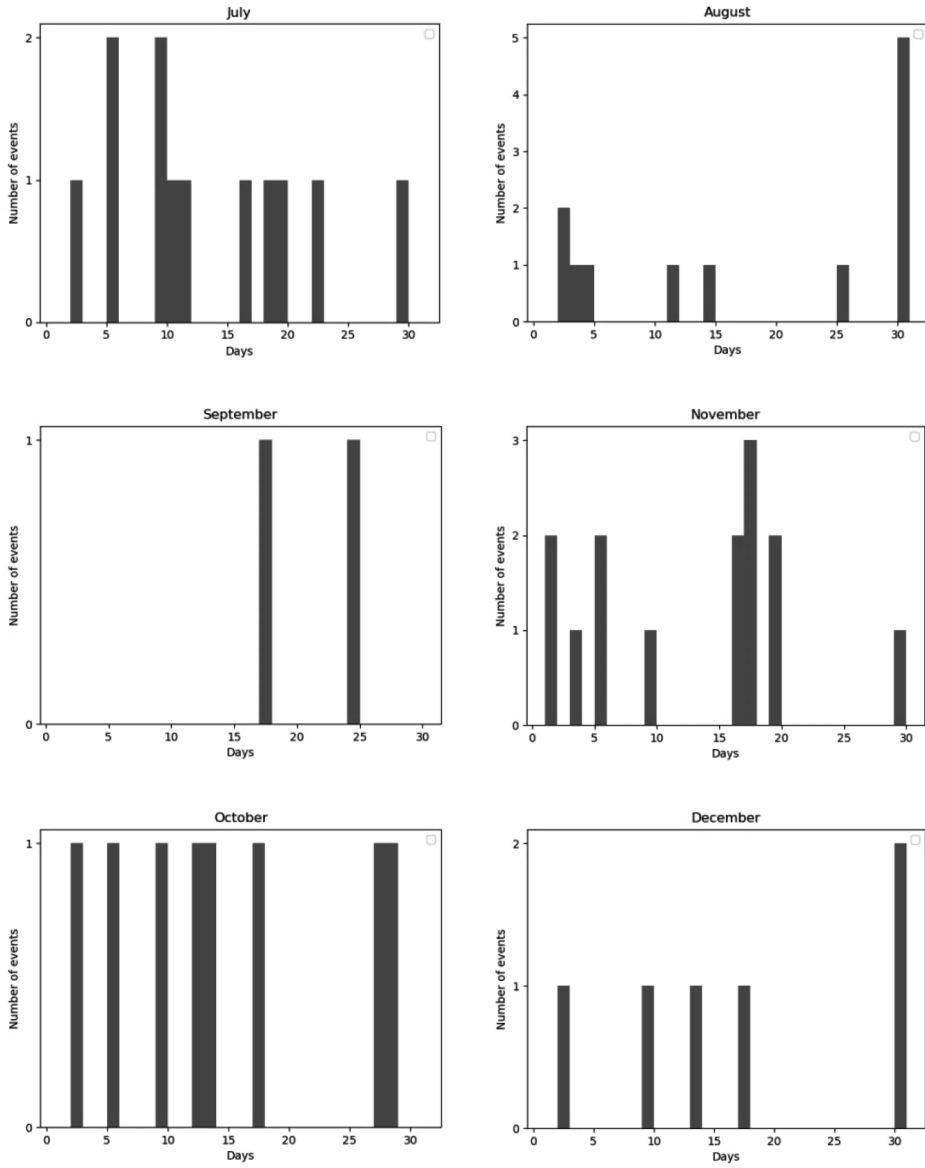


Fig. 8. The distribution of seismicity in time according to the number of events per month

The figures below show the daily distribution of the number of earthquakes/day for each month. We can see that the distribution is not spread out equally and while in some days more than 10 earthquakes may occur, like the first week of January, there are periods, like in August, September, December, where for periods of 10-15 days no events occur on the territory of Bulgaria.

Acknowledgements: The authors express their gratitude towards the seismologists who have worked in NOTSSI for the period 01.01.2018 - 31.12.2018.

References

- Christoskov L., L. Dimitrova, D. Solakov, 2011b. Digital broadband seismometers of NOTSSI for practical magnitude determinations of P waves. BGS. v.XXXVIII, N1-4/2011, ISSN 1311-753X, 62-72.
- D. Solakov, S. Simeonova, P. Raykova, I. Aleksandrova. Empirical relations converting M_d and M_p magnitudes applied in Bulgarian seismological routine practice to moment and magnitude. Comptes rendus de l'Acad'emie bulgare des Sciences, 71, 8, 2018, DOI:DOI:10.7546/CRABS.2018.08.09, 1076-1085. SJR:0.21, ISI IF:0.27

Сеизмичност на територията на България и прилежащите земи по данни от НОТССИ през 2018г.

Д. Драгомиров, Е. Ойнаков, В. Бучакчиев, Й. Милков

Резюме: Представена е карта с епицентрите на 168 земетресения, с магнитуд $M \geq 2.5$ случили се през 2018 г. в България и околностите (сектор ограничен от географска ширина $\phi = 41^\circ - 44.5^\circ N$ и географска дължина $\lambda = 22^\circ - 29^\circ E$) регистрирани от Националната Оперативна Телеметрична Система за Сеизмологична Информация (НОТССИ). Експертен, обобщен анализ е представен. Приложен е каталог със земетресения.

Ключови думи: България, сеизмичност

Благодарности: Авторите изразяват своите благодарности към сеизмолозите, които са работили в НОТССИ за периода 01.01.2018 – 31.12.2018.